



SWISS FEDERAL INSTITUTE OF TECHNOLOGY IN ZÜRICH
DEPARTMENT OF PHYSICS

MASTER'S THESIS

Compatibility of Heavy Neutrinos with Multi-Lepton Signatures at the Large Hadron Collider

Author:
Yannick Burkard

Supervisor:
Prof. Dr. Andreas Crivellin
Co-Supervisor:
Prof. Dr. Klaus Stephan Kirch

July 1, 2023

Abstract

Despite the enormous success of the Standard Model (SM), several experimental results have disagreed with its predictions. In particular, excessive multi-lepton final states measured at the Large Hadron Collider have become increasingly frequent over the past years. One recent CMS publication [1] has reported an overcount of gluon fusion and Z -Higgs production events with two and three final leptons. In this study, we evaluated the compatibility of scalar and vector mediated heavy neutrino production on these anomalous categories. To do so, we first constructed a minimal SM extension containing new scalars, a Z' boson and heavy neutrinos, computing the relevant mass eigenstates and decay widths. We then generated neutrino production events with fast track algorithms, followed by object and event selection procedures to obtain the reconstructed mass distributions found in [1]. At last, we performed a fit of the obtained distributions to CMS data with two distinct methods, and estimated the corresponding cross-section and significance against the SM hypothesis. This analysis was repeated for varying mediator and neutrino masses within selected ranges. We found that the scalar mediated neutrino production is favoured over the SM-only hypothesis in the gluon fusion category, yielding significance $\gtrsim 2.5\sigma$. On the other hand, the Z' mediated neutrino production seems to fit the Z -Higgs results poorly compared to the SM fit, with significance levels $\lesssim 1.0\sigma$. The low significance occurs mainly due to the absence of constraints on the SM normalization parameters, and a more detailed analysis is required to set adequate bounds on them. As further studies, we suggest the evaluation of additional charged and neutral scalar producing signatures on other collider studies.

Acknowledgements

I want to sincerely thank Prof. Dr. Andreas Crivellin for giving me the opportunity to conduct this interesting research project at his group. I truly appreciate the resources and guidance he provided me with to undertake my work and obtain meaningful results in the search for new physics. I am also thankful to Prof. Dr. Klaus Kirch for making this project come into existence. I am deeply grateful to Guglielmo Coloretti for his selfless support and assistance throughout the entire thesis period, engaging in helpful discussions and solving many of my doubts. I wish to extend my gratitude to Prof. Dr. Bruce Mellado, who provided me with the necessary orientation during the sample processing phase. I want to further thank Dr. Sumit Banik for the insightful conversations regarding the two Higgs doublet model. I also appreciate the productive discussions I had with Anza-Tshilidzi Mulaudzi about the event selection criteria. Finally, I wish to express my heartfelt gratitude to my family, friends and girlfriend who unconditionally supported me throughout my studies, and always encouraged me to conduct my work to the best of my abilities.

Contents

Abstract	1
Acknowledgements	2
1 Introduction	6
1.1 Theoretical Framework	8
1.1.1 Gauge Theory of the Standard Model	8
1.1.2 Challenges of the Standard Model	9
1.1.3 Physics Beyond the Standard Model	10
2 Signal Model	13
2.1 Gauge Sector	14
2.2 Fermion Sector	15
2.2.1 Neutrino Mass Eigenstates	15
2.3 Scalar Sector	17
2.3.1 Scalar Mass Eigenstates	18
2.3.2 Gauge Mass Eigenstates	22
2.4 Signal Processes and Parameter Choice	24
2.5 Decay Widths	26
2.5.1 N_i Decay	26
2.5.2 Z' Decay	26
2.5.3 Scalar Decay	27
3 Simulation and Analysis	28
3.1 Event Generation	28
3.2 Object Reconstruction and Event Selection	29
3.3 Smearing and Shifting	32
3.4 Statistical Formalism	34
3.4.1 Chi Squared	36
3.4.2 Likelihood Ratio	37

4 Results and Discussion	39
4.1 Scalar Mediated Neutrino Production	39
4.2 Z' Mediated Neutrino Production	43
5 Conclusion	49
A Mass Matrix Diagonalization	58
A.1 Neutrino Diagonalization	58
A.2 Scalar Sector	58
A.2.1 Identifying Quadratic Terms	58
A.2.2 Complex Scalar Diagonalization	60
A.2.3 Neutral CP-Odd Scalar Diagonalization	60
A.3 Gauge Sector	62
A.3.1 Identifying Quadratic Terms	62
B Decay Width Computations	64
B.1 N Decay	64
B.1.1 $N B\ell$	65
B.1.2 $N h\nu$	67
B.2 Z' Decay	68
B.2.1 $Z' \rightarrow N\bar{N}$	69
B.2.2 $Z' \rightarrow \nu_j \bar{N}$	70
B.2.3 $Z' \rightarrow \nu_j \bar{\nu}_j$	70
B.3 Scalar Decay	70
B.3.1 $h_k \rightarrow N\bar{N}$	71
B.3.2 $h_k \rightarrow \nu_j \bar{N}$	72
B.3.3 $h_k \rightarrow \ell_j^- \ell_j^+$	72
C Signal Model Implementation	73
D Digitalized Values for Literature Distributions	108
D.1 Gluon Fusion Category	108
D.1.1 $p_{T2} < 20$ GeV	108
D.1.2 $p_{T2} > 20$ GeV	108
D.2 Z -Higgs Production Category	109
D.2.1 1-jet	109
D.2.2 2-jet	109
E Standard Model Normalization Parameters	110
E.1 Scalar Mediated Neutrino Production	110

E.2	Z' Mediated Neutrino Production	113
F	Selection Efficiencies	115
F.1	Scalar Mediated Neutrino Production	115
F.2	Z' Mediated Neutrino Production	116
G	Normalized Signal Distributions	117
G.1	Scalar Mediated Neutrino Production	117
G.2	Z' Mediated Neutrino Production	136

Chapter 1

Introduction

Theoretical calculations based on the standard model (SM) of particle physics have shown remarkable agreement with experimental results over the past decades. Various precision studies at the Large Hadron Collider (LHC) involving electroweak bosons [2], top quarks [3] and the Higgs boson [4, 5] have resembled SM predictions with great accuracy. However, there have been several exceptions to such agreements, such as the 2021 muon magnetic moment measurement [6], neutrino oscillations [7] and B-meson anomalies [8], indicating an incompleteness of the SM and serving as a motivation for the search of new physics beyond the standard model (BSM).

Data collected at the LHC from Runs 1 and 2 involving multi-lepton final states have demonstrated various discrepancies with the SM¹. Such variations are typically observed as a localized excess of LHC events against Monte-Carlo (MC) SM predictions in the distributions of reconstructed mass variables. The processes leading to these discrepancies involve various SM interactions, meaning that it is improbable that the mismodelling of a single interaction causes such divergences. Furthermore, these variations have been observed in different experiments made by both the CMS and ATLAS collaborations. The occurrence of multi-lepton anomalies on LHC data has become more prevalent in recent years and could provide important hints for BSM physics.

Divergences from SM predictions in leptonic signatures occur more often in low mass ranges and are mainly observed in recasts of SM searches by CMS and ATLAS. Despite the lack of dedicated BSM searches from experimental collaborations, several individual studies have suggested the existence of low mass resonances by evaluating anomalous data with different signal models. Some analyses [9, 10, 11, 12] made with LHC data have reported significance levels of more than 3σ when considering heavy scalars against the SM hypothesis. A search for

¹For a collection of measurements indicating such discrepancies, see LHC data studied in [9, 10, 11, 12, 13]

a scalar mediator has also been made in $\gamma\gamma$, $Z\gamma$ and $b\bar{b}$ channels, leading to a combined global significance of 4.8σ at mass $m_S = 151.5$ GeV [14]. Moreover, a recent study [13] conducted on a WW channel with CMS and ATLAS data has measured significance levels of $\gtrsim 2.5\sigma$ for mediator masses $m_H = 95$ GeV and 150 GeV. Various LEP and LHC investigations have further indicated the possibility of scalars at masses $m_H = 95$ GeV [15, 16, 17, 18, 19, 20, 21] and $m_H = 680$ GeV [22, 23, 24].

The aforementioned studies have gathered compelling evidence for the existence of new scalars in nature. In order to evaluate BSM scalars on multi-lepton data, a decay chain to leptons must be specified. One possibility is to consider decays via electroweak interactions by introducing one additional $SU(2)_L$ doublet coupled to W and Z bosons, which implies decays of type $H \rightarrow ZZ$. Nevertheless, past searches at the LHC have rejected the possibility of such decay modes in 4 lepton signatures [25]. To circumvent this issue, one can introduce instead a scalar $SU(2)$ triplet of hypercharge 0, whose neutral component does not couple to the diagonal elements of the electroweak sector, as mentioned in [13]. Another alternative is to include massive neutrinos mediating scalar-electroweak interactions as suggested by [14]. The presence of additional neutrinos would also allow for a broader range of possible final states, including multiple combinations of leptons, jets and missing energy, which could therefore be detected in various anomalous channels. It is therefore interesting to evaluate BSM scalar mediated production of heavy neutrinos on anomalous multi-lepton signatures.

Some of the anomalous processes with multi-lepton final states are also mediated by Z and W bosons decaying to Z , W and the SM Higgs boson h . Early studies on leptonic signatures have solely considered Higgs-like mediators, which have scalar properties and could be limiting the significance level against the SM hypothesis. Introducing a new Z' boson coupled to short-lived heavy neutrinos has not been thoroughly explored yet and could increase the significance level for boson mediated multi-lepton production at the LHC. Further motivations for the existence of a Z' boson, as well as for additional scalars and neutrinos are discussed in section 1.1.3.

A recent CMS publication [1] measuring the production cross-section of the Higgs decays to a pair of W bosons has reported an excess of events arising from Higgs mediated gluon fusion (Fig. 1) and Z mediated Z -Higgs production (Fig. 14). This study has been done with data collected over a span of two years, corresponding to a higher integrated luminosity (138 fb^{-1}) than the one found in early studies [9, 10, 11], and hence providing a higher sensitivity for the search for new physics. The more recent results reported in [13] are based on the gluon fusion data, where a scalar decaying to two W bosons was considered as signal hypothesis. While notable significance values were obtained in this search, processes with heavy neutrinos have not yet been evaluated with these data and can possibly show a higher compatibility with such results.

To help explain the anomalies reported in the gluon fusion and Z -Higgs production categories in [1], we consider Z' and H mediated heavy neutrino production at the LHC. In particular, we look at processes of the type $pp \rightarrow H \rightarrow N_i \bar{\nu}_i (\bar{N}_i \nu_i)$ and $pp \rightarrow Z' \rightarrow N_i \bar{N}_i$, where N_i and ν_i are BSM and SM neutrinos. In this project, we construct an extension of the SM containing such particles and required symmetries, investigating the possible mass eigenstates and computing the corresponding decay widths. After implementing the signal model with appropriate parameter selection, we generate and process fast track MC events. To account for discrepancies between fast and full simulations, we implemented a smearing procedure in which jet and missing momentum resolutions were reduced. The resulting BSM histograms were then fitted to data with two distinct methods for comparison, and the corresponding significance levels and cross-sections were computed over given mediator and neutrino mass ranges.

1.1 Theoretical Framework

1.1.1 Gauge Theory of the Standard Model²

The theoretical formulation of the SM is based on a gauge theory. In this framework, we identify each particle by a field belonging to a representation of the Poincaré Group. These are spin- $\frac{1}{2}$ fermions corresponding to spinors of representation $(\frac{1}{2}, 0) \oplus (0, \frac{1}{2})$ ³, spin-1 bosons identified by Lorentz vectors of representation $(\frac{1}{2}, \frac{1}{2})$ and spin-0 bosons identified by spin-0 bosons identified by Lorentz scalars of representation $(0, 0)$. In nature, the fundamental spin- $\frac{1}{2}$ particles are quarks and leptons, whereas the spin-1 bosons are the 8 gluons, the photon γ and the massive electroweak bosons Z and W^\pm , and the only confirmed spin-0 particle is the Higgs boson. The physical spin-1 bosons are also known as exchange particles and mediate the three fundamental forces: strong, weak and electromagnetic.

The dynamics between the particles is determined by the Lagrangian \mathcal{L} , which has to fulfill the internal symmetry group, also referred to as the gauge group. Each particle field belongs to a representation of this group. For the Standard Model, the gauge group is

$$SU(3)_C \otimes SU(2)_L \otimes U(1)_Y \quad (1.1)$$

where the indices C , L and Y refer to color, left-handed and hypercharge respectively. The $SU(3)_C$ group acts only on quarks, whereas the $SU(2)_L$ symmetry acts on the left-handed chiral component of fermions and the Higgs doublet. Each particle also has an assigned weak hypercharge Y , which is given by the transformation under the $U(1)_Y$ group and fulfills the

²The contents in this section are taken from [26]

³We note that the $(\frac{1}{2}, 0)$ and $(0, \frac{1}{2})$ representations correspond to the left- and right-handed chiral components of a spinor, which are treated separately within the electroweak theory, meaning that they transform differently under the $SU(2)_L$ symmetry

relation $Q = I_3 + Y$ where Q and I_3 is the electromagnetic charge and the eigenvalue of the diagonal Pauli matrix σ_z , respectively. Moreover, each subgroup generator corresponds to a spin-1 gauge boson, which is contained in the covariant derivative D_μ .

Although the Standard Model has successfully predicted various experimental results, the Lagrangian cannot account for mass terms by only considering fermion and gauge boson fields. In the early and mid 20th century, experimental results indicated a short-range nature of the strong and weak nuclear forces, suggesting massive exchange bosons. In order to account for gauge boson masses, the concept of spontaneous symmetry breaking (SSB) was developed within the context of gauge theories by Brout, Englert [27], Higgs [28], Guralnik, Hagen and Kibble [29] in 1964. They proposed the introduction of unphysical scalar fields whose degrees of freedom would be exchanged with massless gauge bosons, yielding a 3rd polarization component to the latter and leading to massive gauge particles.

In the SM, the scalar fields are contained in a $SU(2)_L$ doublet Φ , also known as the Higgs field, which loses three degrees of freedom after SSB, giving masses to the Z and W^\pm bosons via a scalar kinetic term. The remaining degree of freedom corresponds to a real CP-even scalar h , also referred to as the Higgs boson. The introduction of a scalar doublet further allows for fermion-fermion- Φ couplings, known as Yukawa couplings, leading to fermion mass terms in the Lagrangian upon acquisition of a vacuum expectation value v by Φ . This means that the scalar $SU(2)_L$ doublet accounts for all mass terms in the SM Lagrangian. In 2012, studies done with LHC data [4, 5] reported the discovery of a Higgs-like scalar of mass around 125 GeV. This particle matches the properties of the SM Higgs boson, serving as evidence for the Higgs mechanism and supporting the validity of the Standard Model.

1.1.2 Challenges of the Standard Model

Despite the great success of the Standard Model, there are several observations which cannot be explained by this theory. Some of these incompatibilities arise from cosmological observations. For instance, data collected from gravitational lensing and galactic motion have indicated the existence of dark matter (DM) in our universe [30], which is radiationless and cannot be explained by the SM. Another observation which is not accounted for by the SM is the prevalence of matter over antimatter in the universe [31]. The SM predicts a symmetrical distribution between both types of matter, but the observed matter-antimatter asymmetry points towards a mechanism favouring the creation of matter in the early cosmos, known as baryogenesis. Moreover, gravity is not included in the Standard Model, and attempts of writing a quantum theory of gravity have resulted in non-renormalizability [32].

The Standard Model also contains some issues related to its theoretical framework. One of them is the hierarchy problem: the Higgs boson is highly sensitive to quantum corrections due to the presence of virtual particles, and a precise level fine-tuning is required to avoid large

correction values [33]. Moreover, quantum chromodynamics (QCD) allows for charge-parity (CP) violating terms, whereas no empirical evidence has been yet found confirming such violation [34]. One more question raised by the SM is whether the three fundamental forces become unified at higher energies, meaning that theory would be described by a simple gauge group with one coupling constant [35]. It has been confirmed at LEP that the electromagnetic and weak forces indeed unify at larger energies [36], and theorists have proposed a further unification with the strong force at energies beyond levels accessible by current experiments.

There are also several experimental results that strongly disagree with Standard Model predictions. For instance, there have been excess events measured at the BaBar experiment for $B\bar{B}$ dimeson channel [37], yielding a 3.4σ significance against the SM. Such excess has also been reported by LHCb [38] and the Belle experiment [39], and a combined analysis on all results has reported a 5σ deviation from the SM prediction [40]. The 2021 measurement of the muon magnetic moment at Fermilab was initially found to deviate by 4.2σ from the SM prediction [6] by using e^+e^- scattering data [41]. However, a later recomputation of this variable with lattice QCD techniques [42] has reduced this tension to $\sim 2\sigma$. The W mass has also been measured in 2022 by the CDF collaboration with a 7σ deviation from the SM value [43], which has been nevertheless challenged by a 2023 measurement made by ATLAS [44] agreeing with the SM prediction. Another empirical phenomenon not yet explained by the SM is neutrino flavour oscillation at the Super-Kamiokande and Sudbury Observatories [45], indicating that neutrinos are massive. As discussed earlier in this chapter, further anomalies have been found at LHC experiments with multi-lepton final states, leading to a significance of more than 3σ when considering new scalars against the SM [9, 10, 11].

1.1.3 Physics Beyond the Standard Model

There have been several proposed theories to explain some of the phenomena which cannot be justified with the SM. Notable extensions of the SM are supersymmetric theories (SUSYs), in which additional symmetries exchanging fermions with bosons are imposed on the Lagrangian, giving rise to supersymmetric particles [46]. Such theories could solve the hierarchy problem and also predict DM candidates. Another class of popular theories are Grand Unified Theories (GUTs), in which only one simple gauge group is imposed on the Lagrangian at higher energies, unifying all three forces [47]. Typical choices for the simple group are $SU(5)$ or $SO(10)$, which at lower energies spontaneously break into the SM gauge group. These theories also predict the existence of new particles and could potentially explain the matter-antimatter asymmetry in the cosmos.

One class of theories yielding particles that could be potentially observed at collision experiments are the so called two Higgs doublet models ($2HDMs$) [48]. They extend the SM with another Higgs-like doublet, yielding three additional scalars: 1 charged, 1 CP-odd neutral

and 1 CP-even neutral. Besides the scalar masses, mixing angles between the Higgs doublets and the neutral scalars appear as new degrees of freedom. As previously mentioned, the addition of new scalars has shown to explain various excesses at leptonic, hadronic and photonic final states at the LHC [9, 10, 11, 13, 14]. *2HDMs* have also predicted the anomalous muon magnetic moment measurement and provide candidates for DM for stable scalars [49]. The main theoretical motivation for *2HDM* is that these models are included in SUSYs, since the latter require a minimum of two Higgs doublets to give mass to up- and down-type quarks simultaneously [50]. The presence of an additional Higgs doublet could also remove strong CP violation from the SM via axion models [51] and account for baryogenesis in the early universe [52].

Another extension of the SM is the addition of a $U(1)'$ symmetry to the gauge group, hence predicting the existence of a new Z' boson [53]. In order for such a boson to be massive, an additional scalar must be included to break the $U(1)'$ symmetry. Direct searches for a massive Z' have been conducted at LEP, Tetravon and LHC by looking at dilepton and dijet channels, but no results have been found favouring its existence so far [54, 55]. However, it is possible to avoid or suppress Z' -quark and Z' -lepton couplings by introducing new mediators like heavy neutrinos and quarks. Such models remain relatively unexplored in collision experiments and could explain anomalous phenomena like the aforementioned excesses seen in electroweak mediated multi-lepton channels. The consequential Z - Z' mixing could also explain the $Z \rightarrow b\bar{b}$ deviations found at LEP and the excess m_W mass measured by CDF [56]. A Z' boson could also mediate interactions between SM and dark particles in frameworks known as Hidden Valley Models [57]. Theoretical motivations for the existence of a $U(1)'$ symmetry come mainly from GUT models containing a $SO(10)$ or E_6 symmetry [53], which breaks into a $SU(3) \otimes SU(2) \otimes U(1) \otimes U(1)^n$ ($n \in \mathbb{N}_{>0}$) symmetry. Several supersymmetric and string theories also include a $U(1)'$ group [58].

A further set of models extend the fermion sector of the SM with heavy neutrinos. One typical scenario is the addition of three right-handed neutrinos, which lead to Majorana and Yukawa mass terms in the Lagrangian, yielding 6 massive physical neutrinos via mixing [59]. This framework referred to as type-I seesaw mechanism, in which the large heavy neutrino mass values allow for small SM neutrino masses. Seesaw mechanisms are generic procedures yielding SM neutrino masses and justify the observed SM neutrino oscillations. Like the previously mentioned models, the inclusion of heavy neutrinos is also contained in several GUT and SUSY theories [60, 61, 62]. Although BSM neutrinos have often been proposed as stable and sterile to explain DM prevalence in the universe [63], there are also motivations for the existence of short-lived massive neutrinos. For instance, as discussed earlier, heavy neutrinos can be introduced as mediators between Z' or neutral scalars and SM leptons to explain multi-lepton discrepancies while maintaining past experimental constraints. One study [64] has also considered neutrinos of single chirality coupled to charged scalars in a linear seesaw

mechanism, containing signatures potentially detectable at collider experiments. Although our model contains vector-like neutrinos with both left- and right-handed chirality, several linear seesaw signatures can also be realized with the proposed theory.

When investigating the existence of certain particles, one can theorize them by extending the SM in a particular way. This procedure begins by first assigning each particle a specific field. In case new gauge bosons are introduced, appropriate symmetries should be included to account for them, and additional scalars are required so that they become massive via SSB. After identifying the fields, one should consider which interactions are to be studied, yielding the necessary coupling terms of the Lagrangian. To obtain such terms, one postulates appropriate gauge representations for each field, and finally writes down all possible gauge invariant Lagrangian terms. Additional global symmetries can be imposed in order to avoid specific couplings which are undesired or forbidden. Once the Lagrangian is obtained, one can identify mass terms and perform a diagonalization procedure in order to obtain mass eigenvalues and physical eigenstates. In this project, we performed the aforementioned steps in order to minimally extend the SM with the proposed scalars, Z' boson and heavy neutrinos, as described in the following section.

Chapter 2

Signal Model

The model considered in this project consists of the SM extended with a $U(1)$ gauge symmetry of charge X and associated field B' , three vector-like neutrino spinors ψ_i , as well as a complex scalar doublet Φ_1 and complex scalar singlet Φ_S . The scalar sector therefore corresponds to a 2 Higgs doublet plus scalar model ($2HDMs$), and since we now have additional heavy neutrinos N_i and a gauge boson Z' , we label to this model as $2HDMs+Z'+N$.

The extended scalar sector allows the new gauge field B' to become the massive, physical gauge boson Z' after SSB. In order to couple the vector-like neutrinos to Z' , we charge them under $U(1)_X$. The additional scalar doublet is also charged under the new symmetry, allowing for scalar-neutrino couplings of Yukawa type. Such couplings lead to mixed neutrino mass eigenstates, which enable heavy neutrinos to interact with electroweak bosons via fermion kinetic terms. Table 2.1 displays the field content with corresponding gauge representations.

We separate the model Lagrangian \mathcal{L} into three terms

$$\mathcal{L} = \mathcal{L}_G + \mathcal{L}_F + \mathcal{L}_H \quad (2.1)$$

where \mathcal{L}_G , \mathcal{L}_F , and \mathcal{L}_H contain gauge, fermion and scalar fields, respectively. We further identify the model covariant derivative as

$$D^\mu = \partial^\mu + i\frac{g_s}{2}T_a G_a^\mu + i\frac{g}{2}\sigma_a W_a^\mu + ig_1 Y B^\mu + ig'_1 X B'^\mu \quad (2.2)$$

where g_s , g , g_1 and g'_1 are the the strong, weak, $U(1)_Y$ and $U(1)_X$ coupling constants, whereas T_a are the $SU(3)_C$ generators, σ_a the Pauli matrices, and Y and X the charges for the $U(1)_Y$ and $U(1)_X$ symmetries. In the following sections we describe each of the Lagrangian terms with their corresponding mass eigenstates, and compute the relevant decay widths. We make recurrent use of the Einstein summation convention. For the corresponding calculations

Field	Generations	Description	Representation
G_i	8	$SU(3)_C$ gauge field	(8, 1, 0, 0)
W_i	3	$SU(2)_L$ gauge field	(1, 3, 0, 0)
B	1	$U(1)_Y$ gauge field	(1, 1, 0, 0)
B'	1	$U(1)_X$ gauge field	(1, 1, 0, 0)
$Q_{i,L}$	3	Left-handed quark doublet	$(3, 2, \frac{1}{6}, \frac{1}{3})$
$u_{i,R}$	3	Right-handed up-type quark singlet	$(3, 1, \frac{2}{3}, \frac{1}{3})$
$d_{i,R}$	3	Right-handed down-type quark singlet	$(3, 2, -\frac{1}{3}, \frac{1}{3})$
$L_{i,L}$	3	Left-handed lepton doublet	$(1, 2, -\frac{1}{2}, 0)$
$l_{i,R}$	3	Right-handed lepton singlet	$(1, 1, -1, 0)$
ψ_i	3	Vector-like neutrino singlet	$(1, 1, 0, -1)$
Φ_1	1	Non-SM scalar doublet	$(1, 2, \frac{1}{2}, -1)$
Φ_2	1	SM scalar doublet	$(1, 2, \frac{1}{2}, 0)$
Φ_S	1	Scalar singlet	$(1, 1, 0, 1)$

Table 2.1: Field content of the $2HDM + Z' + N$ model. The indices i correspond to different generations. The gauge representations (C, L, Y, X) are displayed in terms of the gauge group $SU(3)_C \otimes SU(2)_L \otimes U(1)_Y \otimes U(1)_X$. Values C and L correspond to the dimensions for the $SU(3)_C$ and $SU(2)_L$ representations, whereas Y and X refer to the charges for the $U(1)_Y$ and $U(1)_X$ representations.

implemented with **Mathematica** [65] notebooks, refer to Appendix A.

2.1 Gauge Sector

The Lagrangian gauge term is written as

$$\mathcal{L}_G = -\frac{1}{4}G_a^{\mu\nu}G_{a,\mu\nu} - \frac{1}{4}W_a^{\mu\nu}W_{a,\mu\nu} - \frac{1}{4}B^{\mu\nu}B_{a,\mu\nu} - \frac{1}{4}B'^{\mu\nu}B'_{\mu\nu} \quad (2.3)$$

where for a gauge symmetry with fields \mathcal{F}_a , coupling constant g_i and structure constant f^{abc} we define the field tensor

$$\mathcal{F}_a^{\mu\nu} = \partial^\mu \mathcal{F}_a^\nu - \partial^\nu \mathcal{F}_a^\mu + g_i f^{abc} \mathcal{F}_b^\mu \mathcal{F}_c^\nu \quad (2.4)$$

For the $U(1)_X$ symmetry, the gauge field tensor is hence given by

$$B'^{\mu\nu} = \partial^\mu B'^\nu - \partial^\nu B'^\mu \quad (2.5)$$

2.2 Fermion Sector

The fermion Lagrangian \mathcal{L}_F is equal to the sum of the kinetic, Yukawa and neutrino Dirac mass terms $\mathcal{L}_{F,\text{kin}}$, \mathcal{L}_Y and \mathcal{L}_ψ , respectively. The kinetic term is written as

$$\mathcal{L}_{F,\text{kin}} = \overline{Q}_{i,L} \not{D} Q_{i,L} + \overline{u}_{i,R} \not{D} u_{i,R} + \overline{d}_{i,R} \not{D} d_{i,R} + \overline{L}_{i,L} \not{D} L_{i,L} + \overline{l}_{i,R} \not{D} l_{i,R} + \overline{\psi}_i \not{D} \psi_i \quad (2.6)$$

where $\not{D} := \gamma^\mu D_\mu$.

For a Higgs doublet model, one typically imposes a \mathbb{Z}_2 -symmetry to avoid flavour-changing neutral currents arising from the Yukawa Lagrangian [66]. Nevertheless, by including the $U(1)_X$ symmetry and charging the newly introduced scalars and spinors accordingly we can avoid such flavour violations without the necessity of additional symmetries. We write the Yukawa term as:

$$-\mathcal{L}_Y = Y_{ij}^u \overline{Q}_{i,L} \tilde{\Phi}_2 u_{j,R} + Y_{ij}^d \overline{Q}_{i,L} \Phi_2 d_{j,R} + Y_{ij}^l \overline{L}_{i,L} \Phi_2 l_{j,R} + Y_{ij}^n \overline{L}_{i,L} \tilde{\Phi}_1 \psi_j + \text{h.c.} \quad (2.7)$$

where $(\tilde{\Phi}_k)_m := \varepsilon_{mn}(\Phi_k)_n^*$; Y^u , Y^d and Y^l are SM Yukawa couplings for the up- and down-type quarks and leptons; and Y^n is the Yukawa coupling between SM leptons and BSM neutrino fields.

Lastly, we write the neutrino Dirac mass term as

$$-\mathcal{L}_\psi = M_{ij}^{(\psi)} \overline{\psi}_i \psi_j \quad (2.8)$$

with $M^{(\psi)} \in \mathbb{R}^{3 \times 3}$ as the corresponding mass matrix.

2.2.1 Neutrino Mass Eigenstates

We now determine the physical neutrino mass eigenstates and the corresponding eigenvalues. We first cast all neutrino fields into a single Lagrangian term:

$$-\mathcal{L}_n = M_{jk}^{(\psi)} \overline{\psi}_j \psi_k + Y_{jk}^n \overline{L}_{j,L} \tilde{\Phi}_1 N_k + Y_{jk}^{n,\dagger} \overline{\psi}_k \tilde{\Phi}_1^\dagger L_{j,L} \quad (2.9)$$

Identifying the first lepton doublet components as the neutrino spinors $\eta_{i,L}$ ($i = e, \mu, \tau$) and decomposing the vector-like neutrino singlets into their left- (L) and right-handed (R) chiral components as $\psi_i = \psi_{i,R} + \psi_{i,L}$, we rewrite the neutrino term after SSB (see section 2.3 for scalar components) as

$$-\mathcal{L}_n = \begin{pmatrix} \overline{\eta}_L & \overline{\psi}_L \end{pmatrix} M \begin{pmatrix} N_R \\ \psi_R \end{pmatrix} + \begin{pmatrix} \overline{\psi}_R \\ \psi_L \end{pmatrix} M^\dagger \begin{pmatrix} \eta_L \\ \psi_L \end{pmatrix} \quad (2.10)$$

where we have defined the generalized neutrino fields η_L and ψ , and 6×3 mass matrix M as

$$\eta_L = \begin{pmatrix} \eta_{e,L} \\ \eta_{\mu,L} \\ \eta_{\tau,L} \end{pmatrix}, \quad \psi = \begin{pmatrix} \psi_1 \\ \psi_2 \\ \psi_3 \end{pmatrix}, \quad M = \begin{pmatrix} M^{(Y)} \\ M^{(\psi)} \end{pmatrix} \quad (2.11)$$

with $M_{ij}^{(Y)} := \frac{Y_{ij}v \sin \beta}{\sqrt{2}}$, v the SM vacuum expectation value and β the scalar doublet mixing angle (see section 2.3).

The matrix M has singular value decomposition

$$M = U_L \widehat{M} U_R^\dagger \quad (2.12)$$

with U_L , U_R orthogonal matrices and \widehat{M} containing the mass eigenvalues m_i^ν and m_i^N for the physical light and heavy neutrino fields ν_i and N_i , respectively:

$$\widehat{M} = \begin{pmatrix} m_e^\nu & & \\ & m_\mu^\nu & \\ & & m_\tau^\nu \\ m_1^N & & \\ & m_2^N & \\ & & m_3^N \end{pmatrix} = \begin{pmatrix} 0 & & \\ & 0 & \\ & & 0 \\ m_1^N & & \\ & m_2^N & \\ & & m_3^N \end{pmatrix} \quad (2.13)$$

The physical light neutrinos $\nu_i = \nu_{i,L}$ only contain a left-handed chiral component and are massless, corresponding to the physical SM neutrinos, whereas the physical heavy neutrinos $N = N_{i,L} + N_{i,R}$ are composed of both left- and right-handed chiral fields and are massive. The physical fields are expressed in the unphysical interaction basis by applying the transformation matrices U_L and U_R :

$$\begin{pmatrix} \nu_{e,L} \\ \nu_{\mu,L} \\ \nu_{\tau,L} \\ N_{1,L} \\ N_{2,L} \\ N_{3,L} \end{pmatrix} = U_L^\dagger \begin{pmatrix} \eta_{e,L} \\ \eta_{\mu,L} \\ \eta_{\tau,L} \\ \psi_{1,L} \\ \psi_{2,L} \\ \psi_{3,L} \end{pmatrix}, \quad \begin{pmatrix} N_{1,R} \\ N_{2,R} \\ N_{3,R} \end{pmatrix} = U_R^\dagger \begin{pmatrix} \psi_{1,R} \\ \psi_{2,R} \\ \psi_{3,R} \end{pmatrix} \quad (2.14)$$

The neutrino Lagrangian term can then be expressed in the mass eigenbasis as

$$\mathcal{L}_n = \sum_{k=1}^3 m_k^N (\bar{N}_{k,L} N_{k,R} + \bar{N}_{k,R} N_{k,L}) = \sum_{k=1}^3 m_k^N \bar{N}_k N_k \quad (2.15)$$

In order to avoid SM lepton flavour violation, we only allow for couplings $\eta_e - \psi_1$, $\eta_\mu - \psi_2$ and $\eta_\tau - \psi_3$, leading to diagonal matrices $M^{(\psi)}$ and $M^{(Y)}$. We define the SM-BSM neutrino mixing angles α_j as:

$$\tan \alpha_e := \frac{M_{e1}^{(Y)}}{M_{11}^{(\psi)}}, \quad \tan \alpha_\mu := \frac{M_{\mu 2}^{(Y)}}{M_{22}^{(\psi)}}, \quad \tan \alpha_\tau := \frac{M_{\tau 3}^{(Y)}}{M_{33}^{(\psi)}} \quad (2.16)$$

For the remainder of this document we write $t_j := \tan \alpha_j$, $s_j := \sin \alpha_j$ and $c_j := \cos \alpha_j$. By further assuming non-zero coupling parameters to be positive, we obtain the following transformation matrices:

$$U_L = \begin{pmatrix} c_e & & s_e & & \\ & c_\mu & & s_\mu & \\ & & c_\tau & & s_\tau \\ -s_e & & & c_e & \\ & -s_\mu & & c_\mu & \\ & & -s_\tau & & c_\tau \end{pmatrix} \quad (2.17)$$

$$U_R = \mathbb{1}_{3 \times 3} \quad (2.18)$$

With the corresponding physical neutrinos masses:

$$m_1^h = \sqrt{\left|M_{e1}^{(Y)}\right|^2 + \left|M_{11}^{(\psi)}\right|^2}, \quad m_2^h = \sqrt{\left|M_{\mu 2}^{(Y)}\right|^2 + \left|M_{22}^{(\psi)}\right|^2}, \quad m_3^h = \sqrt{\left|M_{\tau 3}^{(Y)}\right|^2 + \left|M_{33}^{(\psi)}\right|^2} \quad (2.19)$$

We further assume the neutrino masses to be equal, setting $m_1^N = m_2^N = m_3^N := m_N$.

Independent Parameters

In our model, we treat the above defined angles α_j , as well as the heavy neutrino mass m_N as independent parameters and express the coupling constants $M_{ij}^{(N)}$ and $M_{ij}^{(Y)}$ as a function of mixing angles and neutrinos masses:

$$M_{e1}^{(Y)} = s_e m_N, \quad M_{\mu 2}^{(Y)} = s_\mu m_N, \quad M_{\tau 3}^{(Y)} = s_\tau m_N \quad (2.20)$$

$$M_{11}^{(\psi)} = c_e m_N, \quad M_{22}^{(\psi)} = c_\mu m_N, \quad M_{33}^{(\psi)} = c_\tau m_N \quad (2.21)$$

2.3 Scalar Sector

The scalar sector is composed of two $SU(2)_L$ doublets and one $SU(2)_L$ singlet given by

$$\Phi_1 = \begin{pmatrix} \rho_1 \\ \frac{1}{\sqrt{2}}(v_1 + \varphi_1 + i\chi_1) \end{pmatrix}, \quad \Phi_2 = \begin{pmatrix} \rho_2 \\ \frac{1}{\sqrt{2}}(v_2 + \varphi_2 + i\chi_2) \end{pmatrix}, \quad \Phi_S = \frac{1}{\sqrt{2}}(v_S + \varphi_S + i\chi_S) \quad (2.22)$$

where ρ_1, ρ_2 are complex scalars, χ_1, χ_2, χ_S , are real CP-odd scalars, $\varphi_2, \varphi_1, \varphi_S$ are real CP-even scalars, and $v_1, v_2, v_S \in \mathbb{R}$ are vacuum expectation values.

The scalar Lagrangian can be expressed in terms of the kinetic and potential terms $\mathcal{L}_{H,\text{kin}}$ and V_H as $\mathcal{L}_H = \mathcal{L}_{H,\text{kin}} - V_H$. The kinetic term is given by

$$\mathcal{L}_{H,\text{kin}} = (D^\mu \Phi_1) (D_\mu \Phi_1) + (D^\mu \Phi_2) (D_\mu \Phi_2) + (D^\mu \Phi_S) (D_\mu \Phi_S) \quad (2.23)$$

whereas the most general scalar potential is

$$\begin{aligned} V_H = & \mu_1 \Phi_1^\dagger \Phi_1 - \lambda_1 (\Phi_1^\dagger \Phi_1)^2 + \mu_2 \Phi_2^\dagger \Phi_2 - \lambda_2 (\Phi_2^\dagger \Phi_2)^2 \\ & + \mu_S \Phi_S^\dagger \Phi_S - \lambda_S (\Phi_S^\dagger \Phi_S)^2 - \lambda_d (\Phi_1^\dagger \Phi_1)(\Phi_2^\dagger \Phi_2) - \lambda_m (\Phi_1^\dagger \Phi_2)(\Phi_2^\dagger \Phi_1) \\ & - \lambda_{S1} (\Phi_S^\dagger \Phi_S)(\Phi_1^\dagger \Phi_1) - \lambda_{S2} (\Phi_S^\dagger \Phi_S)(\Phi_2^\dagger \Phi_2) - \xi (\Phi_1^\dagger \Phi_2 \Phi_S^\dagger + \Phi_2^\dagger \Phi_1 \Phi_S) \end{aligned} \quad (2.24)$$

where μ_i, λ_i and ξ are real parameters. The quadratic coupling parameters μ_i can be eliminated by assuming the minimization condition

$$\left. \frac{\partial V_H}{\partial \Phi_j} \right|_{\Phi_1=v_1, \Phi_2=v_2, \Phi_S=v_S} = 0 \quad (2.25)$$

which yields relations

$$\mu_1 = \lambda_1 s_\beta^2 v^2 + \frac{1}{2} \left(v^2 c_\beta^2 (\lambda_d + \lambda_m) + v_S^2 \lambda_{S1} + \frac{\sqrt{2}\xi c_\beta v_S}{s_\beta} \right) \quad (2.26)$$

$$\mu_2 = \lambda_2 v^2 c_\beta^2 + \frac{1}{2} \left(v^2 s_\beta^2 (\lambda_d + \lambda_m) + v_S^2 \lambda_{S2} + \frac{\sqrt{2}\xi s_\beta v_S}{c_\beta} \right) \quad (2.27)$$

$$\mu_S = \lambda_S v_S^2 + \frac{v^2}{2} \left(c_\beta^2 \lambda_{S2} + s_\beta^2 \lambda_{S1} + \frac{\sqrt{2}\xi c_\beta s_\beta}{v_S} \right) \quad (2.28)$$

where $s_\beta := \sin\beta$ and $c_\beta := \cos\beta$, and the doublet mixing angle β and vacuum expectation value v are defined by $\tan\beta := \frac{v_1}{v_2}$ and $v := \sqrt{v_1^2 + v_2^2}$.

2.3.1 Scalar Mass Eigenstates

We compute the scalar mass eigenstates and mass eigenvalues arising from the scalar potential. The bilinear terms of the expanded potential V_H in Equation 2.24 define the mass matrices \mathcal{M}_ρ^2 , \mathcal{M}_χ^2 and \mathcal{M}_φ^2 for the complex, real CP-odd and real CP-even fields. After identifying the mass matrices \mathcal{M}_i^2 , we diagonalize them as

$$\mathcal{M}_i^2 = V_i^\dagger \widehat{\mathcal{M}}_i^2 V_i \quad (2.29)$$

where $\widehat{\mathcal{M}}^2$ is diagonal and V unitary. The eigenvalues contained in $\widehat{\mathcal{M}}^2$ are the square values of the physical masses and the physical eigenbasis is obtained by applying V^\dagger to the interaction basis, as in Equation 2.14. We now provide explicit expressions for the mass and transformation matrices for each scalar field category.

Complex Fields

The mass matrix in the unphysical basis $\{\rho_1, \rho_2\}$ is given by

$$M_\rho^2 = \frac{1}{2} \begin{pmatrix} (\lambda_m v^2 c_\beta^2 + \sqrt{2}\xi \frac{v_S c_\beta}{s_\beta}) & -(\lambda_m v^2 s_\beta c_\beta + \sqrt{2}\xi v_S) \\ -(\lambda_m v^2 s_\beta c_\beta + \sqrt{2}\xi v_S) & (\lambda_m v^2 s_\beta^2 + \sqrt{2}\xi \frac{v_S s_\beta}{c_\beta}) \end{pmatrix} \quad (2.30)$$

The corresponding diagonal matrix in the physical basis $\{G^+, H^+\}$ is

$$\widehat{M}_\rho^2 = \begin{pmatrix} 0 & 0 \\ 0 & \frac{1}{2} \left(\lambda_m v^2 + \sqrt{2}\xi \frac{v_S}{s_\beta c_\beta} \right) \end{pmatrix} \quad (2.31)$$

and the transformation matrix $\{\rho_1, \rho_2\} \rightarrow \{G^+, H^+\}$ is

$$V_\rho = \begin{pmatrix} s_\beta & -c_\beta \\ c_\beta & s_\beta \end{pmatrix} \quad (2.32)$$

We identify the physical field G^+ as the SM charged, massless goldstone boson, and H^+ as a BSM charged boson of mass

$$m_+ = \sqrt{\frac{1}{2} \left(\lambda_m v^2 + \sqrt{2}\xi \frac{v_S}{s_\beta c_\beta} \right)} \quad (2.33)$$

Real CP-odd Fields

For the unphysical fields $\{\chi_1, \chi_2, \chi_S\}$ we find the mass matrix

$$M_\chi^2 = \frac{\xi}{\sqrt{2}} \begin{pmatrix} \frac{v_S c_\beta}{s_\beta} & -v_S & v c_\beta \\ -v_S & \frac{v_S s_\beta}{c_\beta} & -v s_\beta \\ v c_\beta & -v s_\beta & \frac{v^2 s_\beta c_\beta}{v_S} \end{pmatrix} \quad (2.34)$$

After diagonalization, we obtain the matrix in the physical basis $\{G^0, G_S^0, A_S\}$

$$\widehat{M}_\chi^2 = \begin{pmatrix} 0 & 0 & 0 \\ 0 & 0 & 0 \\ 0 & 0 & \frac{\xi}{\sqrt{2}} \left(\frac{v_S}{s_\beta c_\beta} + \frac{v^2 s_\beta c_\beta}{v_S} \right) \end{pmatrix} \quad (2.35)$$

with corresponding transformation matrix $\{\chi_1, \chi_2, \chi_S\} \rightarrow \{G^0, G_S^0, A_S\}$

$$V_\chi = \begin{pmatrix} s_\beta & -c_\beta \frac{v s_\beta c_\beta}{\sqrt{v^2 s_\beta^2 c_\beta^2 + v_S^2}} & \frac{c_\beta v_S}{\sqrt{v^2 s_\beta^2 c_\beta^2 + v_S^2}} \\ c_\beta & s_\beta \frac{v s_\beta c_\beta}{\sqrt{v^2 s_\beta^2 c_\beta^2 + v_S^2}} & -\frac{s_\beta v_S}{\sqrt{v^2 s_\beta^2 c_\beta^2 + v_S^2}} \\ 0 & \frac{v_S}{\sqrt{v^2 s_\beta^2 c_\beta^2 + v_S^2}} & \frac{v s_\beta c_\beta}{\sqrt{v^2 s_\beta^2 c_\beta^2 + v_S^2}} \end{pmatrix} \quad (2.36)$$

The field G_0 corresponds to the SM neutral Goldstone boson, whereas G_S^0 corresponds to an additional neutral, massless goldstone boson, whose degree of freedom is absorbed by the massive Z' boson during SSB. The field A_S corresponds to a physical neutral scalar with odd parity and mass.

$$m_A = \sqrt{\frac{\xi}{\sqrt{2}} \left(\frac{v_S}{s_\beta c_\beta} + \frac{v^2 s_\beta c_\beta}{v_S} \right)} \quad (2.37)$$

Real CP-even Fields

The mass matrix for the unphysical fields $\{\varphi_1, \varphi_2, \varphi_S\}$ is given by

$$M_\varphi^2 = \begin{pmatrix} -2\lambda_1 v^2 s_\beta^2 + \frac{\xi}{\sqrt{2}} \frac{v_S c_\beta}{s_\beta} & -(\lambda_d + \lambda_m) v^2 s_\beta c_\beta - \frac{1}{\sqrt{2}} \xi v_S & -\lambda_{S1} v_S v_S s_\beta - \frac{1}{\sqrt{2}} \xi v c_\beta \\ -(\lambda_d + \lambda_m) v^2 s_\beta c_\beta - \frac{1}{\sqrt{2}} \xi v_S & -2\lambda_2 v^2 c_\beta^2 + \frac{\xi}{\sqrt{2}} \frac{v_S s_\beta}{c_\beta} & -\lambda_{S2} v_S v c_\beta - \frac{1}{\sqrt{2}} \xi v_S \beta \\ -\lambda_{S1} v_S v_S s_\beta - \frac{1}{\sqrt{2}} \xi v c_\beta & -\lambda_{S2} v_S v c_\beta - \frac{1}{\sqrt{2}} \xi v_S \beta & -2\lambda_S v_S^2 + \frac{\xi}{\sqrt{2}} \frac{v^2 s_\beta c_\beta}{v_S} \end{pmatrix} \quad (2.38)$$

We diagonalize this matrix by using a general 3×3 rotation matrix

$$R(\omega_1, \omega_2, \omega_3) := \begin{pmatrix} c_1 c_2 & s_1 c_2 & s_2 \\ -(c_1 s_2 s_3 + s_1 c_3) & c_1 c_3 - s_1 s_2 s_3 & c_2 s_3 \\ -c_1 s_2 c_3 + s_1 s_3 & -(c_1 s_3 + s_1 s_2 c_3) & c_2 c_3 \end{pmatrix} \quad (2.39)$$

where $s_j := \sin \omega_j$ and $c_j := \cos \omega_j$. We set the mass matrix in the physical basis $\{H, h, S\}$

with masses $\{m_H, m_h, m_S\}$ as

$$\widehat{M}_\varphi^2 = \begin{pmatrix} m_H^2 & & \\ & m_h^2 & \\ & & m_S^2 \end{pmatrix} = RM_\varphi^2 R^\dagger \quad (2.40)$$

thus obtaining the transformation matrix $\{\varphi_1, \varphi_2, \varphi_S\} \rightarrow \{H, h, S\}$

$$V_\varphi = R^\dagger \quad (2.41)$$

The angles ω_1, ω_2 and ω_S correspond to $\varphi_1 - \varphi_2$, $\varphi_1 - \varphi_S$ and $\varphi_2 - \varphi_S$ mixing, respectively. We identify h as the SM Higgs boson, and therefore find $m_h = 125$ GeV, whereas H and S are additional BSM bosons of even parity with masses determined by Equation 2.40.

Independent Parameters

We set the physical scalar masses $\{m_+, m_A, m_h, m_H, m_S\}$, together with angles $\{\omega_1, \omega_2, \omega_3, \beta\}$ as independent parameters, and express the trilinear and quartic couplings found in Equation 2.24 as a function of the former by using the relations found in Equations 2.33, 2.37 and 2.40:

$$\lambda_1 = \frac{1}{2v^2 s_\beta^2} \left\{ \frac{c_\beta^2 v_S^2}{v^2 s_\beta^2 c_\beta^2 + v_S^2} m_A^2 - \sum_{i=1}^3 R_{i1}^2 m_i^2 \right\} \quad (2.42)$$

$$\lambda_2 = \frac{1}{2v^2 c_\beta^2} \left\{ \frac{s_\beta^2 v_S^2}{v^2 s_\beta^2 c_\beta^2 + v_S^2} m_A^2 - \sum_{i=1}^3 R_{i2}^2 m_i^2 \right\} \quad (2.43)$$

$$\lambda_S = \frac{1}{2v_S^2} \left\{ \frac{v^2 s_\beta^2 c_\beta^2}{v^2 s_\beta^2 c_\beta^2 + v_S^2} m_A^2 - \sum_{i=1}^3 R_{i3}^2 m_i^2 \right\} \quad (2.44)$$

$$\lambda_d = \frac{1}{v^2} \left\{ \frac{v_S^2}{v^2 s_\beta^2 c_\beta^2 + v_S^2} m_A^2 - \frac{1}{s_\beta c_\beta} \left(\sum_{i=1}^3 R_{i1} R_{i2} m_i^2 \right) - 2m_+^2 \right\} \quad (2.45)$$

$$\lambda_m = \frac{2}{v^2} \left\{ m_+^2 - \frac{v_S^2}{v^2 s_\beta^2 c_\beta^2 + v_S^2} m_A^2 \right\} \quad (2.46)$$

$$\lambda_{S1} = - \left\{ \frac{1}{vv_S s_\beta} \left(\sum_{i=1}^3 R_{i1} R_{i3} m_i^2 \right) + \frac{c_\beta^2}{v^2 s_\beta^2 c_\beta^2 + v_S^2} m_A^2 \right\} \quad (2.47)$$

$$\lambda_{S2} = - \left\{ \frac{1}{vv_S c_\beta} \left(\sum_{i=1}^3 R_{i2} R_{i3} m_i^2 \right) + \frac{s_\beta^2}{v^2 s_\beta^2 c_\beta^2 + v_S^2} m_A^2 \right\} \quad (2.48)$$

$$\xi = \frac{\sqrt{2} s_\beta c_\beta v_S}{v^2 s_\beta^2 c_\beta^2 + v_S^2} m_A^2 \quad (2.49)$$

The vacuum expectation values v and v_S can be further expressed as a function of other SM parameters, as well as the Z' mass $m_{Z'}$ and the $U(1)_X$ coupling constant g'_1 , as discussed

section 2.3.2.

2.3.2 Gauge Mass Eigenstates

The kinetic term in Equation 2.23 after SSB also yields mixed gauge terms to which a diagonalization procedure can be applied. After expansion of $\mathcal{L}_{H,\text{kin}}$ and identifying all bilinear terms, we obtain the mass matrices \mathcal{M}_\pm^2 and \mathcal{M}_0^2 in basis $\{W_1, W_2\}$ and $\{B, W_3, B'\}$, respectively

$$\mathcal{M}_\pm^2 = \frac{1}{4} \begin{pmatrix} g^2 v^2 & 0 \\ 0 & g^2 v^2 \end{pmatrix}, \quad \mathcal{M}_0^2 = \frac{1}{4} \begin{pmatrix} g_1^2 v^2 & -g_1 g v^2 & -2g_1 g'_1 v^2 s_\beta^2 \\ -g_1 g v^2 & g^2 v^2 & 2g g'_1 v^2 s_\beta^2 \\ -2g_1 g'_1 v^2 s_\beta^2 & 2g g'_1 v^2 s_\beta^2 & 4g'_1{}^2 (v^2 s_\beta^2 + v_S^2) \end{pmatrix} \quad (2.50)$$

from which we can directly infer physical W boson mass

$$m_W = \frac{gv}{2} \quad (2.51)$$

The diagonalization of matrix \mathcal{M}_0^2 is done in two steps. First we rotate the neutral basis by the Weinberg angle $\tan \theta_w = \frac{g_1}{g}$:

$$\begin{pmatrix} \tilde{B} \\ \tilde{W}^3 \\ B' \end{pmatrix} = \begin{pmatrix} c_w & s_w & 0 \\ -s_w & c_w & 0 \\ 0 & 0 & 1 \end{pmatrix} \begin{pmatrix} B \\ W^3 \\ B' \end{pmatrix} =: V_w^\dagger \begin{pmatrix} B \\ W^3 \\ B' \end{pmatrix} \quad (2.52)$$

where $s_w := \sin \theta_w$ and $c_w := \cos \theta_w$, and express the squared mass matrix in the rotated basis:

$$\widetilde{\mathcal{M}}_0^2 = \frac{1}{4} \begin{pmatrix} 0 & 0 & 0 \\ 0 & (g^2 + g_1^2) v^2 & 2\sqrt{g^2 + g_1^2} g'_1 v^2 s_\beta^2 \\ 0 & 2\sqrt{g^2 + g_1^2} g'_1 v^2 s_\beta^2 & 4g'_1{}^2 (v^2 s_\beta^2 + v_S^2) \end{pmatrix} \quad (2.53)$$

We identify the rotated field \tilde{B} as the physical massless photon A . We further diagonalize $\widetilde{\mathcal{M}}_0^2$ with another rotation by angle θ_z :

$$\begin{pmatrix} A \\ Z \\ Z' \end{pmatrix} = \begin{pmatrix} 1 & 0 & 0 \\ 0 & c_z & s_z \\ 0 & -s_z & c_z \end{pmatrix} \begin{pmatrix} \tilde{B} \\ \tilde{W}^3 \\ B' \end{pmatrix} =: V_z^\dagger \begin{pmatrix} \tilde{B} \\ \tilde{W}^3 \\ B' \end{pmatrix} \quad (2.54)$$

where again $s_z := \sin \theta_z$ and $c_z := \cos \theta_z$. The diagonalized matrix is then:

$$\widehat{\mathcal{M}}_0^2 = \begin{pmatrix} 0 & & \\ & m_Z^2 & \\ & & m_{Z'}^2 \end{pmatrix} = V_z^\dagger V_w^\dagger \mathcal{M}_0^2 V_w V_z =: V_0^\dagger \mathcal{M}_0^2 V_0 \quad (2.55)$$

with complete basis transformation matrix:

$$V_0 = \begin{pmatrix} c_w & -s_w c_z & s_w s_z \\ s_w & c_w c_z & c_w s_z \\ 0 & s_z & c_z \end{pmatrix} \quad (2.56)$$

and relations

$$m_Z^2 = \frac{1}{8} \left\{ (g^2 + g_1^2) v^2 + 4g_1'^2 (v^2 s_\beta^2 + v_S^2) - \sqrt{\left((g^2 + g_1^2) v^2 - 4g_1'^2 (v^2 s_\beta^2 + v_S^2) \right)^2 + 8 (g^2 + g_1^2) g_1'^2 v^4 s_\beta^4} \right\} \quad (2.57)$$

$$m_{Z'}^2 = \frac{1}{8} \left\{ (g^2 + g_1^2) v^2 + 4g_1'^2 (v^2 s_\beta^2 + v_S^2) + \sqrt{\left((g^2 + g_1^2) v^2 - 4g_1'^2 (v^2 s_\beta^2 + v_S^2) \right)^2 + 8 (g^2 + g_1^2) g_1'^2 v^4 s_\beta^4} \right\} \quad (2.58)$$

Independent Parameters

We set the physical masses m_Z and $m_{Z'}$ as independent parameters, and express the newly introduced parameters g'_1 and v_S , as well as the second rotation angle θ_z as a function the masses and parameters g , g_1 , v , s_β . Assuming the condition $4m_{Z'}^2 > (g^2 + g_1^2) v^2 > 4m_Z^2$, which agrees with decay chains of Z' to Z , we obtain the relations

$$g'_1 = \frac{\sqrt{(g^2 + g_1^2) v^2 - 4m_Z^2} \sqrt{4m_{Z'}^2 - (g^2 + g_1^2) v^2}}{2\sqrt{g^2 + g_1^2} v^2 s_\beta^2} \quad (2.59)$$

$$v_S = \frac{v s_\beta \sqrt{(g^2 + g_1^2) v^2 s_\beta^2 (4(m_Z^2 + m_{Z'}^2) - (g^2 + g_1^2) v^2) - ((g^2 + g_1^2) v^2 - 4m_Z^2) (4m_{Z'}^2 - (g^2 + g_1^2) v^2)}}{\sqrt{((g^2 + g_1^2) v^2 - 4m_Z^2) (4m_{Z'}^2 - (g^2 + g_1^2) v^2)}} \quad (2.60)$$

In order to satisfy $(g^2 + g_1^2) v^2 > 4m_Z^2$ we propose the following parameter choice: (1) keep the values of the $U(1)_Y$ and $SU(2)_L$ coupling constants g_1 and g equal to the SM values;

(2) marginally increase the Higgs expectation value $v = v_{\text{SM}} + \delta$, where v_{SM} is the SM Higgs expectation value and $\delta \ll 1 \text{ GeV}$, such that the W boson mass m_W in Equation 2.51 agrees with the SM value within uncertainty.

The rotation angle θ_z is given by

$$\tan \theta_z = \frac{4\sqrt{g^2 + g_1'^2} g_1' v^2 s_\beta^2}{4g_1'^2(v_S^2 + v^2 s_\beta^2) - (g^2 + g_1^2)v^2 + \sqrt{(4g_1'^2(v_S^2 + v^2 s_\beta^2) - (g^2 + g_1^2)v^2)^2 - 16(g^2 + g_1^2)g_1'^2 v^4 s_\beta^4}} \quad (2.61)$$

Since the doublet mixing angle β is expected to be small, we can approximate for computation purposes $s_\beta^2 \approx 0$, yielding

$$\widehat{\mathcal{M}}_0^2 = \widetilde{\mathcal{M}}_0^2 = \begin{pmatrix} 0 & 0 & 0 \\ 0 & (g^2 + g_1^2)v^2 & 0 \\ 0 & 0 & 4g_1'^2(v^2 s_\beta^2 + v_S^2) \end{pmatrix} \quad (2.62)$$

which, together with Equation 2.51, gives the SM relation

$$m_Z = \sqrt{g^2 + g_1^2} v \quad (2.63)$$

as well as the equations

$$m_{Z'} = 2g_1' \sqrt{v^2 s_\beta^2 + v_S^2} \quad (2.64)$$

$$\theta_z = 0 \quad (2.65)$$

We hence fix g , g_1 and v to SM values, are agreement with Equations 2.51 and 2.63, and set $g_1' = 0.2$. The remaining degree of freedom is contained in $m_{Z'}$, and we use Equation 2.64 to determine the vacuum expectation value v_S .

2.4 Signal Processes and Parameter Choice

To help explain the excesses seen in [1], two distinct groups of processes are considered within the $2HDM S+Z'+N$ scenario, each one involving different parameter choices. Since the gluon fusion excess found in section 5.1 of [1] arises from a Higgs mediated interaction with two opposite-sign, different flavour (OSDF) leptons and no jets, we consider as signal hypothesis the heavy scalar scalar production $pp \rightarrow H$, with subsequent decays $H \rightarrow \bar{N}_i \nu_i$ and $H \rightarrow N_i \bar{\nu}_i$, as shown in Figure 2.1. The two OSDF lepton are then observed with the following decay chains $N_i \rightarrow W^+ \ell_i^-$, $W^+ \rightarrow \ell_i^- \bar{\nu}_i$ and $\bar{N}_i \rightarrow W^- \ell_i^+$, $W^- \rightarrow \ell_i^+ \nu_i$ where ℓ_i^- (ℓ_i^+) are charged (anti-)leptons. We label these processes as $N\nu$.

The anomaly originating from Z mediated Z -Higgs production in section 7.3 of [1] involves

three final charged leptons with total charge ± 1 and two jets. One dilepton pair originates from a Z boson, whereas the remaining lepton and the two jets arise from W decays. Such final states can be reproduced by a Z' mediated production of heavy neutrino pairs $N_i \bar{N}_i$, as depicted in Figure 2.1. The heavy neutrinos subsequently decay to W and Z bosons, which further decay to quarks and leptons. We refer to this group of processes by NN .

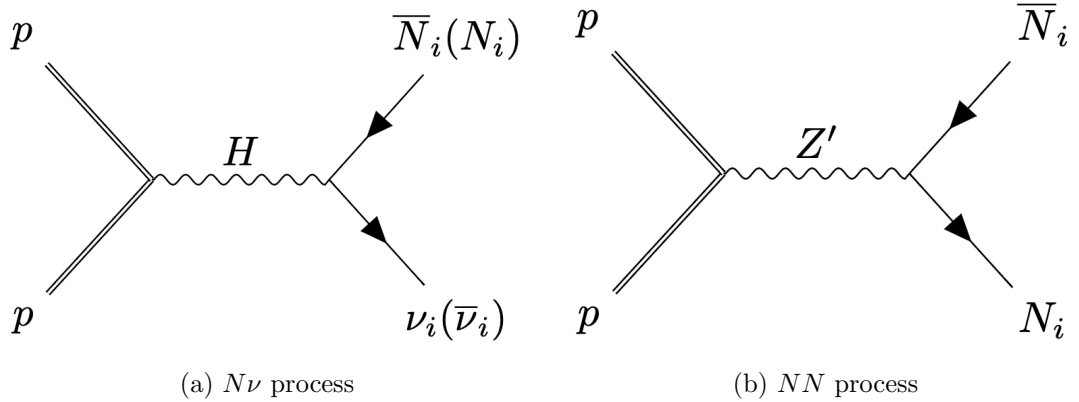


Figure 2.1: Feynman diagrams for signal processes

Each of the two aforementioned process types involves distinct parameter constraints. For the scalar mediated processes, we require the condition $m_H > m_N > m_W$, whereas for the Z' mediated interaction, we have $m_{Z'} > 2m_N > 2m_Z$. We further avoid CP-even scalar mixing and fix $\omega_1 = \omega_2 = \omega_3 = 0$, which prevents heavy neutrinos from decaying to the SM Higgs and maximizes the presence of W and Z mediated decays. In order to avoid additional BSM interactions, we set the masses of other BSM particles not present in NN or $N\nu$ processes to very high values. For both cases, we fix the neutrino and scalar doublet mixing angles to $\alpha_i = 0.1$ and $\beta = 0.1$, and set the $U(1)_X$ coupling constant to $g'_1 = 0.2$, as discussed in section 2.3.2. Table 2.2 summarizes the parameter choice for each BSM scenario, and also displays the investigated scalar, Z' and heavy neutrino mass ranges.

Parameter	Value for NN	Value for $N\nu$
g'_1		0.2
β		0.1
$\alpha_1, \alpha_2, \alpha_3$		0.1
$\omega_1, \omega_2, \omega_3$		0
m_H	$\{100, 120, 140, 160, 180, 200, 210\}$ GeV	20 TeV
$m_{Z'}$	20 TeV	$\{300, 350, 400, 450, 500, 550, 600, 650, 700, 750, 800, 850, 900, 1000, 1100\}$ GeV
m_N	$\{90, 100, 110, 130, 150, 170, 180\}$ GeV	$\{100, 150, 200, 250, 300, 350, 400, 500\}$ GeV
m_+, m_A, m_S		20 TeV

Table 2.2: Parameter values for processes $N\nu$ and NN .

2.5 Decay Widths

We provide a list of relevant decay widths for the $2HDM + Z' + N$ model as a function of independent parameters mentioned in sections 2.2 and 2.3. Since the signal processes mentioned in section 2.4 involve the Z' boson, H scalar and N_i neutrinos, we give analytical expressions for their decay widths in the following subsections. Such formulas are useful to compute corresponding branching ratios and cross-sections. Detailed calculations for the decay widths can be found in Appendix B.

Only dominant 2-body decays without mediating particles are considered, and we do not include interactions involving the charged and CP-odd scalars H^+ and A_S , as they are not considered in this study. We further ignore Z' and scalar decays to quarks, since this is experimentally forbidden for masses up to ~ 4 TeV according to several searches done at LEP and LHC [54]. This poses a weakness in our model, since these decays should occur for highly energetic Z' and H . Nonetheless, such decay channels can be easily avoided by introducing heavy quarks as mediators between SM quarks and BSM particles.

2.5.1 N_i Decay

The BSM neutrinos N_i can decay to electroweak bosons and scalars accompanied by leptons. Decays to Z' are not considered because in the studied scenarios we always have $m_N < m_{Z'}$. Decay widths to electroweak bosons Z and W^\pm , charged (anti-)leptons $\ell_i^- (\ell_i^+)$ and SM neutrinos ν_i are:

$$\Gamma_{N_i \rightarrow W^+ \ell_i^-} = \Gamma_{\bar{N}_i \rightarrow W^- \ell_i^+} = \frac{e^2 s_i^2}{64\pi m_N^3 m_Z^2 s_w^2} (m_N^2 (m_N^2 + m_Z^2) - 2m_Z^4) (m_N^2 - m_Z^2) \quad (2.66)$$

$$\Gamma_{N_i \rightarrow Z \nu_i} = \Gamma_{\bar{N}_i \rightarrow Z \bar{\nu}_i} = \frac{e^2 s_i^2 c_i^2}{128\pi m_N^3 m_W^2 s_w^2 c_w^2} (m_N^2 (m_N^2 + m_W^2) - 2m_W^4) (m_N^2 - m_W^2) \quad (2.67)$$

where $s_i = \sin \alpha_i$ and $c_i = \cos \alpha_i$ as defined in section 2.2.1, and e is the elementary charge.

Decay widths to scalars $\{h_1, h_2, h_3\} := \{H, h, S\}$, provided that $m_N > m_{h_k}$, are

$$\Gamma_{N \rightarrow h_k \nu_j} = \Gamma_{\bar{N}_i \rightarrow h_k \bar{\nu}_j} = \frac{s_j^2 c_j^2}{32\pi m_N v^2 s_\beta^2} |(V_\varphi)_{k1}|^2 (m_N^2 - m_{h_k}^2)^2 \quad (2.68)$$

where V_φ is the transformation matrix for real CP-even fields defined in section 2.3.1.

2.5.2 Z' Decay

The Z' boson decays to neutrinos with three possible final arrangements: two BSM neutrinos ($N_i \bar{N}_i$), one BSM and one SM neutrino ($N_i \bar{\nu}_i$) or ($\nu_i \bar{N}_i$), and two SM neutrinos ($\nu_i \bar{\nu}_i$). The respective decay widths are:

$$\Gamma_{Z' \rightarrow N_i \bar{N}_i} = g_1'^2 \frac{\sqrt{m_{Z'}^2 - 4m_N^2}}{4\pi m_{Z'}^2} \left[\frac{1}{6}(1 + c_i^4)(m_{Z'}^2 - m_N^2) + c_i^2 m_N^2 \right] \quad (2.69)$$

$$\Gamma_{Z' \rightarrow \nu_i \bar{N}_i} = \Gamma_{Z' \rightarrow N_i \bar{\nu}_i} = g_1'^2 \frac{s_i^2 c_i^2}{48\pi m_{Z'}^5} (2m_{Z'}^4 - m_N^2(m_{Z'}^2 + m_N^2)) (m_{Z'}^2 - m_N^2) \quad (2.70)$$

$$\Gamma_{Z' \rightarrow \nu_i \bar{\nu}_i} = g_1'^2 \frac{s_i^4 m_{Z'}}{24\pi} \quad (2.71)$$

where again $s_i = \sin \alpha_i$ and $c_i = \cos \alpha_i$ as in section 2.2.1.

2.5.3 Scalar Decay

We consider the decay of CP-even scalars $\{h_1, h_2, h_3\} = \{H, h, S\}$ to leptons. The finite decay widths are:

$$\Gamma_{h_k \rightarrow N_i \bar{N}_i} = \frac{s_i^4 m_N^2}{8\pi m_{h_k}^2 v^2 s_\beta^2} (m_{h_k}^2 - 4m_N^2)^{\frac{3}{2}} |V_{\varphi 1k}|^2 \quad (2.72)$$

$$\Gamma_{h_k \rightarrow N_i \bar{\nu}_i} = \frac{s_i^2 c_i^2 m_N^2}{16\pi m_{h_k}^3 v^2 s_\beta^2} (m_{h_k}^2 - m_N^2)^2 |V_{\varphi 1k}|^2 \quad (2.73)$$

$$\Gamma_{h_k \rightarrow \ell_i^- \ell_i^+} = \frac{1}{16\pi m_{h_k}^2} (m_{h_k}^2 - 4m_{\ell_i}^2)^{\frac{3}{2}} |Y_{ii}^l|^2 |V_{\varphi 2k}|^2 \quad (2.74)$$

where V_φ is again the transformation matrix from section 2.3.1, and $\ell_i^- (\ell_i^+)$ is a charged (anti-)lepton of mass m_{ℓ_i} .

Chapter 3

Simulation and Analysis

We describe the methodology used for the sample generation and processing, as well as for the statistical analysis. Events were generated using a fast track algorithm, followed by a series of object and event selection criteria. A smearing procedure was subsequently implemented to reduce discrepancies between fast and full MC generations. At last, we used two distinct statistical procedures to extract a significance level and cross-section for both the NN and $N\nu$ processes.

3.1 Event Generation

The $2HDMs+Z'+N$ model was implemented with the `FeynRules` package [67] (see Appendix C), which was then interfaced with `MadGraph5` [68] version 2.7.3 to generate MC pp collision events with a center-of-mass energy of 13 TeV. The parton shower and hadronization stages were simulated with `Pythia8` [69] and the detector response and reconstruction was implemented with `Delphes` [70] version 3.5. For the $N\nu$ processes with $m_N < 100$ GeV we generated 1M events due to small efficiencies, whereas for all other processes we generated 500k events. Tables showing the efficiencies corresponding to each mass combination are found in Appendix F.

To minimize computation efforts, we only generated processes at tree level. Moreover, the event selection criteria are flavour independent, which means that including only one neutrino generation suffices to evaluate the significance level of the signal hypothesis. Therefore, we only simulated H and Z' decays to electron neutrinos ν_e and first generation heavy neutrinos N_1 .

The production mode $pp \rightarrow H$ is possible via a top-loop mediated gluon fusion. Since we only simulate tree-level interactions, we account for the ggH vertex by adding an effective

Lagrangian term

$$\mathcal{L}_{gg\Phi_2} = -\frac{1}{4}c_H G_a^{\mu\nu} G_{a,\mu\nu} H - \frac{1}{4}c_h G_a^{\mu\nu} G_{a,\mu\nu} h \quad (3.1)$$

where

$$c_H = -\frac{\alpha_s}{2\pi v c_\beta} (V_\varphi)_{21} F\left(\frac{4m_t^2}{m_H^2}\right) \quad (3.2)$$

$$c_h = -\frac{\alpha_s}{2\pi v c_\beta} (V_\varphi)_{22} F\left(\frac{4m_t^2}{m_h^2}\right) \quad (3.3)$$

with

$$F(r) = r \left(1 + (1-r) \left(\arcsin \frac{1}{\sqrt{r}} \right)^2 \right) \quad (3.4)$$

as described in [71]. For the implementation with the **FeynRules** package, we expand Equations 3.2 and 3.3 to the third order in $\left(\frac{m_H}{2m_t}\right)^2$ and $\left(\frac{m_h}{2m_t}\right)^2$, respectively:

$$c_H = -\frac{g_s}{12\pi^2 v c_\beta} (V_\varphi)_{21} \text{sert} \left[\left(\frac{m_H}{2m_t} \right)^2 \right] \quad (3.5)$$

$$c_h = -\frac{g_s}{12\pi^2 v c_\beta} (V_\varphi)_{21} \text{sert} \left[\left(\frac{m_h}{2m_t} \right)^2 \right] \quad (3.6)$$

with

$$\text{sert}[x] = 1 + \frac{7}{30}x + \frac{2}{21}x^2 + \frac{26}{525}x^3 \quad (3.7)$$

3.2 Object Reconstruction and Event Selection

After implementing the MC simulations, a series of object and event selection criteria was applied to the generated samples. Such criteria intend to reject misidentified particles and isolate the SM signal processes involving Higgs decays to two W bosons for both the gluon fusion and the Z-Higgs production in [1]. Among the final objects are electrons, muons, jets and missing momentum P^{miss} , which are all reconstructed by the **Delphes3** modular framework. The subsequent sample processing was implemented within the **ROOT** [72] framework. Both electrons and muons were additionally required to have transverse momentum $p_T > 10$ GeV, as well as pseudorapidity $|\eta| < 2.5$ and $|\eta| < 2.4$, respectively, whereas jets are required to fulfill $p_T > 20$ GeV and $|\eta| < 4.7$. Selected jets with $p_T > 30$ GeV are labeled as signal jets.

In order to further reduce the number of misidentified objects, an overlap removal procedure was applied to jets and leptons. Such procedures have shown to efficiently reduce ambiguities arising from independent particle reconstruction algorithms [73]. Electrons were removed if they located within a distance of $\Delta R := \sqrt{(\Delta\phi)^2 + (\Delta\eta)^2} = 0.2, 0.3$ or 0.4 of a p_T leading electron, p_T leading muon or b-tagged jet, respectively. Similarly, muons within a distance

$\Delta R = 0.3$, 0.3 or 0.4 of a higher p_T muon, higher p_T electron or b-tagged jet, respectively, were rejected. After lepton removal, we further non b-tagged jets which were within a radius of $\Delta R = 0.2$ from electrons or muons.

After object reconstruction and selection, several conditions were imposed on sample events. Such criteria were elaborated to select for the SM signal processes $pp \rightarrow h \rightarrow WW$ and $pp \rightarrow Z \rightarrow Zh, h \rightarrow WW$ in the anomalous gluon fusion and Z-Higgs categories in [1], and were applied to $N\nu$ and NN events, respectively. For the gluon fusion category, events were required to have exactly two OSDF leptons with $p_T > 25$ (> 13) GeV for the (sub)leading lepton. Moreover, for the dilepton system $\ell\ell$, the lepton invariant mass $m_{\ell\ell}$ and transverse momentum $p_{T,\ell\ell}$ were required to exceed 12 GeV and 30 GeV, respectively, and a lower bound of 12 GeV was imposed in the missing momentum p_T^{miss} . Events were further rejected if they had at least one b-tagged or signal jet. Defining the transverse mass variable for a group of objects $\{S_i\}$ with transverse momenta $\{\vec{p}_{T,i}\}$

$$m_T(\{S_i\}) = \sqrt{\left(\sum_i |\vec{p}_{T,i}| \right)^2 - \left| \sum_i \vec{p}_{T,i} \right|^2} \quad (3.8)$$

we further imposed the constraints $m_T(\{\ell_2, P^{\text{miss}}\}) > 30$ GeV and $m_T^H := m_T(\{\ell\ell, P^{\text{miss}}\}) > 60$ GeV on sample events, where ℓ_2 is the subleading lepton and m_T^H is referred to as the *Higgs transverse mass*. Events were subsequently categorized into those with $p_{T,2} \gtrless 20$ GeV, where $p_{T,2}$ is the transverse momentum of the subleading lepton.

For the Z -Higgs category, events were required to have 3 final leptons with charge ± 1 , as well as one opposite-sign, same flavour (OSSF) lepton pair $\ell_Z\ell_Z$ with invariant mass fulfilling $|m_{\ell_Z\ell_Z} - m_Z| < 25$ GeV. The remaining lepton decaying from the W boson is labeled as ℓ_W . Events with three final electrons or muons with two OSSF lepton pairs $\ell_i\ell_i$ fulfilling the mentioned constraint on the invariant mass result in an ambiguous definition for the lepton ℓ_W . In such cases, the lepton ℓ_W was taken as the one which did not minimize $|m_{\ell_i\ell_i} - m_Z|$. The transverse momenta of the leading, subleading and subsubleading leptons were required to exceed 25 GeV, 20 GeV and 15 GeV, respectively. For invariant masses $m_{\ell\ell}$ for any of the three possible dilepton systems $\ell\ell$ and for the 3-lepton system m_{3l} were constrained with $m_{\ell\ell} > 12$ GeV and $m_{3l} > 20$ GeV. Events were further required to have no b-tagged jets, and were categorized into those containing exactly one or at least two signal jets. The azimuthal angle separation $\Delta\phi$ between the $\ell_W + P^{\text{miss}}$ system and the (two p_T leading) signal jet system was required to fulfill $|\Delta\phi| < \pi/2$ for the 1-jet (2-jet) category.

After event selection, we constructed histograms in terms of the *Higgs transverse mass* m_T^H for each of the mentioned categories, which correspond to the plots containing excesses in [1]. The *Higgs transverse mass* is defined as $m_T^H := m_T(\{\ell\ell, P^{\text{miss}}\})$ for the gluon-fusion

category, and as $m_T^H := m_T(\{\ell_W, P^{\text{miss}}, j_1, j_2\})$ for the 1-jet (2-jet) Z -Higgs category (j_1 and j_2 symbolizing the leading and subleading signal jet). For $N\nu$ samples with $p_{T,2} < 20$ GeV and $p_{T,2} > 20$ GeV, bin edges were set to $[60, 80, 90, 110, 130, 150, 200]$ GeV and $[60, 80, 90, 100, 110, 120, 130, 150, 200]$ GeV, whereas for the NN samples with 1 jet and at least 2 jets, the bin edges were set from 0 to 250 GeV and 50 to 250 GeV with bin size 25 GeV, respectively. The overflow events were added to the last bin for all histograms. Figure 3.1 shows the histograms found in [1] for both the gluon fusion and Z -Higgs production categories which were used in this work.

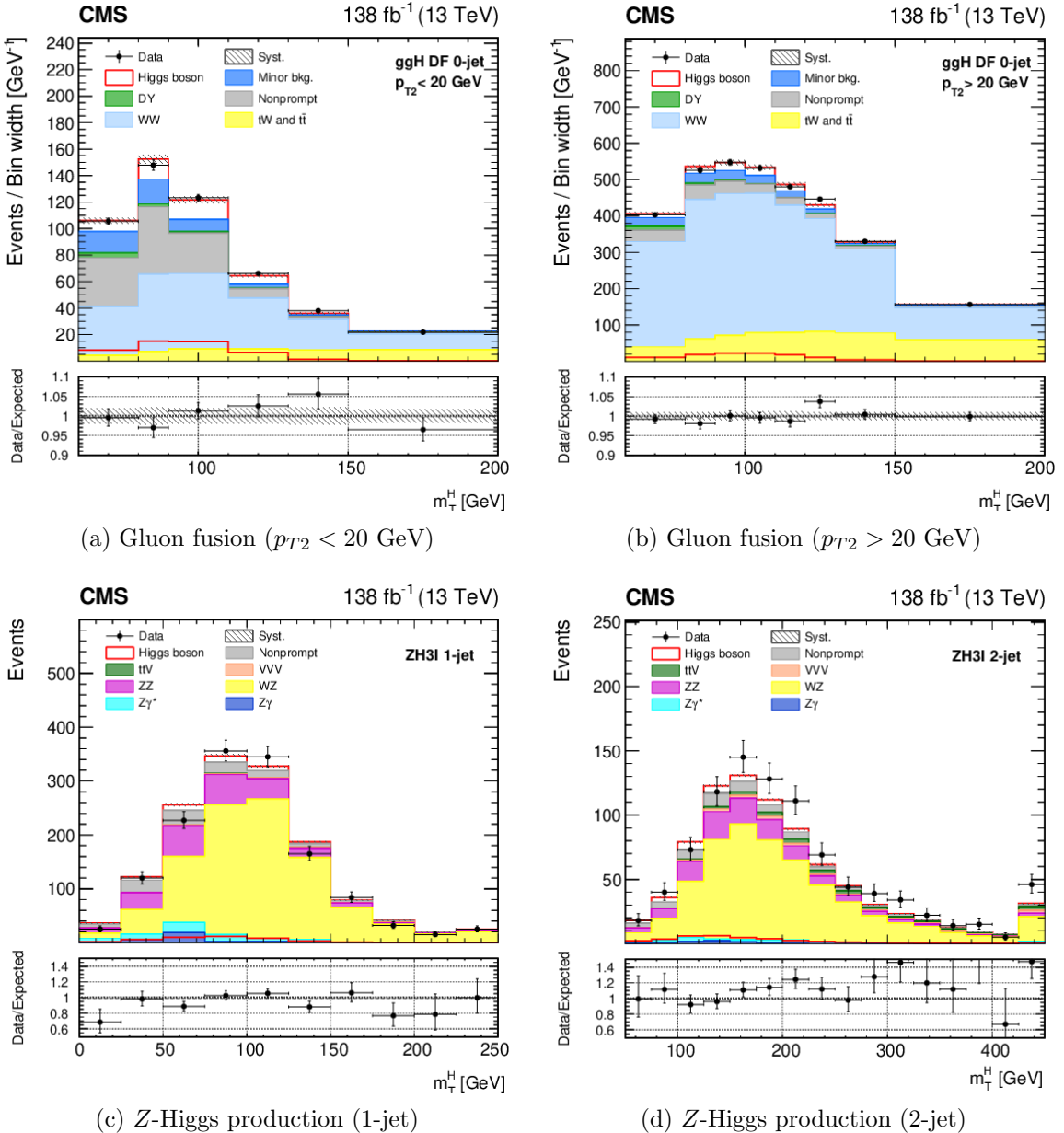


Figure 3.1: Histograms found in [1] for the gluon fusion and Z -Higgs production categories

3.3 Smearing and Shifting

The framework **Delphes** efficiently simulates the detector response and reconstructs final state objects based on parametric algorithms [70]. Despite being faster than the framework **GEANT4** [74] used at CMS searches, it is based on simplified models and assumptions to increase computation efficiency, leading to inaccuracies in jet and missing momentum reconstruction. To compensate for discrepancies seen between **Delphes** and the CMS generations, we intentionally decreased the resolution of the soft missing energy – reconstructed only with leptons – and jets in a procedure known as smearing. We additionally shifted the generated histograms by a factor s to optimally approach the CMS simulation.

The soft missing momentum $P_{\text{soft}}^{\text{miss}} = (E^s, p_x^s, p_y^s, p_z^s)$ only includes final leptons in its reconstruction, for which we have the relation

$$P_{\text{soft}}^{\text{miss}} = P^{\text{miss}} + \sum_i P_i^{\text{jet}} \quad (3.9)$$

where P_i^j is the 4-momentum for jet i , and the sum symbol indicates a sum of 3-momenta while maintaining the energy-momentum relation. The soft missing momentum was smeared by adding a random factor to its transverse components while keeping the longitudinal component p_z^s constant:

$$p_x^s \rightarrow p_x^s + \text{Rand}[0, K] \cdot \cos(\text{Rand}[0, 2\pi]) \cdot \text{GeV} \quad (3.10)$$

$$p_y^s \rightarrow p_y^s + \text{Rand}[0, K] \cdot \sin(\text{Rand}[0, 2\pi]) \cdot \text{GeV} \quad (3.11)$$

where $\text{Rand}[0, x]$ is uniformly distributed between 0 and x , and $[K] = 1$. The smearing on jets was done by adding a factor to their energy E_j , while maintaining the vectorial orientation:

$$E_j \rightarrow E_j + \sqrt{E_j} \cdot \text{Gauss}(0, \sigma) \cdot \sqrt{\text{GeV}} \quad (3.12)$$

where $\text{Gauss}(0, \sigma)$ is normally distributed around 0 with standard deviation σ , and $[\sigma] = 1$. All randomly distributed values were generated using the **TRandom2** class from the **ROOT** library. In case of the **Delphes** distributions not adequately resembling the **GEANT4** data after smearing, we additionally considered shifting the histograms by adding a factor s to the *Higgs transverse mass* variable

$$m_T^H \rightarrow m_T^H + s \quad (3.13)$$

where $[s] = \text{GeV}$.

Values for K , σ and s were estimated by comparing the histograms obtained with the fast and full simulations. After generating events for the SM signal processes in [1], we applied the smearing and shifting procedures together with the event selection criteria, and generated

the corresponding distributions. Defining $N_{\text{MG},i}$ and $N_{\text{lit},i}$ as the number of events for bin i in the generated and CMS simulation histograms, we measured the distance Δ_h between both distributions with:

$$\Delta_h = \sum_i \left(\frac{N_{\text{MG},i}}{N_{\text{MG,tot}}} - \frac{N_{\text{lit},i}}{N_{\text{lit,tot}}} \right)^2 \quad (3.14)$$

where $N_{\text{MG,tot}}$ and $N_{\text{lit,tot}}$ are the corresponding total number of events. The smearing and shifting parameters were adjusted such that Δ_h is minimized.

The earlier study [13] on the gluon fusion process in [1] had found that value $K = 30$ and $s = 0$ GeV minimize Δ_h for both subcategories with $p_{T,2} \gtrless 20$. For the Z -Higgs category, we fixed $K = 30$ and varied σ and s over a chosen range to identify the optimal values. Figure 3.2 shows a 2-dimensional scan of Δ_h over the parameter space (σ, s) .

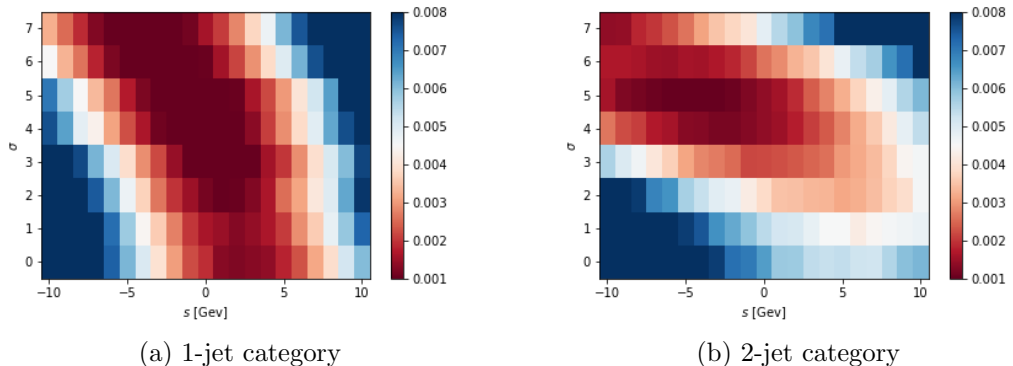
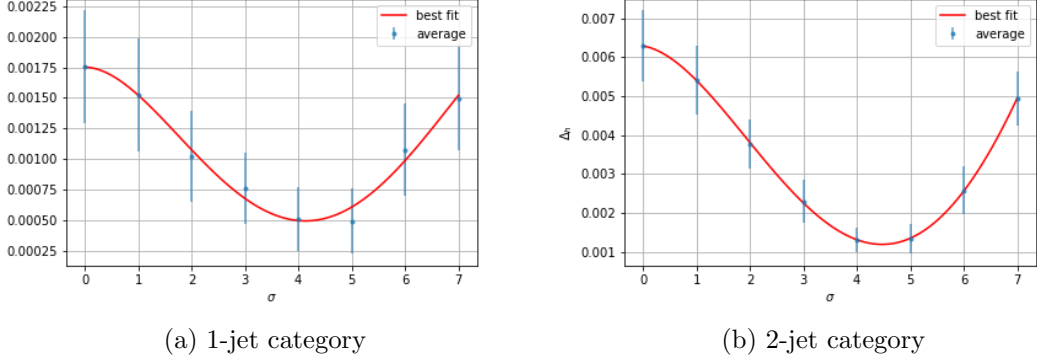


Figure 3.2: Computed averages for Δ_h over 50 iterations as a function of parameters σ and s with fixed $K = 30$ for both 1-jet (a) and 2-jet (b) categories

We see that low values of Δ_h are achieved with some jet smearing and a negative shift of the m_T^H variable. However, we notice that the negative shift has a relatively low impact on Δ_h , and including a mass shift on the BSM results would involve a more careful analysis. For these reasons, we decided not to include any shifting and hence keep $s = 0$ GeV. To better estimate the σ value, we plotted the Δ_h values as a function of the jet smearing parameter, as shown in Figure 3.3.

After performing a polynomial fit on the average Δ_h values, we notice that, within unitary precision, a jet smearing parameter of $\sigma = 4$ minimizes Δ_h for both the 1-jet and 2-jet categories. The corresponding fast simulation histograms with and without jet and soft missing momenta smearing are shown in Figure 3.4 together with literature distributions.



(a) 1-jet category

(b) 2-jet category

Figure 3.3: Computed average and standard deviation for Δ_h over 50 iterations as a function of parameter σ with fixed $K = 30$ and no shifting for both 1-jet (a) and 2-jet (b) categories

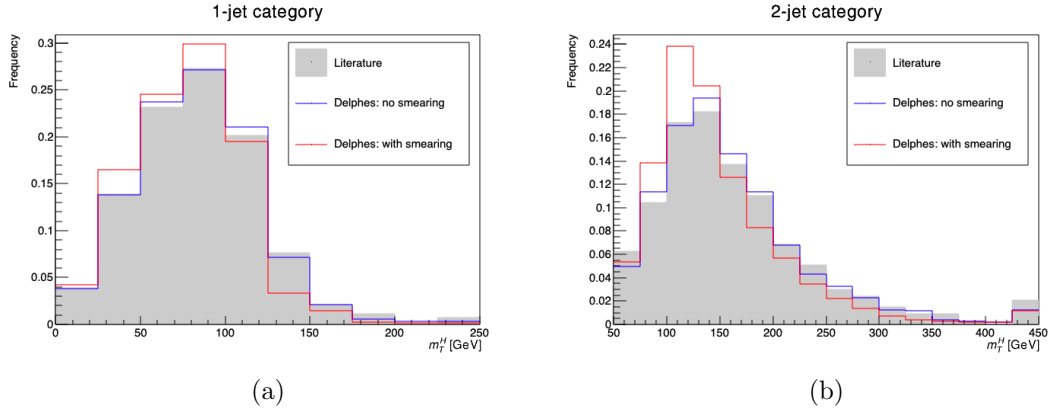


Figure 3.4: Normalized histograms for the Z -Higgs category found in literature [1] and obtained with the **Delphes** framework with and without the smearing procedure for $8 \cdot 10^6$ events

3.4 Statistical Formalism¹

The statistical framework used in this project is based on the concept of hypothesis testing. In the context of particle physics, one typically has a signal hypothesis H_S postulating the existence of unobserved phenomena, as well as a background hypothesis H_B where these phenomena are absent, taking only known physics into account. In our case, the signal hypothesis corresponds to the scalar and Z' mediated neutrino productions in addition to SM processes, whereas the background hypothesis only considers SM interactions. After experimental data \vec{x} has been collected, one can compute a so called test statistics $t = t(\vec{x})$, which obeys a distribution $g(t|H_i)$ under assumption of hypothesis H_i . Given the computed

¹The content found in this section is based on reference [75]

test statistics \tilde{t} and hypothesis H_i , the associated p-value is

$$p = \int_{\tilde{t}}^{\infty} g(t|H_i) dt \quad (3.15)$$

which corresponds to probability of obtaining results that are equally or less compatible with hypothesis H_i than the measured data \vec{x} . The smaller the p-value, the less likely it is for the data \vec{x} to be described by hypothesis H_i . Note that Equation 3.15 is valid for a one-sided test statistics; for a two-sided one should integrate over range $t > |\tilde{t}|$.

Test statistics used in particle physics are usually constructed in such a way that they take both the signal and background predictions into account and are often computed by fitting these predictions to experimental results. Popular choices are χ^2 differences and likelihood ratios, the latter due to the Neyman-Pearson lemma. One then evaluates the p-value assuming the background hypothesis as true, which may be rejected against the signal hypothesis for sufficiently small p-values. Instead of the p-value one often reports a significance Z , typically given in terms of the number of standard deviations σ the test statistics \tilde{t} is away from its expectation value. By using asymptotic formulas, one can approximate $Z \approx \sqrt{\tilde{t}}$ for a likelihood ratio derived test statistics and large enough sample sizes. A lower threshold of $Z = 5\sigma$ is the currently accepted value to claim a new discovery, which corresponds to a p-value of $p \approx 2.87 \cdot 10^{-7}$.

In this project, we first performed a normalization fit of the signal and background m_T^H distributions to the experimental plots found in [1] and then extracted the corresponding test statistics and significance level from it. The signal distributions correspond to the BSM plus SM histograms, whereas the background distributions are composed of SM-only data. We used two distinct fitting methods: χ^2 minimization and likelihood maximization. The fitting parameters correspond to the BSM and SM histogram normalization factors μ_{BSM} and $\mu_{\text{SM}}^{(k)}$ in the signal scenario, and the SM normalization factor $\tilde{\mu}_{\text{SM}}^{(k)}$ in the background scenario, where k denotes the histogram for a given subcategory. This means that a different SM parameter was fitted for each subcategory, whereas a common parameter was BSM parameter fitted for all histograms corresponding to a certain process. The minimization was implemented with the `MIGRAD` algorithm found within the `TMinuit2` class of the `ROOT` library.

For the SM and experimental data we used the values found in [1], which were digitalized with the platform `PlotDigitizer` [76]. Numerical values obtained after digitalization are found in Appendix D. Before conducting the fit, we rescaled the BSM histogram entries with factor

$$R = \frac{1}{N_{\text{tot}}^{\text{BSM}}} Lr \quad (3.16)$$

where $L = 138 \text{ fb}^{-1}$ is the luminosity corresponding to the collected LHC data and $N_{\text{tot}}^{\text{MG}}$ is

the total number of BSM events generated. We have also included the efficiency ratio

$$r = \frac{\varepsilon_{\text{lit}}}{\varepsilon_{\text{MG}}} \quad (3.17)$$

where ε_{lit} and ε_{MG} are the event selection efficiencies found in literature [1] and obtained with the `MadGraph5` library after the smearing procedure, respectively, for the corresponding SM signal process. The efficiency ratio corrects for further inaccuracies during object reconstruction and event selection. The previous study done on the gluon fusion data has found an efficiency ratio of $r \approx 0.012/0.032$ [13] for this process type, whereas for the Z -Higgs category, we have obtained an efficiency ratio of $r \approx 0.00061/0.00039$. After rescaling BSM events, the fitting is done directly on the BSM signal cross-section σ_{BSM} , now being equal to the normalization parameter μ_{BSM} .

The two distinct fitting methods were chosen because, while the χ^2 allows to include bin-to-bin correlations arising from systematic errors, the likelihood function performs better in the low-statistics limit [75]. After the fit, the significance level of the BSM signal against the SM background hypothesis was extracted by computing two different test statistics for each fitting method: χ^2 difference and likelihood ratio. In the following subsections, we explain each of the methods used for the statistical analysis. Global variables are the number of events N_i^D , N_i^{SM} and N_i^{BSM} for bin i in subcategory k from the Data and SM distributions found in [1], and the obtained BSM histograms, respectively, as well as the SM (BSM) fitting parameters $\mu_{\text{SM}}^{(k)}$ (μ_{BSM}) for the signal hypothesis, and the SM fitting parameters $\tilde{\mu}_{\text{SM}}^{(k)}$ for the background hypothesis.

3.4.1 Chi Squared

A fit of the signal (S) and background (B) distributions is done by minimizing chi squared functions. For a given subcategory k , we define

$$\chi_{\text{S},(k)}^2 = \vec{D}_{\text{S}}^T V^{-1} \vec{D}_{\text{S}} = D_{\text{S},i} V_{ij}^{-1} D_{\text{S},j} \quad (3.18)$$

$$\chi_{\text{B},(k)}^2 = \vec{D}_{\text{B}}^T V^{-1} \vec{D}_{\text{B}} = D_{\text{B},i} V_{ij}^{-1} D_{\text{B},j} \quad (3.19)$$

where

$$D_{\text{S},i} = N_i^D - \mu_{\text{SM}}^{(k)} N_i^{\text{SM}} - \mu_{\text{BSM}} N_i^{\text{BSM}} \quad (3.20)$$

$$D_{\text{B},i} = N_i^D - \tilde{\mu}_{\text{SM}}^{(k)} N_i^{\text{SM}} \quad (3.21)$$

$$V_{ij} = \delta_{ij} N_i^D + \sum_a \epsilon_a^2 N_i^a N_j^a \quad (3.22)$$

with V_{ij} the covariance matrix, for which we include

- the (uncorrelated) statistical error from data, which assuming Poissonian errors is equal

$\sqrt{N_i^D}$ for bin i , hence accounting for the term $\delta_{ij} N_i^D$

- the relative (fully correlated) systematic uncertainties ε_a arising from the background channel a , with corresponding number of events N_i^a for bin i . For the gluon fusion category, we applied a 7% error on the process $gg \rightarrow h \rightarrow WW$ and a 11% error for the summed Drell-Yan, nonprompt and minor background events, as extracted from an ATLAS analysis [77]. For the Z -Higgs category we did not include any systematic errors due to lack of available information about them in [1].

The combined chi squared functions are then given by the sum of the individual ones

$$\chi_S^2 = \sum_k \chi_{S,(k)}^2, \quad \chi_B^2 = \sum_k \chi_{B,(k)}^2 \quad (3.23)$$

We fit of parameters μ_{BSM} , $\mu_{\text{SM}}^{(k)}$ and $\tilde{\mu}_{\text{SM}}^{(k)}$ by minimizing functions χ_S^2 and χ_B^2 . After minimization, we compute the test statistics t_χ and extract the corresponding significance Z_χ from it:

$$t_\chi = \chi_B^2 - \chi_S^2 \quad (3.24)$$

$$Z_\chi = \sqrt{t_\chi} = \sqrt{\chi_B^2 - \chi_S^2} \quad (3.25)$$

3.4.2 Likelihood Ratio

We perform fit on the signal (S) and background (B) histograms by maximizing the likelihood functions $L_S = L(\mu_{\text{SM}}^{(k)}, \mu_{\text{BSM}} | \vec{N}^D)$ and $L_B = L(\tilde{\mu}_{\text{SM}}^{(k)} | \vec{N}^D)$. Assuming a Poissonian distribution for each bin, the likelihood functions for subcategory k are given by

$$L_S^{(k)} = \prod_i \left(\frac{\mu_{\text{SM}}^{(k)} N_i^{\text{SM}} + \mu_{\text{BSM}} N_i^{\text{BSM}}}{N_i^D!} \right)^{N_i^D} \times \exp \left\{ - (\mu_{\text{SM}}^{(k)} N_i^{\text{SM}} + \mu_{\text{BSM}} N_i^{\text{BSM}}) \right\} \quad (3.26)$$

$$L_B^{(k)} = \prod_i \left(\frac{\tilde{\mu}_{\text{SM}}^{(k)} N_i^{\text{SM}}}{N_i^D!} \right)^{N_i^D} \times \exp \left\{ - (\tilde{\mu}_{\text{SM}}^{(k)} N_i^{\text{SM}}) \right\} \quad (3.27)$$

Since values for $N_i^D!$ are considerably large and the exponential part is small, the defined likelihood functions yield very small values, surpassing the precision level of most computers. Moreover, optimization packages typically minimize instead of maximizing functions. To circumvent these issues, we minimize the negative logarithm of the likelihood functions subtracted by the unimportant constant $C^{(k)} = \sum_i N_i^D \log(N_i^D!)$, thus obtaining:

$$l_S^{(k)} := -\log(L_S^{(k)}) - C^{(k)} = \sum_i \left\{ -N_i^D \log \left(\mu_{\text{SM}}^{(k)} N_i^{\text{SM}} + \mu_{\text{BSM}} N_i^{\text{BSM}} \right) + \left(\mu_{\text{SM}}^{(k)} N_i^{\text{SM}} + \mu_{\text{BSM}} N_i^{\text{BSM}} \right) \right\} \quad (3.28)$$

$$l_B^{(k)} := -\log(L_B^{(k)}) - C^{(k)} = \sum_i \left\{ -N_i^D \log(\tilde{\mu}_{SM}^{(k)} N_i^{SM}) + \tilde{\mu}_{SM}^{(k)} N_i^{SM} \right\} \quad (3.29)$$

The total likelihood function for each hypothesis is defined by the product of the individual ones:

$$L_S = \prod_k L_S^{(k)}, \quad L_B = \prod_k L_B^{(k)} \quad (3.30)$$

which is equivalent to performing a sum over the negative logarithm of likelihood functions:

$$l_S := -\log(L_S) - C = \sum_k l_S^{(k)}, \quad l_B := -\log(L_B) - C = \sum_k l_B^{(k)} \quad (3.31)$$

where $C := \sum_k C^{(k)}$. A fit of the signal and background distributions is hence done by minimizing functions l_S and l_B , respectively. The corresponding test statistics t_L and significance Z_L are then extracted with a likelihood ratio

$$t_L = -2 \log \frac{L_B}{L_S} \quad (3.32)$$

$$Z_L = \sqrt{t_L} = \sqrt{-2 \log \frac{L_B}{L_S}} \quad (3.33)$$

Chapter 4

Results and Discussion

We present the relevant significance levels of the signal versus background hypotheses computed over the corresponding mass space for each process type. In addition, we provide the fitted cross-section σ_{BSM} for each mass choice. The signal histograms scaled by the fitted parameters are then plotted for each fitting method together with the data values. The results for each category are discussed.

4.1 Scalar Mediated Neutrino Production

We display the results for the processes $pp \rightarrow H \rightarrow N_1\bar{\nu}_e$ and $pp \rightarrow H \rightarrow \bar{N}_1\nu_e$ evaluated on the gluon fusion data from [1]. Figures 4.1 and 4.2 show the significance and BSM cross-section values obtained with the χ^2 and likelihood functions, respectively, for each combination of masses m_H and m_N . The obtained background SM normalization parameters are $\tilde{\mu}_{\text{SM}}^{<20} = 1.01 \pm 0.02$ and $\tilde{\mu}_{\text{SM}}^{>20} = 1.01 \pm 0.01$ for the χ^2 fit, and $\tilde{\mu}_{\text{SM}}^{<20} = 1.01 \pm 0.01$ and $\tilde{\mu}_{\text{SM}}^{>20} = 1.0 \pm 0.01$ for the likelihood fit, where $\gtrless 20$ denote the $p_{T2} \gtrless 20$ GeV subcategories. The SM normalization parameters $\mu_{\text{SM}}^{\gtrless 20}$ in the signal hypothesis remained within an interval of $[0.93, 1.01]$ after fitting, with uncertainty ranges nearly always overlapping with 1, as seen in Appendix E.1. From Figures 4.1a and 4.2a we can identify maximum significances of $Z_\chi = 2.5\sigma$ and $Z_L = 2.6\sigma$. The corresponding fitted signal and data plots for $p_{T2} > 20$ and $p_{T2} < 20$ for each minimization method are shown in Figures 4.3 and 4.4 together with their ratios and fitted parameter values. In Appendix G.1 one finds the normalized m_T^H distributions for the $N\nu$ processes.

In Figures 4.1a and 4.2a we see that the significance peaks at masses $m_H = 200$ GeV and $m_N = 140$ GeV for both fitting methods, and also stays $\gtrsim 2.0\sigma$ for mass ranges $m_H \in [150, 200]$ GeV and $m_N \in [90, 150]$ GeV. Although the mass $m_H = 200$ GeV is not in agreement with the predicted mass of around 150 GeV in [9, 10, 11, 14], the latter searches

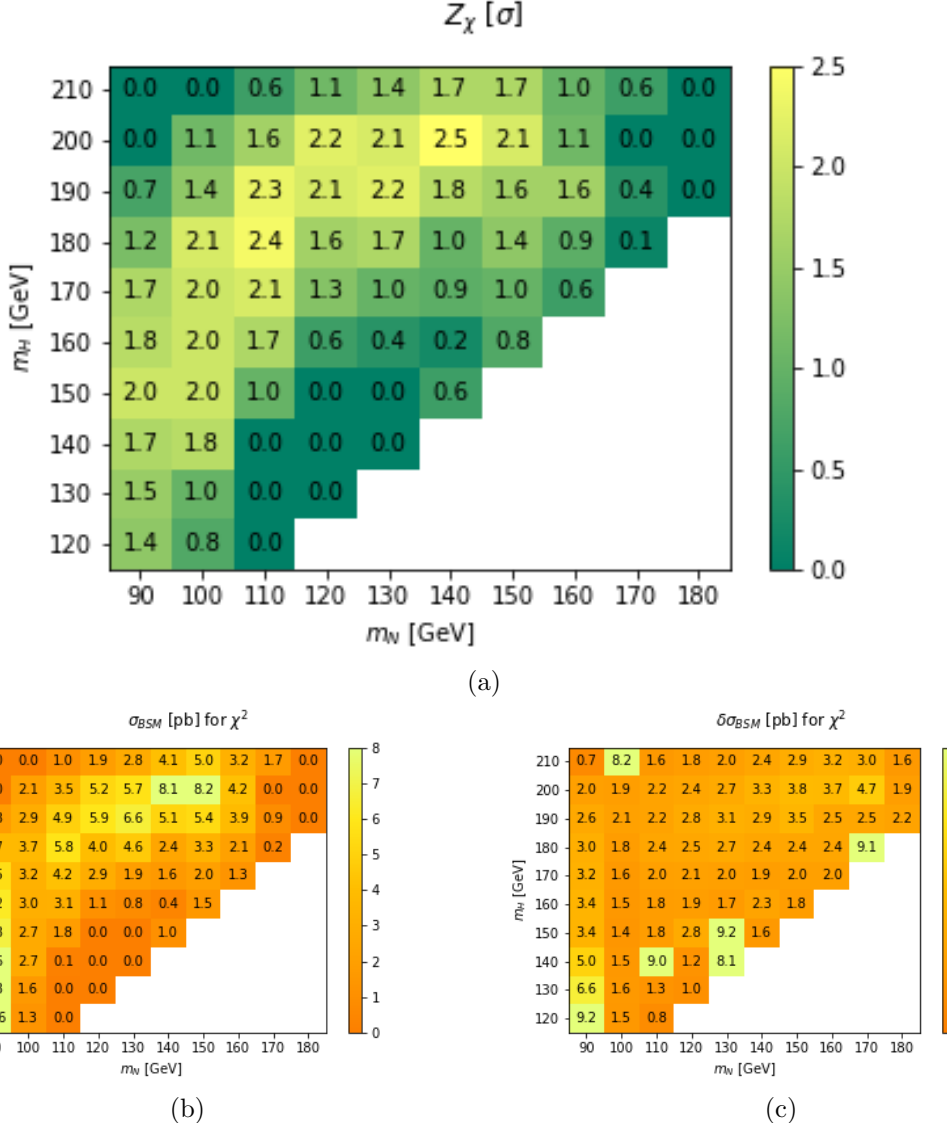


Figure 4.1: Significance Z_χ (a), cross-section σ_{BSM} (b) and associated uncertainty $\delta\sigma_{BSM}$ (c) for processes $pp \rightarrow H \rightarrow N_1\bar{\nu}_e(\bar{N}_1\nu_e)$ computed with the χ^2 function

were conducted by considering only scalars coupled directly to electroweak bosons without intermediate particles. Moreover, the significance for mass $m_H = 150$ GeV still stays around 2.0σ for neutrino masses $m_N = 90$ and 100 GeV in Figure 4.1a, which could serve as further evidence for a scalar with this mass. In particular, the predictions made in [14] with $\gamma\gamma$, $Z\gamma$ and $b\bar{b}$ resonances can also be explained by the $2HDM + Z' + N$ model, and combining both results could significantly increase the global significance value. On the other hand, we see that the significance decreases notably for masses $m_H < 140$ and $m_H > 200$ GeV, which therefore challenges the existence of neutrinos coupled to a scalar candidate of masses $m_H = 95$ GeV or $m_H = 680$ GeV, or to the SM Higgs.

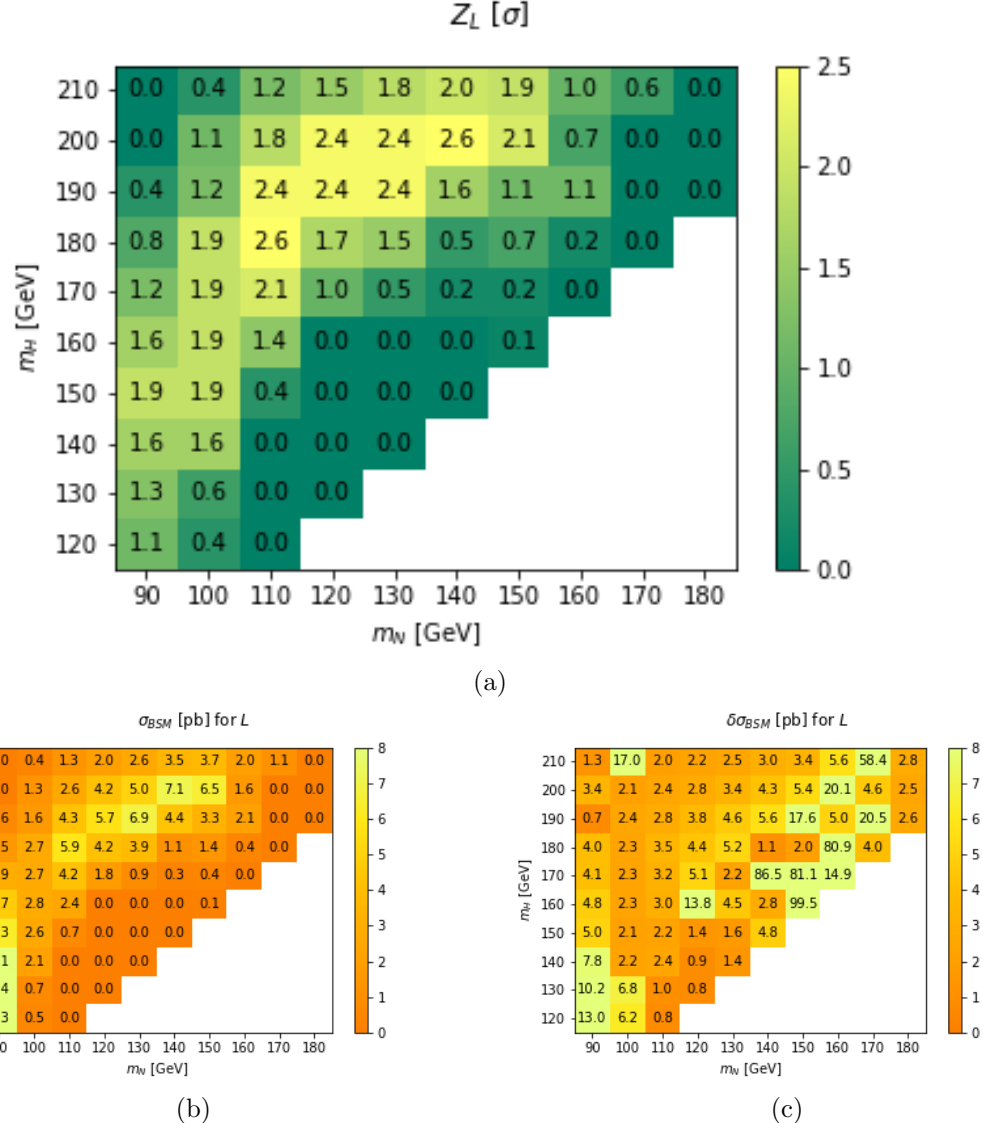


Figure 4.2: Significance Z_L (a), cross-section σ_{BSM} (b) and associated uncertainty $\delta\sigma_{BSM}$ (c) for processes $pp \rightarrow H \rightarrow N_1\bar{\nu}_e(\bar{N}_1\nu_e)$ computed with the likelihood function

Comparing the obtained significance levels with values from past searches on multi-lepton data, we see similar or better results when coupling scalars to neutrinos. The significance found for the same category in [10] is relatively small (0.43σ), whereas the search in [13] made with the same CMS data yields comparable significance levels of $\gtrsim 2.5\sigma$ for scalar masses $m_H < 130$ GeV. Here we note that the latter study also included the excess reported by ATLAS in [77], and evaluating the $H \rightarrow N_i\nu_i$ decays on these results could further increase the BSM-SM discrepancies.

Referring to the BSM plots in Appendix G.1, a change a change of shape is observed with varying neutrino and scalar masses. We see that increasing the scalar mass shifts the peak

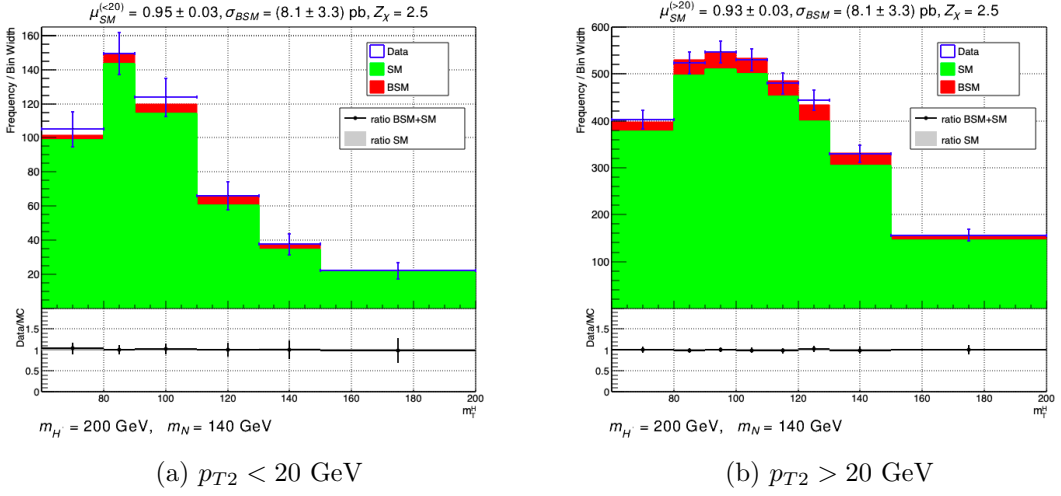


Figure 4.3: Histograms rescaled with parameters σ_{BSM} and $\mu_{SM}^{(k)}$ after fitting by minimizing the χ^2 function, along with LHC data values. Below the histograms one finds the corresponding ratios of LHC events over MC predictions of the SM hypothesis without rescaling ("ratio SM") and SM plus BSM hypothesis after rescaling ("ratio SM+BSM").

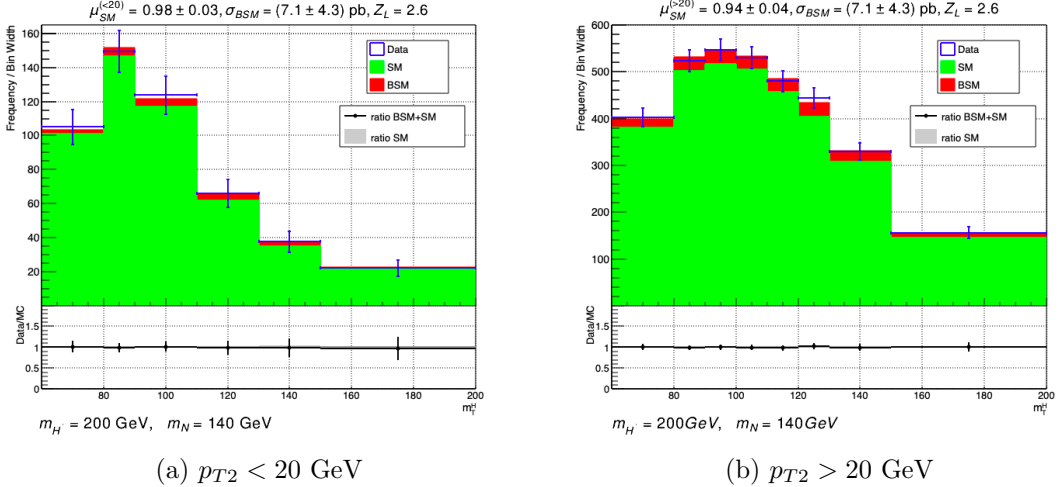


Figure 4.4: Histograms rescaled with parameters σ_{BSM} and $\mu_{SM}^{(k)}$ after fitting by maximizing the likelihood function, along with LHC data values. Below the histograms one finds the corresponding ratios (see caption of Figure 4.3 for details)

from left to right, implying that the m_T^H gets increased. This change is due to the *Higgs transverse mass* being a reconstruction of the transverse mediator mass based on dilepton \vec{p}_T and missing momentum, meaning that a higher mediator mass naturally increases the value of m_T^H . On the other hand, it can be seen that increasing the neutrino mass slightly broadens the m_T^H distributions. This broadening can be interpreted as an increased variance of the m_T^H variable, which in turn can be justified in a higher missing momentum arising from an increased momentum deposition of the heavy neutrino on the SM neutrino. The

augmented missing momentum will be detected with an increased statistical fluctuation, hence also increasing the fluctuations measured for m_T^H .

We further observe in Figures 4.1b and 4.2b that the cross-sections found for the significance levels $\gtrsim 2.0$ GeV are in the range $\sigma_{\text{BSM}} \in [2, 9]$ pb. This cross-section interval corresponds to a total number of events ranging from 250k to 1.4M events for a luminosity of $L = 138$ fb^{-1} , and given that the selection efficiencies are larger than 0.01% as seen in Appendix F, the BSM process is not excluded by the estimated cross-sections. We also see a notably large cross-section for masses $m_N = 90$ GeV and $m_H < 150$ GeV in Figures 4.1b and 4.2b, with high associated uncertainties. These large errors imply that both the χ^2 and likelihood function are less sensitive to the BSM fitting parameter for low neutrino and scalar masses, which can in turn be attributed to a smaller statistics caused by the reduced selection efficiencies in this mass range. In addition, most of the $\mu_{\text{SM}}^{\gtrless 20}$ and $\tilde{\mu}_{\text{SM}}^{\gtrless 20}$ values found in Appendix E.1 agree with 1 within uncertainty, indicating consistency with the SM. However, large BSM cross-sections occasionally reduce the SM fitting parameter significantly, as seen in Figures 4.3 and 4.4 for the parameters maximizing the significance. Although the disagreeing uncertainty ranges are still close to 1, a more careful analysis should be done to determine whether such parameter values are within accepted ranges.

One can also note some differences and similarities between the results obtained with each fitting method. Both significance scans in Figures 4.1a and 4.2a have a similar distribution, with significance values usually not varying by more than 0.6σ and peaking at the same mass combination $(m_H, m_N) = (200, 140)$ GeV. However, the distribution obtained with the likelihood function in Figure 4.2a is narrower, with a slightly increased peak. This difference could be attributed to the inclusion of systematic errors in the χ^2 function, which is known to yield more conservative results upon the introduction of non-diagonal terms in the correlation matrix.

The cross-section seen in Figures 4.1b and 4.2b are also similarly distributed, with values that mostly do not differ by more than 2 pb. However, there is a notable difference between the uncertainty values found in Figures 4.1c and 4.2c. Cross-sections estimated with the likelihood function possess considerably larger errors than the ones obtained with χ^2 . This difference indicates that the likelihood function is often less sensitive to the rescaling of BSM histograms, hence yielding less precise fitting parameters after minimization. The higher precision achieved with the χ^2 function reflects more reliable results.

4.2 Z' Mediated Neutrino Production

We show the results for $pp \rightarrow Z' \rightarrow N_1 \bar{N}_1$ against the Z -Higgs production data from [1] in a similar fashion as for the $N\nu$ processes. Figures 4.5 and 4.6 display the significance values and

estimated cross-sections with their corresponding uncertainties over the considered parameter space. The background SM normalization parameters for the 1-jet and 2-jet categories are $\tilde{\mu}_{\text{SM}}^{1j} = 0.95 \pm 0.03$ and $\tilde{\mu}_{\text{SM}}^{1j} = 1.09 \pm 0.04$ with the χ^2 function, and $\tilde{\mu}_{\text{SM}}^{1j} = 0.96 \pm 0.04$ and $\tilde{\mu}_{\text{SM}}^{1j} = 1.11 \pm 0.05$ with the likelihood function. The signal SM parameters μ_{SM}^{1j} and μ_{SM}^{2j} remained within intervals $[0.94, 0.96]$ and $[1.08, 1.11]$, respectively, and often did not agree with 1 (see Appendix E.2). In Figures 4.7 and 4.8 we display the rescaled signal distributions after fitting for the maximum significance levels $Z_\chi = 1.0\sigma$ and $Z_L = 1.4\sigma$ together with the data histograms. The normalized m_T^H histograms for the NN processes are displayed in Appendix G.2

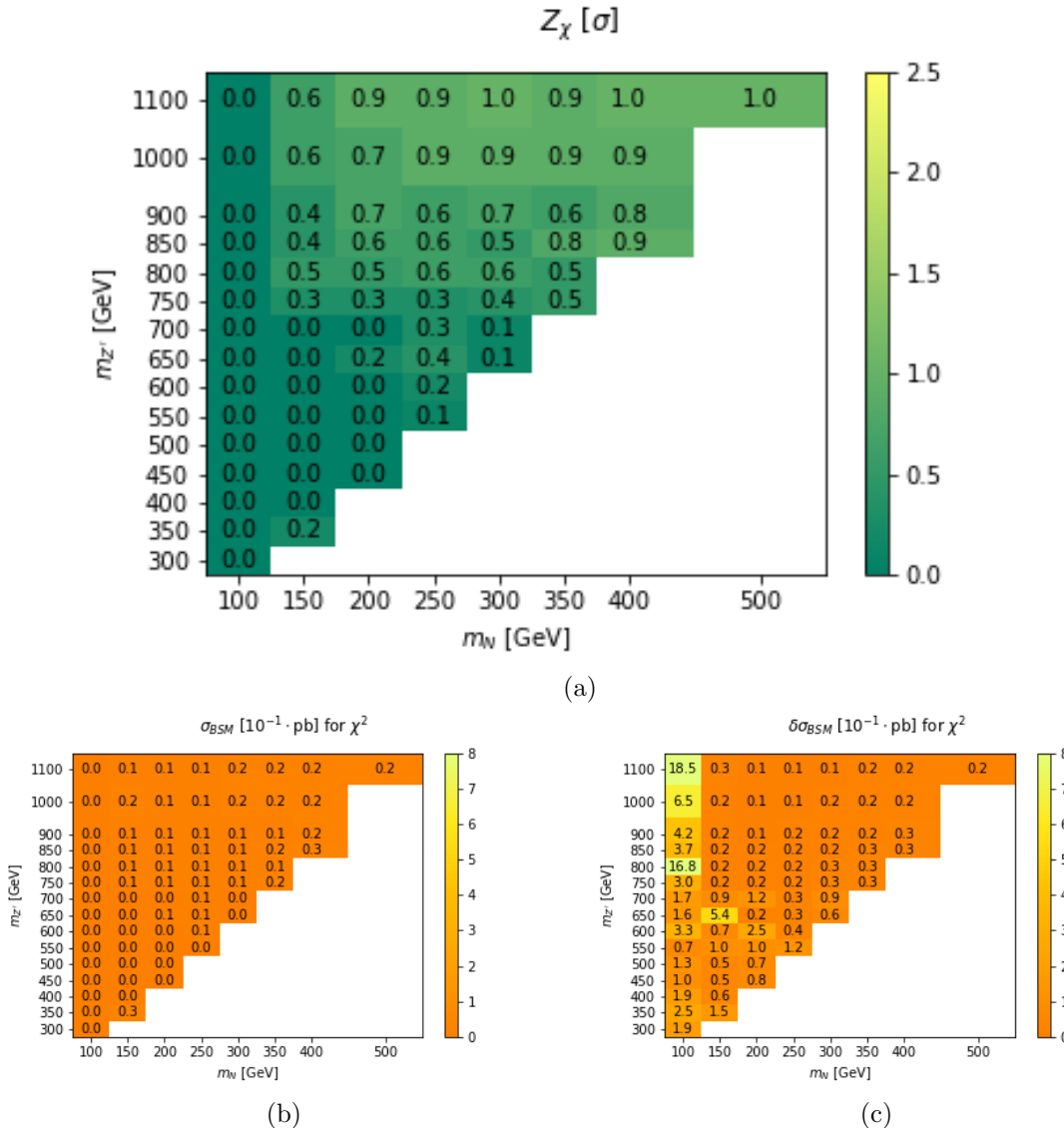


Figure 4.5: Significance Z_χ (a), cross-section σ_{BSM} (b) and associated uncertainty $\delta\sigma_{\text{BSM}}$ (c) for processes $pp \rightarrow Z' \rightarrow N_1 \bar{N}_1$ computed with the χ^2 function

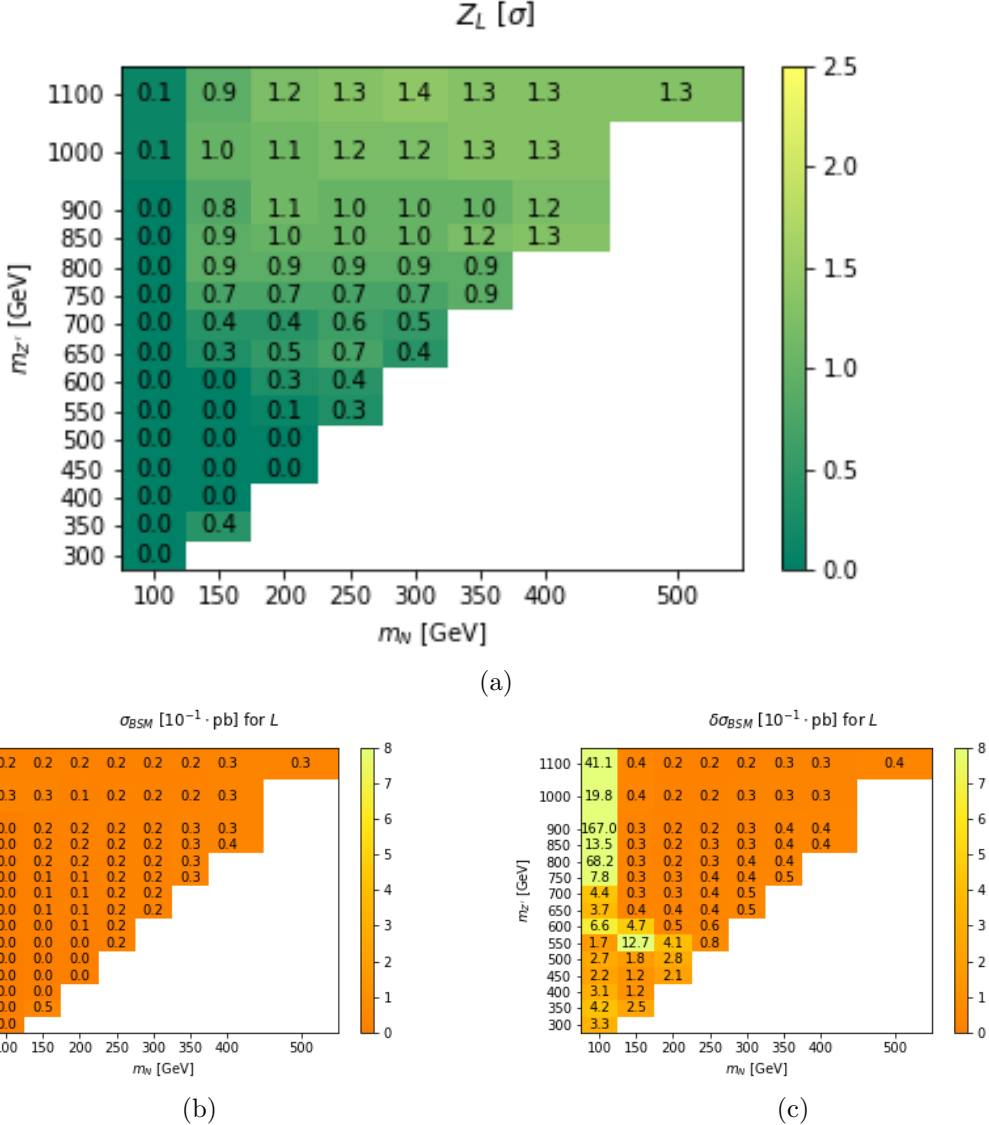


Figure 4.6: Significance Z_L (a), cross-section σ_{BSM} (b) and associated uncertainty $\delta\sigma_{BSM}$ (c) for process $pp \rightarrow Z' \rightarrow N_1 \bar{N}_1$ computed with the likelihood function

In contrast to the results in section 4.1, the analysis done on the Z -Higgs category yields notably low significance values. Most of the significances remain $\lesssim 1.0\sigma$, with a considerable fraction being equal to 0.0σ . Despite the Z -Higgs results in [1] presenting two prominent excesses for the 2-jet category (see Figure 3.1d), several reasons can be listed as contributing to a reduced significance. In Figure 3.4 we can note that, for the 2-jet case, the smearing procedure markedly broadens the SM distributions. Such broadening was also observed for the BSM histogram, hence hindering the fitting of a localized excess. Another reason for lower significance levels is the inclusion of the anomaly-free 1-jet category in the analysis, as seen in Figure 3.1c. For the gluon fusion analysis, there is some excess seen in both $p_{T2} \gtrless 20$ GeV

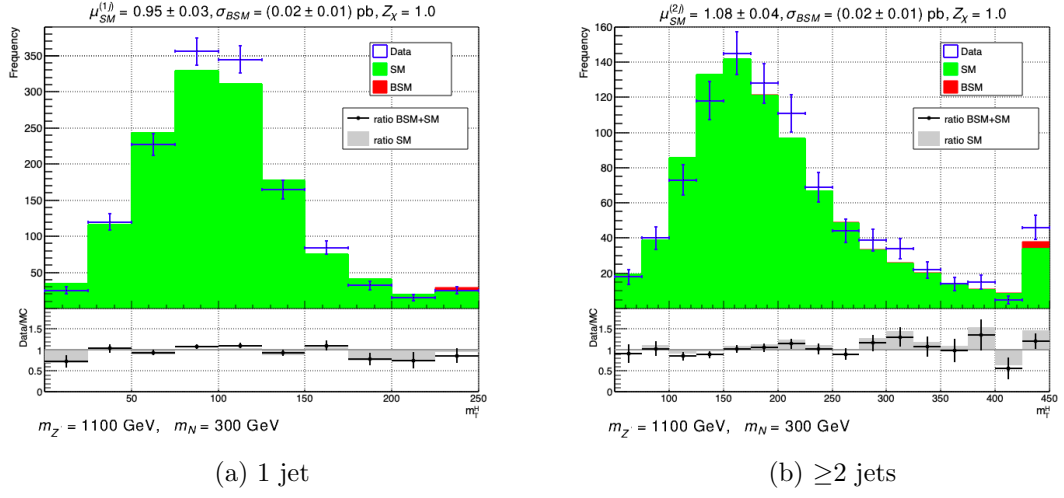


Figure 4.7: Histograms rescaled with parameters σ_{BSM} and $\mu_{SM}^{(k)}$ after fitting by minimizing the χ^2 function, along with LHC data values. Below the histograms one finds the corresponding ratios (see caption of Figure 4.3 for details)

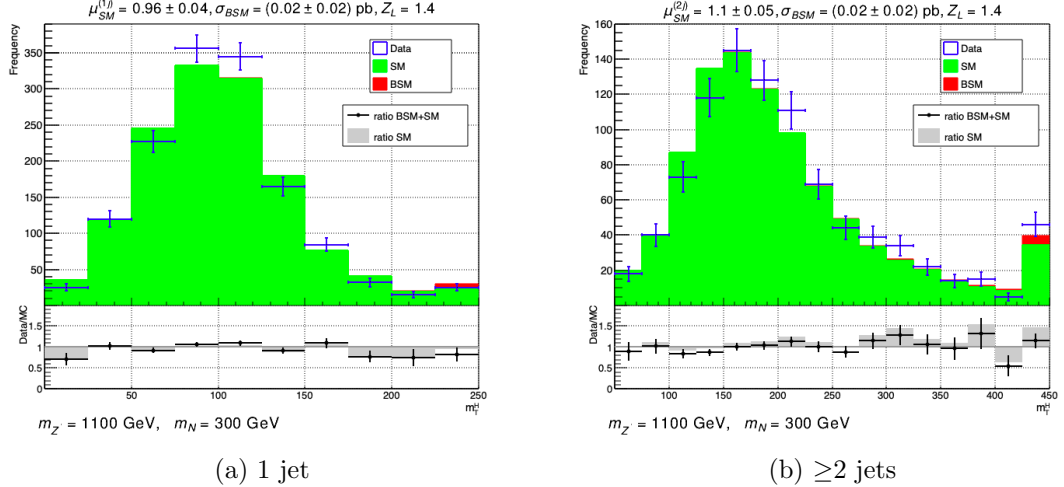


Figure 4.8: Histograms rescaled with parameters σ_{BSM} and $\mu_{SM}^{(k)}$ after fitting by maximizing the likelihood function, along with LHC data values. Below the histograms one finds the corresponding ratios (see caption of Figure 4.3 for details)

cases for masses $m_T^H \sim 130$ GeV, as noticed in Figures 3.1a and 3.1b, while for the Z -Higgs we only see anomalies for the 2-jet category. The number of events falling into the 1-jet and 2-jet categories is similar, usually not diverging by more than factor 2, meaning that the 1-jet case cannot be excluded from the analysis. A BSM process with mainly a 2-jet signature would likely explain better the Z -Higgs excess.

One more factor reducing the significance values is the fact that we consider the SM distributions as an additional degree of freedom in both the signal and background hypotheses without

imposing any constraints. By fitting the SM normalization factors, we observe that this parameter is typically reduced to 0.95-0.96 for the 1-jet category, and increased to 1.08-1.11 for the 2-jet category, as seen in Appendix E.2. The 2-jet normalization factor is increased to compensate for the excess of data events, which, in the signal hypothesis, leads to a low or vanishing BSM cross-section. The resulting low significance indicates that the BSM distribution has little to no effect in the signal fitting, and the obtained χ^2 and likelihood values do not differ much from the ones obtained by fitting the SM distributions alone. Nonetheless, most of the fitted SM parameters $\tilde{\mu}_{\text{SM}}^{1j/2j}$ and $\mu_{\text{SM}}^{1j/2j}$ deviate significantly from 1. In [1], no explicit bounds are given to the main backgrounds WW and WZ , and a dedicated analysis is required to constrain the SM parameters.

When looking at the cross-section in Figures 4.5b and 4.6b, we observe considerably smaller values compared to the ones obtained for the gluon fusion study. Most of the non-vanishing cross-sections are of around $\sim 10 - 30 \text{ fb}$, and considering an efficiency of $\lesssim 0.4\%$ for the 2-jet category, we would obtain $\lesssim 15$ events observed in the study. Taking into account that there are 16 bins for the 2-jet distribution as well as the large width of the BSM distributions, in Appendix G.2 it is unlikely that such cross-section would be observed in the CMS analysis. By constraining the background normalization parameters one would possibly obtain larger cross-section values. As in the previous subsection, we encounter large cross-section uncertainties $\delta\sigma_{\text{BSM}}$ in Figures 4.5c and 4.6c for low neutrino masses, suggesting a low sensitivity of the fitting functions to the BSM cross-section, which could again be due to low selection efficiencies.

The mass ranges considered in our analysis are exhaustive. The lower mass bounds are $m_N > m_Z$ and $m_{Z'} > 2m_Z$ in order to allow for decay chains $Z' \rightarrow N_1 \bar{N}_1 \rightarrow Z \nu_e Z \bar{\nu}_e$. As we can see in Appendix G.2, the 2-jet distributions for the minimum masses $(m_{Z'}, m_N) = (300, 100) \text{ GeV}$ peaks around $m_T^H = 150 \text{ GeV}$, whereas excesses are seen for $m_T^H \gtrsim 175 \text{ GeV}$. For lower masses, the peak would further shift to the left, likely yielding vanishing significance. On the other hand, we see that masses $m_Z > 900 \text{ GeV}$ and $m_N > 200 \text{ GeV}$ yield the highest significance levels. We observe that most of the events for the distributions in these mass ranges are located in the overflow bin, meaning that the higher significance is attributed to the excess seen in this bin and not to the remaining excess events at $m_T^H \sim 200 \text{ GeV}$ and $\sim 300 \text{ GeV}$, as seen in Figure 3.1d. This can also be observed in Figures 4.7 and 4.8, where the BSM distribution is the highest in the rightmost bin. A further increase in the masses would enhance the overflow bin, but marginally increase the significance level.

One can also observe changes in the shapes of the BSM histograms in Appendix G.2 with varying Z' and neutrino masses. We see that higher $m_{Z'}$ values broaden the m_T^H distributions, whereas higher m_N values shift these distributions to the right. The broadening of the m_T^H distributions can be again interpreted as larger statistical fluctuations, which are in turn

caused by larger oscillations in the p_T values of the reconstructed final objects. The shift to the right can be justified with the fact that the *Higgs transverse mass* variable is the mass reconstruction of a secondary mediator h in the SM chain $pp \rightarrow Z \rightarrow Zh$. Since the heavy neutrino is also a secondary mediator in the chain $pp \rightarrow Z' \rightarrow N_1 \bar{N}_1$, increasing its mass will directly increase the mass m_T^H .

As for the gluon fusion analysis, both the χ^2 and likelihood methods yield similar results, with a few exceptions. We can notice that the significance values obtained with the likelihood function are slightly higher than the ones obtained with the χ^2 function. The difference between both distributions is not larger than 0.5σ . It is worth pointing out that we did not include systematics in this analysis, which likely would likely decrease the significance levels further. The differences here can hence attributed to the assumption of Gaussian and Poissionian statistics for the χ^2 and likelihood, respectively. The cross-section values σ_{BSM} also differ marginally, most of them not varying by more than 0.02 pb. However, like in the gluon fusion case, we have often larger cross-section uncertainties $\delta\sigma_{\text{BSM}}$ for the likelihood analysis, implying that this function is less sensitive to the BSM distribution. Again, the more precise results achieved with the χ^2 method suggest higher reliability.

Chapter 5

Conclusion

The $2HDM S+Z'+N$ model contains multiple signatures which are detectable at collider experiments and could help explain various experimental excesses. The high numbers of independent BSM parameters (14) and particles (8) give rise to a rich phenomenology which can be explored in different anomalous scenarios while maintaining constraints set by past results. Here we have focused on scalar and Z' mediated neutrino production at the LHC, generating and processing MC samples, and evaluating these with two distinct methods on CMS data collected for gluon fusion and Z -Higgs production categories presenting an excess.

The results obtained for each category differ considerably. For the $pp \rightarrow H \rightarrow \bar{N}_i \nu_i (N_i \bar{\nu}_i)$ processes evaluated on the gluon fusion category, we obtained significance levels of $\gtrsim 2.5\sigma$, which are comparable to other results considering signatures with only BSM scalars. However the predicted scalar masses for these previous studies are significantly lower than the ones maximizing our significance. Our findings also challenge neutrino-scalar couplings at masses $m_H = 95$ GeV, $m_H = 680$ GeV and $m_H = 125$ GeV. In contrast, the significance levels obtained for the $pp \rightarrow Z' \rightarrow N_i \bar{N}_i$ process on Z -Higgs production data are $\lesssim 1.0\sigma$, being notably lower than the ones estimated with the scalar mediated processes. The fitted cross-section is ~ 0.1 pb, which potentially excludes the BSM signature. The main reason for the low significance is likely the absence of constraints imposed on the SM fitting parameter μ_{SM} . Both fitting methods give similar results, with the χ^2 function yielding slightly more conservative and precise values.

The methodology and results present some limitations too. Regarding the signal model, we recognize that we purposefully excluded BSM particles which were not involved in the NN and $N\nu$ processes by setting them to high masses. One issue with this is that scalar particles arising from the same doublet are expected to have similar masses [78]. However, we note that the production modes $pp \rightarrow A_S$ and $pp \rightarrow H^+$ can be suppressed by a small $\sin \beta$ value. We also set all CP-even mixing angles to zero, which excludes the SM Higgs from BSM

interactions and forces decay types $N_i \rightarrow Z\nu_i$ and $N_i \rightarrow W\ell_i$. Nonetheless, in the case of a finite ω_1 , processes $pp \rightarrow h \rightarrow N_i \bar{N}_i (N_i \bar{\nu}_i)$ and decays $N_i \rightarrow h\nu_i$ would be highly suppressed by factor $\sin^2 \omega_1$, as seen from Equations 2.72, 2.73 and 2.68. One could also argue that other Z' and H decays to leptons were not considered in this search. However, we see in Equations 2.69-2.74 that $Z' \rightarrow N_i \bar{N}_i$ and $H \rightarrow N_i \bar{\nu}_i (\bar{N}_i \nu_i)$ are in fact dominant. While hadronic decay channels $Z' \rightarrow q\bar{q}_i$ would in principle be possible within the studied $m_{Z'}$ range, they have been excluded by past experiments [54], and could be avoided by introducing e.g. heavy quarks, as mentioned in section 2.4.

There were also some challenges encountered during the event generation and statistical analysis phases. First, we acknowledge that all processes were simulated at tree level, without the inclusion of next-to-leading-order effects caused by loop interactions. The shower hadronization processes computed by the **Pythia8** framework is based on a simplified modelling which might lead to some inaccuracies [69]. We also recognize the fact that missing energy and jet smearing is also an approximate procedure to resemble full detector reconstruction algorithms. These approximations might decrease the precision level of our results, but the obtained values are still useful to estimate the effect of the proposed BSM signatures on LHC data. Furthermore, the absence of systematic uncertainties arising from major background processes $pp \rightarrow WW$ and $pp \rightarrow WZ$ in the χ^2 fit may yield slightly biased results. We also acknowledge that we assumed fixed masses for our analyses while only maintaining one BSM degree of freedom, which could potentially result in a look-elsewhere effect. Such effect can be accounted for by appropriately correcting the local significance, as discussed in [79]. A further point of criticism is the small statistics observed for BSM processes with low neutrino masses, which possibly leads to high cross-section errors, yielding less precise results.

Lastly, we recognize that the fitted values for $\mu_{\text{SM}}^{(2j)}$ and $\tilde{\mu}_{\text{SM}}^{(2j)}$ are fairly large, surpassing the predicted value in [1] by at least 8% and consequentially decreasing the BSM cross-section. There are no explicit bounds provided for the main WW and WZ background normalizations in the CMS analysis, making it difficult to constrain this parameter in a precise manner. A more detailed analysis is needed in order to determine uncertainty bands for the two dominant backgrounds. Furthermore, the NN signature would also be identified in other searches, such as the $3W$ and $4W$ studies in [80, 81, 82] with three and four lepton final states. This means that, the cross-section σ_{BSM} would be adequately constrained by performing a simultaneous fit with these results.

To further verify the existence of heavy neutrinos, as well as scalar and vector-like mediators, we suggest additional processes for future studies. For instance, one could assess the effect of including neutrino decays to scalars and associated leptons on both the gluon fusion and Z -Higgs production channels, which would introduce additional degrees of freedom in the analysis. There has also been a recent excess measured by ATLAS in [83], which could be

explained by the NN process with subsequent decay mode $N \rightarrow H\nu_i$. Moreover, as stated in section 1.1.3, a recent study [64] analysing the phenomenology of a linear seesaw mechanism has proposed a series of processes to be evaluated against experimental data. Such model introduces 6 neutrino singlets and an additional scalar doublet, producing signatures which are testable at various collider studies.

In particular, processes $e^+e^- \rightarrow NN$, $e^+e^- \rightarrow H^\pm H^\pm$ and $e^-\gamma \rightarrow NH^-$ with subsequent $H^\pm \rightarrow \ell^\pm N \rightarrow \text{leptons+jets}$ decay chains could yield detectable events at e^+e^- and $e^-\gamma$ colliders. However, we note that the seesaw model contains lepton number and flavour violating signatures due to Majorana terms in the Lagrangian and neutrino mixing among different flavours. While our model could reproduce lepton flavour violating processes upon introduction of non-diagonal elements in mass matrices $M^{(\psi)}$ and $M^{(Y)}$, the field content must be altered in order to account for lepton number violation. One possibility is to disentangle the left- and right-handed chiral components of ψ and assign them adequate symmetries in order to obtain Majorana-like terms. A more elaborated analysis is needed in order fully reproduce the linear seesaw phenomenology with the $2HDM+Z'+N$ model, which would provide another way to test the existence of heavy neutrinos coupled to scalars in nature.

Bibliography

- [1] CMS Collaboration, *Measurements of the higgs boson production cross section and couplings in the w boson pair decay channel in proton-proton collisions at $\sqrt{s} = 13$ tev*, 2206.09466.
- [2] G. Hamel de Monchenault, *Electroweak measurements at the LHC*, *Ann. Rev. Nucl. Part. Sci.* **67** (2017) 19.
- [3] R. Hawkings, *Top quark physics at the lhc*, *Comptes Rendus Physique* **16** (2015) 424.
- [4] CMS Collaboration, *Observation of a new boson at a mass of 125 GeV with the CMS experiment at the LHC*, *Physics Letters B* **716** (2012) 30.
- [5] ATLAS Collaboration, *Observation of a new particle in the search for the standard model higgs boson with the ATLAS detector at the LHC*, *Physics Letters B* **716** (2012) 1.
- [6] B. Abi, T. Albahri, S. Al-Kilani, D. Allspach, L. Alonzi, A. Anastasi et al., *Measurement of the positive muon anomalous magnetic moment to 0.46 ppm*, *Physical Review Letters* **126** (2021) .
- [7] T. Kajita, *Atmospheric neutrino results from super-kamiokande and kamiokande: Evidence for neutrino(mu) oscillations*, *Nuclear Physics B - Proceedings Supplements* **77** (1999) 123.
- [8] J. Alda, J. Guasch and S. Penaranda, *Anomalies in b mesons decays: Present status and future collider prospects*, 2021.
- [9] S. von Buddenbrock, N. Chakrabarty, A.S. Cornell, D. Kar, M. Kumar, T. Mandal et al., *The compatibility of lhc run 1 data with a heavy scalar of mass around 270 gev*, 1506.00612.
- [10] S. von Buddenbrock, A.S. Cornell, A. Fadol, M. Kumar, B. Mellado and X. Ruan, *Multi-lepton signatures of additional scalar bosons beyond the standard model at the lhc*, 1711.07874.

- [11] S. von Buddenbrock, A.S. Cornell, Y. Fang, A.F. Mohammed, M. Kumar, B. Mellado et al., *The emergence of multi-lepton anomalies at the LHC and their compatibility with new physics at the EW scale*, *Journal of High Energy Physics* **2019** (2019) .
- [12] Y. Hernandez, M. Kumar, A.S. Cornell, S.-E. Dahbi, Y. Fang, B. Lieberman et al., *The anomalous production of multi-leptons and its impact on the measurement of wh production at the LHC*, *The European Physical Journal C* **81** (2021) .
- [13] G. Coloretti, A. Crivellin, S. Bhattacharya and B. Mellado, *Searching for low-mass resonances decaying into w bosons*, 2302.07276.
- [14] A. Crivellin, Y. Fang, O. Fischer, A. Kumar, M. Kumar, E. Malwa et al., *Accumulating evidence for the associate production of a neutral scalar with mass around 151 gev*, 2109.02650.
- [15] T. Biekötter, S. Heinemeyer and G. Weiglein, *Mounting evidence for a 95 GeV higgs boson*, *Journal of High Energy Physics* **2022** (2022) .
- [16] S. Iguro, T. Kitahara and Y. Omura, *Scrutinizing the 95–100 GeV di-tau excess in the top associated process*, *The European Physical Journal C* **82** (2022) .
- [17] U. Haisch and A. Malinauskas, *Let there be light from a second light higgs doublet*, *Journal of High Energy Physics* **2018** (2018) .
- [18] A. Crivellin, J. Heeck and D. Müller, *Large $h \rightarrow bs$ in generic two-Higgs-doublet models*, *Phys. Rev. D* **97** (2018) 035008 [1710.04663].
- [19] T. Biekötter, M. Chakraborti and S. Heinemeyer, *A 96 GeV Higgs boson in the N2HDM*, *Eur. Phys. J. C* **80** (2020) 2 [1903.11661].
- [20] J. Cao, X. Guo, Y. He, P. Wu and Y. Zhang, *Diphoton signal of the light Higgs boson in natural NMSSM*, *Phys. Rev. D* **95** (2017) 116001 [1612.08522].
- [21] CMS collaboration, *Search for a standard model-like Higgs boson in the mass range between 70 and 110 GeV in the diphoton final state in proton-proton collisions at $\sqrt{s} = 8$ and 13 TeV*, *Phys. Lett. B* **793** (2019) 320 [1811.08459].
- [22] CMS collaboration, *Measurements of properties of the Higgs boson decaying into the four-lepton final state in pp collisions at $\sqrt{s} = 13$ TeV*, *JHEP* **11** (2017) 047 [1706.09936].
- [23] ATLAS collaboration, *Search for resonances decaying into photon pairs in 139 fb^{-1} of pp collisions at $\sqrt{s}=13$ TeV with the ATLAS detector*, *Phys. Lett. B* **822** (2021) 136651 [2102.13405].

- [24] M. Consoli and L. Cosmai, *Experimental signals for a second resonance of the Higgs field*, *Int. J. Mod. Phys. A* **37** (2022) 2250091 [2111.08962].
- [25] ATLAS Collaboration, *Search for heavy ZZ resonances in the $\ell^+\ell^-\ell^+\ell^-$ and $\ell^+\ell^-\nu\bar{\nu}$ final states using proton-proton collisions at $\sqrt{s} = 13$ TeV with the ATLAS detector*, *The European Physical Journal C* **78** (2018) .
- [26] A. Rubbia, *Phenomenology of Particle Physics*, Cambridge University Press (2022), 10.1017/9781009023429.
- [27] F. Englert and R. Brout, *Broken symmetry and the mass of gauge vector mesons*, *Phys. Rev. Lett.* **13** (1964) 321.
- [28] P.W. Higgs, *Broken symmetries and the masses of gauge bosons*, *Phys. Rev. Lett.* **13** (1964) 508.
- [29] G.S. Guralnik, C.R. Hagen and T.W.B. Kibble, *Global conservation laws and massless particles*, *Phys. Rev. Lett.* **13** (1964) 585.
- [30] G. Bertone, D. Hooper and J. Silk, *Particle dark matter: Evidence, candidates and constraints*, *Phys. Rept.* **405** (2005) 18 [hep-ph/0404175].
- [31] L. Canetti, M. Drewes and M. Shaposhnikov, *Matter and antimatter in the universe*, *New Journal of Physics* **14** (2012) 095012.
- [32] A. Shomer, *A pedagogical explanation for the non-renormalizability of gravity*, 2007.
- [33] S. Koren, *The hierarchy problem: From the fundamentals to the frontiers*, 2020.
- [34] T. Mannel, *Theory and phenomenology of CP violation*, *Nucl. Phys. B Proc. Suppl.* **167** (2007) 115.
- [35] A.J. Buras, J. Ellis, M.K. Gaillard and D.V. Nanopoulos, *Aspects of the grand unification of strong, weak and electromagnetic interactions*, *Nuclear Physics B* **135** (1978) 66.
- [36] M.E. Peskin, *Precision theory of electroweak interactions*, 2020.
- [37] J.P. Lees, V. Poireau, V. Tisserand, J.G. Tico, E. Grauges, A. Palano et al., *Evidence for an excess of $\overline{B} \rightarrow d^{(*)}\tau^-\bar{\nu}_\tau$* , *Physical Review Letters* **109** (2012) .
- [38] The LCHb Collaboration, *Measurement of the ratio of branching $\mathcal{B}(\overline{B}^0 \rightarrow d^*\tau^-\bar{\nu}_\tau)/\mathcal{B}(\overline{B}^0 \rightarrow d^*\mu^-\bar{\nu}_\mu)$* , *Physical Review Letters* **115** (2015) .
- [39] Belle Collaboration, *Angular analysis of $b^0 \rightarrow k^*(892)^0\ell^+\ell^-$* , 2016.

- [40] B. Capdevila, A. Crivellin, S. Descotes-Genon, J. Matias and J. Virto, *Patterns of new physics in $b \rightarrow s\ell^+\ell^-$ transitions in the light of recent data*, *Journal of High Energy Physics* **2018** (2018) .
- [41] M. Davier, A. Hoecker, B. Malaescu and Z. Zhang, *A new evaluation of the hadronic vacuum polarisation contributions to the muon anomalous magnetic moment and to $\alpha(m_Z^2)$* , *Eur. Phys. J. C* **80** (2020) 241 [1908.00921].
- [42] S. Borsanyi, Z. Fodor, J.N. Guenther, C. Hoelbling, S.D. Katz, L. Lellouch et al., *Leading hadronic contribution to the muon magnetic moment from lattice QCD*, *Nature* **593** (2021) 51.
- [43] CDF collaboration, *High-precision measurement of the W boson mass with the CDF II detector*, *Science* **376** (2022) 170.
- [44] ATLAS collaboration, *Improved W boson Mass Measurement using 7 TeV Proton-Proton Collisions with the ATLAS Detector*, .
- [45] A. McDonald, *Evidence for neutrino oscillations i: Solar and reactor neutrinos*, *Nuclear Physics A* **751** (2005) 53.
- [46] H.E. Haber and L.S. Haskins, *Supersymmetric theory and models*, in *Anticipating the Next Discoveries in Particle Physics*, WORLD SCIENTIFIC, may, 2018, DOI.
- [47] E.W. Kolb and M.S. Turner, *Grand Unified Theories and the Origin of the Baryon Asymmetry*, *Ann. Rev. Nucl. Part. Sci.* **33** (1983) 645.
- [48] G. Branco, P. Ferreira, L. Lavoura, M. Rebelo, M. Sher and J.P. Silva, *Theory and phenomenology of two-higgs-doublet models*, *Physics Reports* **516** (2012) 1.
- [49] L. Wang, J.M. Yang and Y. Zhang, *Two-higgs-doublet models in light of current experiments: a brief review*, *Communications in Theoretical Physics* **74** (2022) 097202.
- [50] H.E. Haber and G.L. Kane, *The Search for Supersymmetry: Probing Physics Beyond the Standard Model*, *Phys. Rept.* **117** (1985) 75.
- [51] J.E. Kim, *Light Pseudoscalars, Particle Physics and Cosmology*, *Phys. Rept.* **150** (1987) 1.
- [52] L. Fromme, S.J. Huber and M. Seniuch, *Baryogenesis in the two-Higgs doublet model*, *JHEP* **11** (2006) 038 [hep-ph/0605242].
- [53] P. Langacker, *The Physics of Heavy Z' Gauge Bosons*, *Rev. Mod. Phys.* **81** (2009) 1199 [0801.1345].
- [54] C. Patrignani et al. (Particle Data Group), *Review of particle physics*, *Chinese Physics C* **40** (2016) 100001.

- [55] CDF Collaboration, *Search for $z' \rightarrow e^+e^-$ using dielectron mass and angular distribution*, *Physical Review Letters* **96** (2006) .
- [56] A. Crivellin, *Anomalies in Particle Physics*, in *8th Symposium on Prospects in the Physics of Discrete Symmetries*, 4, 2023 [2304.01694].
- [57] M.J. Strassler, *Possible effects of a hidden valley on supersymmetric phenomenology*, 2006.
- [58] M. Cvetič and P. Langacker, *Implications of abelian extended gauge structures from string models*, *Phys. Rev. D* **54** (1996) 3570.
- [59] Z.-Z. Xing, *Neutrino Physics*, in *1st Asia-Europe-Pacific School of High-Energy Physics*, pp. 177–217, 2014, DOI [1406.7739].
- [60] I. Dorsner and P. Fileviez Pérez, *Unification without supersymmetry: Neutrino mass, proton decay and light leptoquarks*, *Nuclear Physics B* **723** (2005) 53.
- [61] J. Harvey, D. Reiss and P. Ramond, *Mass relations and neutrino oscillations in an $so(10)$ model*, *Nuclear Physics B* **199** (1982) 223.
- [62] W.G. Hollik, *Neutrinos meet supersymmetry: Quantum aspects of neutrino physics in supersymmetric theories*, 2015.
- [63] S. Dodelson and L.M. Widrow, *Sterile-neutrinos as dark matter*, *Phys. Rev. Lett.* **72** (1994) 17 [hep-ph/9303287].
- [64] A. Batra, P. Bharadwaj, S. Mandal, R. Srivastava and J.W.F. Valle, *Phenomenology of the simplest linear seesaw mechanism*, 2023.
- [65] W.R. Inc., “Mathematica, Version 13.2.”
- [66] G. Branco, P. Ferreira, L. Lavoura, M. Rebelo, M. Sher and J.P. Silva, *Theory and phenomenology of two-higgs-doublet models*, *Physics Reports* **516** (2012) 1.
- [67] A. Alloul, N.D. Christensen, C. Degrande, C. Duhr and B. Fuks, *FeynRules 2.0 — a complete toolbox for tree-level phenomenology*, *Computer Physics Communications* **185** (2014) 2250.
- [68] J. Alwall, M. Herquet, F. Maltoni, O. Mattelaer and T. Stelzer, *MadGraph 5: going beyond*, *Journal of High Energy Physics* **2011** (2011) .
- [69] C. Bierlich, S. Chakraborty, N. Desai, L. Gellersen, I. Helenius, P. Ilten et al., *A comprehensive guide to the physics and usage of pythia 8.3*, 2022.

- [70] J. de Favereau, , C. Delaere, P. Demin, A. Giammacco, V. Lemaître et al., *DELPHES 3: a modular framework for fast simulation of a generic collider experiment*, *Journal of High Energy Physics* **2014** (2014) .
- [71] T. Plehn, *Lectures on LHC Physics*, Springer Berlin Heidelberg (2012), 10.1007/978-3-642-24040-9.
- [72] R. Brun and F. Rademakers, *Root — an object oriented data analysis framework*, *Nuclear Instruments and Methods in Physics Research Section A: Accelerators, Spectrometers, Detectors and Associated Equipment* **389** (1997) 81.
- [73] E. Ting, “Overlap removal at the atlas experiment.” https://indico.cern.ch/event/1131431/contributions/5059616/attachments/2512765/4319357/Ting_AIPabstract.pdf.
- [74] J. Allison et al., *Geant4 developments and applications*, *IEEE Trans. Nucl. Sci.* **53** (2006) 270.
- [75] M. Donegà and C. Grab, “Statistical methods and analysis techniques in experimental physics.” 2017.
- [76] Plot Digitizer, “Plot digitizer.” <https://plotdigitizer.com/>, n.d.
- [77] ATLAS Collaboration, *Measurements of higgs boson production by gluon–gluon fusion and vector-boson fusion using $h \rightarrow ww^* \rightarrow e\nu\mu\nu$ decays in pp collisions at $\sqrt{s} = 13$ tev with the atlas detector*, 2022.
- [78] A. Biswas and A. Lahiri, *Masses of Physical Scalars in Two Higgs Doublet Models*, *Springer Proc. Phys.* **174** (2016) 605.
- [79] E. Gross and O. Vitells, *Trial factors for the look elsewhere effect in high energy physics*, *The European Physical Journal C* **70** (2010) 525.
- [80] ATLAS collaboration, *Observation of WWW Production in pp Collisions at $\sqrt{s} = 13$ TeV with the ATLAS Detector*, *Phys. Rev. Lett.* **129** (2022) 061803 [2201.13045].
- [81] ATLAS collaboration, *Search for Higgs boson pair production in the $WW^{(*)}WW^{(*)}$ decay channel using ATLAS data recorded at $\sqrt{s} = 13$ TeV*, *JHEP* **05** (2019) 124 [1811.11028].
- [82] CMS Collaboration, *Search for higgs boson pairs decaying to $wwww$, $ww\tau\tau$, and $\tau\tau\tau\tau$ in proton-proton collisions at $\sqrt{s} = 13$ tev*, 2022.
- [83] ATLAS collaboration, *Measurement of the $t\bar{t}$ production cross-section and lepton differential distributions in $e\mu$ dilepton events from pp collisions at $\sqrt{s} = 13$ TeV with the ATLAS detector*, *Eur. Phys. J. C* **80** (2020) 528 [1910.08819].

Appendix A

Mass Matrix Diagonalization

We present here the **Mathematica** notebooks used to identify and diagonalize mass matrices for neutrino, scalars and gauge bosons, as well as to express internal parameters as a function of independent ones.

A.1 Neutrino Diagonalization

```
M = {{M1e, M2e, M3e}, {M1mu, M2mu, M3mu}, {M1tau, M2tau, M3tau},  
{MN11, MN12, MN13}, {MN12, MN22, MN23}, {MN13, MN23, MN33}};  
conditions = M1e >= 0 && M2e == 0 && M3e == 0 && M1mu == 0 && M2mu >= 0 &&  
M3mu == 0 && M1tau == 0 && M2tau == 0 && M3tau >= 0 && MN11 >= 0 &&  
MN12 == 0 && MN13 == 0 && MN22 >= 0 && MN23 == 0 && MN33 >= 0;  
M = FullSimplify[M, Assumptions -> conditions];  
{UL, Mhat, URdag} = SingularValueDecomposition[M];  
UL = FullSimplify[UL, Assumptions -> conditions];  
Mhat = FullSimplify[Mhat, Assumptions -> conditions];  
URdag = FullSimplify[URdag, Assumptions -> conditions];  
UL // MatrixForm  
Mhat // MatrixForm  
URdag // MatrixForm
```

A.2 Scalar Sector

A.2.1 Identifying Quadratic Terms

```
Subscript[\[CapitalPhi]],  
1] = {{Subscript[\[Phi]]^C,
```

```

1]], {(1/Sqrt[2]) (Subscript[v, 1] + Subscript[\[Phi], 1] +
I Subscript[\[Chi], 1])}};
Subscript[\[CapitalPhi],
2] = {{Subscript[\[Phi]]^C,
2]}, {(1/Sqrt[2]) (Subscript[v, 2] + Subscript[\[Phi], 2] +
I Subscript[\[Chi], 2])}};
Subscript[\[CapitalPhi],
S] = {{(1/Sqrt[2]) (Subscript[v, S] + Subscript[\[Phi], S] +
I Subscript[\[Chi], S])}};
VH=Subscript[\[Mu], 1]ConjugateTranspose[Subscript[\[CapitalPhi], \
1]].Subscript[\[CapitalPhi], 1] - Subscript[\[Lambda], \
1](ConjugateTranspose[Subscript[\[CapitalPhi], 1]].Subscript[\
\[CapitalPhi], 1])^2
+ Subscript[\[Mu], \
2]ConjugateTranspose[Subscript[\[CapitalPhi], 2]].Subscript[\
\[CapitalPhi], 2] - Subscript[\[Lambda], \
2](ConjugateTranspose[Subscript[\[CapitalPhi], 2]].Subscript[\
\[CapitalPhi], 2])^2
+ Subscript[\[Mu], S]ConjugateTranspose[Subscript[\[CapitalPhi], \
S]].Subscript[\[CapitalPhi], S] - Subscript[\[Lambda], \
S](ConjugateTranspose[Subscript[\[CapitalPhi], S]].Subscript[\
\[CapitalPhi], S])^2
- Subscript[\[Lambda], d](ConjugateTranspose[Subscript[\
\[CapitalPhi], 1]].Subscript[\[CapitalPhi], \
1]).(ConjugateTranspose[Subscript[\[CapitalPhi], 2]].Subscript[\
\[CapitalPhi], 2]) - Subscript[\[Lambda], \
m](ConjugateTranspose[Subscript[\[CapitalPhi], 1]].Subscript[\
\[CapitalPhi], 2]).(ConjugateTranspose[Subscript[\[CapitalPhi], \
2]].Subscript[\[CapitalPhi], 1])
- Subscript[\[Lambda], S1](ConjugateTranspose[Subscript[\
\[CapitalPhi], S]].Subscript[\[CapitalPhi], \
S]).(ConjugateTranspose[Subscript[\[CapitalPhi], 1]].Subscript[\
\[CapitalPhi], 1]) - Subscript[\[Lambda], \
S2](ConjugateTranspose[Subscript[\[CapitalPhi], S]].Subscript[\
\[CapitalPhi], S]).(ConjugateTranspose[Subscript[\[CapitalPhi], \
2]].Subscript[\[CapitalPhi], 2])
- \[Xi](Subscript[\[CapitalPhi], S].ConjugateTranspose[Subscript[\
\[CapitalPhi], 2]].Subscript[\[CapitalPhi], \

```

```

1]+ConjugateTranspose[Subscript[\[CapitalPhi], \[S]].ConjugateTranspose[Subscript[\[CapitalPhi], 1]].Subscript[\[CapitalPhi], 2]);
VH=ExpandAll[VH];
VH=ExpandAll[FullSimplify[VH, Assumptions->Subscript[v, 1]\[Element]Reals&&Subscript[\[Phi], 1]\[Element]Reals&&Subscript[\[Chi], 1]\[Element]Reals&&Subscript[v, 2]\[Element]Reals&&Subscript[\[Phi], 2]\[Element]Reals&&Subscript[\[Chi], 2]\[Element]Reals&&Subscript[v, S]\[Element]Reals&&Subscript[\[Phi], S]\[Element]Reals]];
VH;

```

A.2.2 Complex Scalar Diagonalization

```

factor = Sqrt[2];
Mpm2 = -{{-(1/2) (lam4 v2^2 + factor mu v2 vS / v1), (1/
2) (lam4 v1 v2 + factor mu vS )}, {(1/2) (lam4 v1 v2 +
factor mu vS ), -(1/2) (lam4 v1^2 + factor mu v1 vS / v2)}};
Mpm2 = Simplify[Mpm2, Assumptions -> v1 > 0 && v2 > 0 && vS > 0];
Mpm2 // MatrixForm
Mpm2diag = DiagonalMatrix[Eigenvalues[Mpm2]] // MatrixForm
Vpm = Transpose[Eigenvectors[Mpm2]] // Simplify;
Vpm // MatrixForm

```

A.2.3 Neutral CP-Odd Scalar Diagonalization

```

Modd2 = (-\[Xi]/
Sqrt[2]) {{-Subscript[v, S] Subscript[v, 2]/Subscript[v, 1],
Subscript[v, S], -Subscript[v, 2]}, {Subscript[v,
S], -Subscript[v, S] Subscript[v, 1]/Subscript[v, 2], Subscript[v,
1]}, {-Subscript[v, 2], Subscript[v,
1], -Subscript[v, 1] Subscript[v, 2]/Subscript[v, S]}};
Modd2 // MatrixForm;
W = {{Subscript[v, 1]/
Sqrt[(Subscript[v, 1]^2 + Subscript[v, 2]^2)], -Subscript[v, 2]/
Sqrt[(Subscript[v, 1]^2 + Subscript[v, 2]^2)], 0},
{Subscript[v, 2]/Sqrt[(Subscript[v, 1]^2 + Subscript[v, 2]^2)],
Subscript[v, 1]/Sqrt[(Subscript[v, 1]^2 + Subscript[v, 2]^2)], 0},
0},

```

```

{0, 0, 1}};

Modd2EHB = Inverse[W] . Modd2 . W // FullSimplify;
Modd2EHB // MatrixForm;
Modd2EHBhat = DiagonalMatrix[Eigenvalues[Modd2EHB]];
Modd2EHBhat // MatrixForm
U = Transpose[Eigenvectors[Modd2EHB]];
U // MatrixForm;
u3 = Transpose[U[[All, 3]]];
U12 = Transpose[U[[All, 1 ;; 2]]];
u3 = Normalize[u3];
u3 = Simplify[u3,
  Assumptions ->
    Subscript[v, 1] >= 0 && Subscript[v, 2] >= 0 &&
    Subscript[v, S] >= 0];
Transpose[u3] // MatrixForm;
U12 = Orthogonalize[U12];
U12 = Simplify[U12,
  Assumptions ->
    Subscript[v, 1] >= 0 && Subscript[v, 2] >= 0 &&
    Subscript[v, S] >= 0];
Transpose[U12] // MatrixForm;
U = Transpose[{U12[[1]], U12[[2]], u3}];
V = W . U;
FullSimplify[Transpose[V] . Modd2 . V,
  Assumptions ->
    Subscript[v, 1] >= 0 && Subscript[v, 2] >= 0 &&
    Subscript[v, S] >= 0] // MatrixForm;
FullSimplify[Transpose[V] . V,
  Assumptions ->
    Subscript[v, 1] >= 0 && Subscript[v, 2] >= 0 &&
    Subscript[v, S] >= 0] // MatrixForm;
V = V /. {Subscript[v, 1] -> sb*v, Subscript[v, 2] -> cb*v}
FullSimplify[V,
  Assumptions ->
    v >= 0 && sb >= 0 && cb >= 0 && sb^2 + cb^2 == 1 &&
    Subscript[v, S] >=
      0 && -1 +
      sb^2 == -cb^2] // MatrixForm

```

A.3 Gauge Sector

A.3.1 Identifying Quadratic Terms

```

Phi1 = {{0}, {v1/Sqrt[2]}};
Phi2 = {{0}, {v2/Sqrt[2]}};
PhiS = {{vS/Sqrt[2]}};

DmuPhi1 = ((g/2) (PauliMatrix[1] W1 + PauliMatrix[2] W2 +
    PauliMatrix[3] W3) + g1 (1/2) B IdentityMatrix[2] +
    g1p (-1) Bp IdentityMatrix[2]) . Phi1;
DmuPhi2 = ((g/2) (PauliMatrix[1] W1 + PauliMatrix[2] W2 +
    PauliMatrix[3] W3) + g1 (1/2) B IdentityMatrix[2]) . Phi2;
DmuPhiS = g1p (+1) Bp IdentityMatrix[1] . PhiS;
LagrHKin =
    ConjugateTranspose[DmuPhi1] . DmuPhi1 +
    ConjugateTranspose[DmuPhi2] . DmuPhi2 +
    Transpose[DmuPhiS] . DmuPhiS;
Simplify[LagrHKin,
Assumptions ->
W1 \[Element] Reals && W2 \[Element] Reals && W3 \[Element] Reals &&
B \[Element] Reals && Bp \[Element] Reals &&
v1 \[Element] Reals && v2 \[Element] Reals &&
vS \[Element] Reals && g \[Element] Reals && g1 \[Element] Reals &&
g1p \[Element] Reals] // ExpandAll

```

Gauge Boson Diagonalization

```

M02 = (1/
4) {{g1^2 v^2, -g1 g v^2, -2 g1 g1p v^2 Subscript[
    s, \[Beta]]^2}, {-g1 g v^2, g^2 v^2,
2 g1p g v^2 Subscript[s, \[Beta]]^2 }, {-2 g1 g1p v^2 Subscript[
    s, \[Beta]]^2, 2 g1p g v^2 Subscript[s, \[Beta]]^2 ,
4*g1p^2 (v^2 Subscript[s, \[Beta]]^2 +
    vS^2)}]; M02 // MatrixForm;
M02 = Simplify[M02, Assumptions];
M02 // MatrixForm;
V0 = Transpose[Eigenvectors[M02]];
M02Diag = DiagonalMatrix[Eigenvalues[M02]];
V0 // MatrixForm;
FullSimplify[M02Diag, Assumptions] // MatrixForm
Transpose[V0] . V0 // ExpandAll // FullSimplify // MatrixForm;

```

```

VSM = (1/Sqrt[g^2 + g1^2]) {{g, -g1, 0}, {g1, g, 0}, {0, 0,
Sqrt[g^2 + g1^2]}};

VSM // MatrixForm

M02SM = Transpose[VSM] . M02 . VSM // ExpandAll // FullSimplify;
M02SM // MatrixForm

M2SMDiag =
Simplify[DiagonalMatrix[Eigenvalues[M02SM]], Assumptions] //
ExpandAll // FullSimplify;

M2SMDiag // MatrixForm

V0BSM = Transpose[Eigenvectors[M02SM]];
V0BSM // MatrixForm

(*Parameter Dependance*)

exprZ = 1/8 ((g^2 + g1^2) v^2 + 4 g1p^2 vS^2 + 4 g1p^2 v^2
\!(*SubsuperscriptBox[(s), (\Beta), (2)]*) -
Sqrt[((g^2 + g1^2) v^2 - 4 g1p^2 vS^2)^2 + 8 g1p^2 v^2
\!(*SubsuperscriptBox[(s), (\Beta), (2)]*) (-((g^2 +
g1^2) v^2) + 4 g1p^2 vS^2 +
2 (g^2 + g1^2 + g1p^2) v^2
\!(*SubsuperscriptBox[(s), (\Beta), (2)])] == mZ^2;
exprZp = 1/8 ((g^2 + g1^2) v^2 + 4 g1p^2 vS^2 + 4 g1p^2 v^2
\!(*SubsuperscriptBox[(s), (\Beta), (2)]*) +
Sqrt[((g^2 + g1^2) v^2 - 4 g1p^2 vS^2)^2 + 8 g1p^2 v^2
\!(*SubsuperscriptBox[(s), (\Beta), (2)]*) (-((g^2 +
g1^2) v^2) + 4 g1p^2 vS^2 +
2 (g^2 + g1^2 + g1p^2) v^2
\!(*SubsuperscriptBox[(s), (\Beta), (2)])] == mZp^2;
FullSimplify[Solve[exprZ && exprZp, {g1p, g}]]

```

Appendix B

Decay Width Computations

We compute the decay widths for the Z' boson, CP-even scalars and heavy neutrinos in terms of the signal ($2HDM + Z' + N$) model parameters. For simplicity we remove the index i from the heavy neutrinos and label them by N . Each decay mode is a two body decay $M \rightarrow 1 + 2$ with differential width

$$d\Gamma = \frac{\langle |\mathcal{M}|^2 \rangle}{2M} \frac{d^3 p_1}{(2\pi)^3 2E_1} \frac{d^3 p_2}{(2\pi)^3 2E_2} (2\pi)^4 \delta^4(p - p_1 - p_2) \quad (\text{B.1})$$

where $p_1 = (E_1, \vec{p}_1)$ and $p_2 = (E_2, \vec{p}_2)$ are the 4-momenta of the daughter particles, p and M are the 4-momentum and mass of the mother particle, and $\langle |\mathcal{M}|^2 \rangle$ is the squared scattering amplitude. In the rest frame of N and for a momentum-independent $\langle |\mathcal{M}|^2 \rangle$, we obtain after integration

$$\Gamma = \frac{\langle |\mathcal{M}|^2 \rangle}{16\pi M^3} \sqrt{(M^2 - m_1^2 - m_2^2)^2 - 4m_1^2 m_2^2} \quad (\text{B.2})$$

where $m_1^2 = p_1^2$ and $m_2^2 = p_2^2$ are the squared masses of daughter particles. We now proceed to explicitly compute the decay widths for each mother particle.

B.1 N Decay

We categorize the possible decay modes of the N neutrino into two types of processes:

- $N \rightarrow B + \ell$ or $\bar{N} \rightarrow \bar{B} + \bar{\ell}$, where B and ℓ are a SM electroweak gauge boson and lepton, respectively
- $N \rightarrow h + \nu$ or $\bar{N} \rightarrow h + \bar{\nu}$, where h and ν are a CP-even scalar and a neutrino, respectively

B.1.1 $NB\ell$

We calculate the decay width for the process $N \rightarrow B + \ell$ by first computing the average squared scattering amplitude $\langle |\mathcal{M}|^2 \rangle$. For an initial heavy neutrino N with 4-momentum p_N and spin t , final electroweak boson B with 4-momenta p_B and polarization λ , and final lepton ℓ with 4-momenta p_ℓ and spin s , find that the scattering amplitude is given by

$$\mathcal{M} = \bar{u}^s(p_\ell) V^\mu u^t(p_N) (B_\mu^\lambda(p_B))^* \quad (\text{B.3})$$

where u^p is a Dirac spinor and B^μ is the gauge field for the electroweak boson. Moreover, V^μ describes the $NB\ell$ vertex factor, and can be decomposed as $V^\mu = V\gamma^\mu P_L$, where $P_L = \frac{1}{2}(1 - \gamma^5)$ is the left-handed chiral projection operator and $V = V_{BN\ell}$ is a constant depending on signal model parameters and is specific to the coupling $BN\ell$. Summing over the final state degrees of freedom and averaging over the initial ones, we find:

$$\begin{aligned} \langle |\mathcal{M}|^2 \rangle &= \frac{1}{2} \sum_t \sum_s \sum_\lambda \left[\bar{u}^s(p_\ell) V^\mu u^t(p_N) (B_\mu^\lambda(p_B))^* \right] \left[\bar{u}^s(p_\ell) V^\nu u^t(p_N) (B_\nu^\lambda(p_B))^* \right]^* \\ &= \frac{1}{2} |V|^2 \frac{1}{2} \frac{1}{2} \sum_\lambda (B_\mu^\lambda(p_B))^* (B_\nu^\lambda(p_B)) \sum_s \sum_t \left[\bar{u}^s(p_\ell) \gamma^\mu (1 - \gamma^5) u^t(p_N) \right] \left[\bar{u}^s(p_\ell) \gamma^\nu (1 - \gamma^5) u^t(p_N) \right]^* \end{aligned} \quad (\text{B.4})$$

We find that the sum over the gauge field components yields

$$\sum_\lambda (B_\mu^\lambda(p_B))^* (B_\nu^\lambda(p_B)) = -g_{\mu\nu} + \frac{p_{B,\mu} p_{B,\nu}}{m_B^2} \quad (\text{B.5})$$

The remaining summation over the spin degrees of freedom can be simplified using Casimir's trick:

$$\begin{aligned} \sum_s \sum_t \left[\bar{u}^s(p_\ell) \gamma^\mu (1 - \gamma^5) u^t(p_N) \right] \left[\bar{u}^s(p_\ell) \gamma^\nu (1 - \gamma^5) u^t(p_N) \right]^* \\ = \text{Tr}[\gamma^\mu (1 - \gamma^5)(\not{p}_N + m_N)\gamma^0(\gamma^\mu(1 - \gamma^5))^\dagger\gamma^0(\not{p}_\ell + m_\ell)] \end{aligned} \quad (\text{B.6})$$

We further have

$$\gamma^0(\gamma^\mu(1 - \gamma^5))^\dagger\gamma^0 = \gamma^0(1 - (\gamma^5)^\dagger)(\gamma^\mu)^\dagger\gamma^0 = (1 + \gamma^5)\gamma^0(\gamma^\mu)^\dagger\gamma^0 = (1 + \gamma^5)\gamma^\mu \quad (\text{B.7})$$

as well as

$$\not{p}_N(1 + \gamma^5) = (1 - \gamma^5)\not{p}_N \quad (\text{B.8})$$

and taking into account that the trace of a product of an uneven number of γ -matrices is zero, we can further simplify Eq. (B.6) as:

$$\begin{aligned}\text{Tr}[\gamma^\mu(1-\gamma^5)\not{p}_N(1+\gamma^5)\gamma^\mu\not{p}_\ell] &= \text{Tr}[\gamma^\mu(1-\gamma^5)(1-\gamma^5)\not{p}_N\gamma^\mu\not{p}_\ell] = 2\text{Tr}[\gamma^\mu(1-\gamma^5)\not{p}_N\gamma^\mu\not{p}_\ell] \\ &= 8(p_N^\mu p_\ell^\nu + p_\ell^\mu p_N^\nu - g^{\mu\nu}(p_N \cdot p_\ell))\end{aligned}\quad (\text{B.9})$$

Introducing Eq. (B.5) and (B.9) in Eq. (B.4), we obtain:

$$\langle|\mathcal{M}|^2\rangle = |V|^2 \left(-g_{\mu\nu} + \frac{p_{B,\mu}p_{B,\nu}}{m_B^2} \right) (p_N^\mu p_\ell^\nu + p_\ell^\nu p_N^\mu - g^{\mu\nu}p_N^\sigma p_{\ell,\sigma}) = |V|^2 \left(p_N \cdot p_\ell + 2 \frac{(p_B \cdot p_N)(p_B \cdot p_\ell)}{m_B^2} \right) \quad (\text{B.10})$$

Taking the rest frame of the neutrino N , we find:

$$m_N^2 = p_N^2 = (p_B + p_\ell)^2 = m_B^2 + m_\ell^2 + 2(p_B \cdot p_\ell) \implies p_B \cdot p_\ell = \frac{1}{2}(m_N^2 - m_B^2 - m_\ell^2) \quad (\text{B.11})$$

We hence find that the average squared scattering amplitude $\langle|\mathcal{M}|^2\rangle$ only depends on the particles masses, and we can directly use Eq. (B.2) to finally obtain:

$$\Gamma_{N \rightarrow B\ell} = \frac{|V_{NB\ell}|^2}{16\pi m_N^3} \left(\frac{m_N^2 + m_\ell^2}{2} + \frac{(m_N - m_\ell)^2}{2m_B^2} - m_B^2 \right) \sqrt{(m_N^2 - m_B^2 - m_\ell^2)^2 - 4m_B^2 m_\ell^2} \quad (\text{B.12})$$

The decay width $\Gamma_{\bar{N} \rightarrow \bar{B}\ell}$ can be obtained following an analogous procedure and is equal to $\Gamma_{N \rightarrow B\ell}$. Since the mass of leptons is low compared to the heavy neutrino and electroweak bosons, we can approximate $m_\ell \approx 0$, yielding:

$$\Gamma_{N \rightarrow B\ell} = \frac{|V_{NB\ell}|^2}{32\pi m_N^3 m_B^2} (m_N^2 (m_N^2 + m_B^2) - 2m_B^4) (m_N^2 - m_B^2) \quad (\text{B.13})$$

For SM lepton ℓ_j^- and associated neutrino ν_j , we find the squared vertex factors:

$$|V_{NW^+\ell_j^-}|^2 = |V_{\bar{N}W^-\ell_j^+}|^2 = \frac{e^2 s_j^2}{2s_w^2} \quad (\text{B.14})$$

$$|V_{NZ\nu_j}|^2 = |V_{\bar{N}Z\nu_j}|^2 = \frac{e^2 s_j^2 c_j^2}{4s_w^2 c_w^2} \quad (\text{B.15})$$

where we have written $s_j = \sin \alpha_j$ and $c_j = \cos \alpha_j$ for $j = e, \mu, \tau$ and $s_w = \sin \theta_w$ and $c_w = \cos \theta_w$ for the weak mixing angle θ_w . Hence, the total decay width to SM charged

leptons is:

$$\Gamma_{N \rightarrow W^+ \ell_j^-} = \Gamma_{\bar{N} \rightarrow W^- \ell_j^+} = \frac{e^2 s_j^2}{64\pi m_N^3 m_Z^2 s_w^2} (m_N^2 (m_N^2 + m_Z^2) - 2m_Z^4) (m_N^2 - m_Z^2) \quad (\text{B.16})$$

whereas the total decay width to SM neutrinos is given by:

$$\Gamma_{N \rightarrow Z \nu_j} = \Gamma_{\bar{N} \rightarrow Z \bar{\nu}_j} = \frac{e^2 s_j^2 c_j^2}{128\pi m_N^3 m_W^2 s_w^2 c_w^2} (m_N^2 (m_N^2 + m_W^2) - 2m_W^4) (m_N^2 - m_W^2) \quad (\text{B.17})$$

B.1.2 $N h\nu$

We now consider the process $\langle |\mathcal{M}|^2 \rangle$, and calculate first the average squared scattering amplitude $\langle |\mathcal{M}|^2 \rangle$ for it. Let the initial heavy neutrino 4-momentum and spin be p_N and t , the final neutrino 4-momentum and spin be p_ν and s , and the final scalar 4-momentum be p_h . The scattering amplitude is:

$$\mathcal{M} = \bar{u}^s(p_\nu) V_h u^t(p_N) \quad (\text{B.18})$$

where u is again a Dirac spinor and $V_h = VP_R$, with $P_R = \frac{1}{2}(1 + \gamma^5)$ the chiral right-handed projection operator and $V = V_{Nh\nu}$ a constant factor depending on the process. We then find:

$$\begin{aligned} \langle |\mathcal{M}|^2 \rangle &= \frac{1}{2} \sum_t \sum_s |\bar{u}^s(p_\nu) V_h u^t(p_N)|^2 = \frac{1}{2} |V|^2 \frac{1}{4} \sum_s \sum_t |\bar{u}^s(p_\nu)(1 + \gamma^5) u^t(p_N)|^2 \\ \frac{|V|^2}{8} \text{Tr} \left[(1 + \gamma^5)(\not{p}_N + m_N) \gamma^0 (1 - \gamma^5)^\dagger \gamma^0 (\not{p}_\nu) \right] &= \frac{|V|^2}{8} \text{Tr} \left[(1 + \gamma^5)(\not{p}_N + m_N)(1 - \gamma^5)(\not{p}_\nu) \right] \\ = \frac{|V|^2}{8} \text{Tr} \left[(1 + \gamma^5)^2 \not{p}_N \not{p}_\nu \right] &= \frac{|V|^2}{8} 2 \text{Tr} \left[(1 + \gamma^5) \not{p}_N \not{p}_\nu \right] = \frac{|V|^2}{4} \text{Tr} \left[\not{p}_N \not{p}_\nu \right] = |V|^2 (p_N \cdot p_\nu) \end{aligned} \quad (\text{B.19})$$

where in the second line we implemented Casimir's trick, and used the identities $\gamma^\mu \gamma^5 = -\gamma^5 \gamma^\mu$, $(\gamma^5)^2 = 1$, $\text{Tr}[\gamma^5 \gamma^\mu \gamma^\nu] = 0$, $\text{Tr}[\gamma^\mu \gamma^\nu] = 4g^{\mu\nu}$, and $\text{Tr}[\gamma^\alpha \gamma^\beta \dots] = 0$ for an odd number of γ -matrices.

Considering the rest frame of the initial neutrino N , we have:

$$m_N^2 = p_N^2 = (p_h + p_\nu)^2 = m_h^2 + 2(p_h \cdot p_\nu) \implies p_N \cdot p_\nu = p_\nu^2 + p_h \cdot p_\nu = p_h \cdot p_\nu = \frac{1}{2}(m_N^2 - m_h^2) \quad (\text{B.20})$$

Using Eq. (B.14) and (B.15) in Eq. (B.2), we arrive at the expression:

$$\Gamma_{N \rightarrow h\nu} = \frac{|V_{Nh\nu}|^2}{32\pi m_N^3} (m_N^2 - m_h^2)^2 \quad (\text{B.21})$$

Following an analogous procedure, we obtain $\Gamma_{\bar{N} \rightarrow h\bar{\nu}} = \Gamma_{N \rightarrow h\nu}$

For a decay to SM neutrino ν_j and CP-even scalar h_k (where $\{h_1, h_2, h_3\} = \{H, h, S\}$), we find the squared vertex factor:

$$|V_{Nh_k\nu_j}|^2 = |V_{\bar{N}h_k\bar{\nu}_j}|^2 = \frac{m_N^2 s_j^2 c_j^2}{v^2 s_\beta^2} |(V_\varphi)_{k1}|^2 \quad (\text{B.22})$$

giving the decay width (provided $m_N > m_{h_k}$):

$$\Gamma_{N \rightarrow h_k \nu_j} = \Gamma_{\bar{N} \rightarrow h_k \bar{\nu}_j} = \frac{s_j^2 c_j^2}{32\pi m_N v^2 s_\beta^2} |(V_\varphi)_{k1}|^2 (m_N^2 - m_{h_k}^2)^2 \quad (\text{B.23})$$

B.2 Z' Decay

We consider the decays of the type $Z' \rightarrow \nu_1 \bar{\nu}_2$, where ν_1 and ν_2 are SM or heavy neutrinos. The scattering amplitude \mathcal{M} for such process is:

$$\mathcal{M} = B_\mu^\lambda(p_{Z'}) \bar{u}_\ell^s(p_1) V^\mu v_N^t(p_2) \quad (\text{B.24})$$

where $p_{Z'}$, p_1 and p_2 are the 4-momenta for the initial Z' boson, and final neutrinos ν_1 and ν_2 , respectively. The fields $u(v)$ and B are Dirac (anti-)spinors and the gauge field for a massive boson. The indices s and t indicate the spin degrees of freedom, whereas the index λ refers of the polarization. The factor V^μ can be further decomposed into $V^\mu = V_L \gamma^\mu P_L + V_R \gamma^\mu P_R$, with V_L and V_R constants depending on signal parameters and decay products. The squared average amplitude is

$$\begin{aligned} \langle |\mathcal{M}|^2 \rangle &= \frac{1}{3} \sum_t \sum_s \sum_\lambda \left| B_\mu^\lambda(p_{Z'}) \bar{u}_\ell^s(p_1) V^\mu v_N^t(p_2) \right|^2 = \frac{1}{3} \sum_\lambda \left[B_\mu^\lambda(p_{Z'}) \right] \left[B_\nu^\lambda(p_{Z'}) \right]^* \\ &\quad \sum_t \sum_s \left[\bar{u}_\ell^s(p_1) V^\mu v_N^t(p_2) \right] \left[\bar{u}_\ell^s(p_1) V^\nu v_N^t(p_2) \right]^* = \frac{1}{12} \sum_\lambda \left[B_\mu^\lambda(p_{Z'}) \right] \left[B_\nu^\lambda(p_{Z'}) \right]^* \\ &\quad \sum_t \sum_s \left[\bar{u}_\ell^s(p_1) (V_L \gamma^\mu (1 - \gamma^5) + V_R \gamma^\mu (1 + \gamma^5)) v_N^t(p_2) \right] \left[\bar{u}_\ell^s(p_1) (V_L \gamma^\nu (1 - \gamma^5) + V_R \gamma^\nu (1 + \gamma^5)) v_N^t(p_2) \right]^* \end{aligned} \quad (\text{B.25})$$

Using the identities mentioned in section B.1.1, we have:

$$\sum_\lambda \left[B_\mu^\lambda(p_{Z'}) \right] \left[B_\nu^\lambda(p_{Z'}) \right]^* = -g_{\mu\nu} + \frac{p_{Z',\mu} p_{Z',\nu}}{m_{Z'}^2} \quad (\text{B.26})$$

and

$$\begin{aligned}
& \sum_t \sum_s [\bar{u}^s(p_1) (V_L \gamma^\mu (1 - \gamma^5) + V_R \gamma^\mu (1 + \gamma^5)) v^t(p_2)] [\bar{u}^s(p_1) (V_L \gamma^\nu (1 - \gamma^5) + V_R \gamma^\nu (1 + \gamma^5)) v^t(p_2)]^* \\
&= \text{Tr} [(V_L \gamma^\mu (1 - \gamma^5) + V_R \gamma^\mu (1 + \gamma^5)) (\not{p}_2 - m_2) \gamma^0 (V_L \gamma^\nu (1 - \gamma^5) + V_R \gamma^\nu (1 + \gamma^5))^\dagger \gamma^0 (\not{p}_1 + m_1)] \\
&= \text{Tr} [(V_L \gamma^\mu (1 - \gamma^5) + V_R \gamma^\mu (1 + \gamma^5)) (\not{p}_2 - m_2) (V_L^* (1 + \gamma^5) \gamma^\nu + V_R^* (1 - \gamma^5) \gamma^\nu) (\not{p}_1 + m_1)] \\
&= \text{Tr} [(V_L \gamma^\mu (1 - \gamma^5) + V_R \gamma^\mu (1 + \gamma^5)) (\not{p}_2) (V_L^* (1 + \gamma^5) \gamma^\nu + V_R^* (1 - \gamma^5) \gamma^\nu) (\not{p}_1)] \\
&\quad - \text{Tr} [(V_L \gamma^\mu (1 - \gamma^5) + V_R \gamma^\mu (1 + \gamma^5)) (m_2) (V_L^* (1 + \gamma^5) \gamma^\nu + V_R^* (1 - \gamma^5) \gamma^\nu) (m_1)] \\
&= \text{Tr} [(V_L \gamma^\mu (1 - \gamma^5) + V_R \gamma^\mu (1 + \gamma^5)) (V_L^* (1 - \gamma^5) \not{p}_2 \gamma^\nu + V_R^* (1 + \gamma^5) \not{p}_2 \gamma^\nu) (\not{p}_1)] \\
&\quad - m_1 m_2 \text{Tr} [(V_L \gamma^\mu (1 - \gamma^5) + V_R \gamma^\mu (1 + \gamma^5)) (V_L^* (1 + \gamma^5) \gamma^\nu + V_R^* (1 - \gamma^5) \gamma^\nu)] \\
&= 2|V_L|^2 p_{1,\alpha} p_{2,\beta} \text{Tr} [\gamma^\mu (1 - \gamma^5) \gamma^\beta \gamma^\nu \gamma^\alpha] + 2|V_R|^2 p_{1,\alpha} p_{2,\beta} \text{Tr} [\gamma^\mu (1 + \gamma^5) \gamma^\beta \gamma^\nu \gamma^\alpha] \\
&\quad - 2V_L V_R^* m_1 m_2 \text{Tr} [\gamma^\mu (1 - \gamma^5) \gamma^\nu] - 2V_R V_L^* m_1 m_2 \text{Tr} [\gamma^\mu (1 + \gamma^5) \gamma^\nu] \\
&= 8(|V_L|^2 + |V_R|^2) (-g^{\mu\nu}(p_1 \cdot p_2) + p_1^\mu p_2^\nu + p_1^\nu p_2^\mu) - 8(V_L V_R^* + V_L^* V_R) m_1 m_2 g^{\mu\nu} \quad (\text{B.27})
\end{aligned}$$

Merging the expressions found in Eq. (B.26) and (B.27) and considering the rest frame of Z' , we obtain:

$$\begin{aligned}
\langle |\mathcal{M}|^2 \rangle &= \frac{2}{3} (|V_L|^2 + |V_R|^2) \left[p_1 \cdot p_2 + 2 \frac{(p_1 \cdot p_{Z'}) (p_2 \cdot p_{Z'})}{m_{Z'}^2} \right] + 2 (V_L V_R^* + V_L^* V_R) m_1 m_2 \\
&= \frac{2}{3} (|V_L|^2 + |V_R|^2) \left[m_{Z'}^2 - \frac{1}{2} (m_1^2 + m_2^2) - \frac{1}{2} \frac{(m_1^2 - m_2^2)^2}{m_{Z'}^2} \right] + 2 (V_L V_R^* + V_L^* V_R) m_1 m_2
\end{aligned} \quad (\text{B.28})$$

We now identify three types of decay, and give explicit formulas for each.

B.2.1 $Z' \rightarrow N\bar{N}$

For the decay of Z' to two heavy neutrinos N , we have

$$V_L^{N\bar{N}} = -g'_1 c_j^2, \quad V_R^{N\bar{N}} = -g'_1 \quad (\text{B.29})$$

which gives the decay width

$$\Gamma_{Z' \rightarrow N\bar{N}} = g'^2 \frac{\sqrt{m_{Z'}^2 - 4m_N^2}}{4\pi m_{Z'}^2} \left[\frac{1}{6} (1 + c_j^4) (m_{Z'}^2 - m_N^2) + c_j^2 m_N^2 \right] \quad (\text{B.30})$$

B.2.2 $Z' \rightarrow \nu_j \bar{N}$

We consider now the decay of Z' to a heavy neutrino N and a SM neutrino ν_j . We have

$$V_L^{\nu_j \bar{N}} = -g'_1 s_j c_j, \quad V_R^{\nu_j \bar{N}} = 0 \quad (\text{B.31})$$

yielding

$$\Gamma_{Z' \rightarrow \nu_j \bar{N}} = \Gamma_{Z' \rightarrow N \bar{\nu}_j} = g'^2_1 \frac{s_j^2 c_j^2}{48\pi m_{Z'}^5} (2m_{Z'}^4 - m_N^2 (m_{Z'}^2 + m_N^2)) (m_{Z'}^2 - m_N^2) \quad (\text{B.32})$$

B.2.3 $Z' \rightarrow \nu_j \bar{\nu}_j$

For the decay of Z' to two SM neutrinos ν_j , the vertex factors are

$$V_L^{\nu_j \bar{\nu}_j} = -g'_1 s_j^2, \quad V_R^{\nu_j \bar{\nu}_j} = 0 \quad (\text{B.33})$$

giving us

$$\Gamma_{Z' \rightarrow \nu_j \bar{\nu}_j} = g'^2_1 \frac{s_j^4 m_{Z'}}{24\pi} \quad (\text{B.34})$$

B.3 Scalar Decay

We compute the decay widths for a process $h_k \rightarrow \nu_1 \bar{\nu}_2$, where where $\{h_1, h_2, h_3\} = \{H, h, S\}$ the CP-even scalars. The scattering amplitude for this process is given by:

$$\mathcal{M} = \bar{u}_\ell^s(p_1) V v_N^t(p_2) \quad (\text{B.35})$$

where p_j are the 4-momenta for the final neutrino ν_j , $u(v)$ are Dirac (anti-)spinors for spin $s(t)$ and $V = V_L P_L + V_R P_R$, with $V_{L/R}$ a constant depending on signal parameters and $P_{L/R} = \frac{1}{2}(1 \mp \gamma^5)$ the left-/right-handed chirality projection operator. We compute the

squared average amplitude:

$$\begin{aligned}
4\langle|\mathcal{M}|^2\rangle &= \sum_t \sum_s [\bar{u}^s(p_1) (V_L(1-\gamma^5) + V_R(1+\gamma^5)) v^t(p_2)] [\bar{u}^s(p_1) (V_L(1-\gamma^5) + V_R(1+\gamma^5)) v^t(p_2)]^* \\
&= \text{Tr} [(V_L(1-\gamma^5) + V_R(1+\gamma^5)) (\not{p}_2 - m_2) \gamma^0 (V_L(1-\gamma^5) + V_R(1+\gamma^5))^{\dagger} \gamma^0 (\not{p}_1 + m_1)] \\
&= \text{Tr} [(V_L(1-\gamma^5) + V_R(1+\gamma^5)) (\not{p}_2 - m_2) (V_L^*(1+\gamma^5) + V_R^*(1-\gamma^5)) (\not{p}_1 + m_1)] \\
&= \text{Tr} [(V_L(1-\gamma^5) + V_R(1+\gamma^5)) (\not{p}_2) (V_L^*(1+\gamma^5) + V_R^*(1-\gamma^5)) (\not{p}_1)] \\
&\quad - \text{Tr} [(V_L(1-\gamma^5) + V_R(1+\gamma^5)) (m_2) (V_L^*(1+\gamma^5) + V_R^*(1-\gamma^5)) (m_1)] \\
&= \text{Tr} [(V_L(1-\gamma^5) + V_R(1+\gamma^5)) (V_L^*(1-\gamma^5) \not{p}_2 + V_R^*(1+\gamma^5) \not{p}_2) (\not{p}_1)] \\
&\quad - m_1 m_2 \text{Tr} [(V_L(1-\gamma^5) + V_R(1+\gamma^5)) (V_L^*(1+\gamma^5) + V_R^*(1-\gamma^5))] \\
&= 2|V_L|^2 p_{1,\alpha} p_{2,\beta} \text{Tr} [(1-\gamma^5) \gamma^\beta \gamma^\alpha] + 2|V_R|^2 p_{1,\alpha} p_{2,\beta} \text{Tr} [(1+\gamma^5) \gamma^\beta \gamma^\alpha] \\
&\quad - 2V_L V_R^* m_1 m_2 \text{Tr} [(1-\gamma^5)] - 2V_R V_L^* m_1 m_2 \text{Tr} [(1+\gamma^5)] \\
&= 8 \{ (|V_L|^2 + |V_R|^2) (p_1 \cdot p_2) - (V_L V_R^* + V_L^* V_R) m_1 m_2 \} \quad (\text{B.36})
\end{aligned}$$

Using Eq. (B.2) and considering the rest frame of h_k , we obtain for the decay width of process $h_k \rightarrow \nu_1 \bar{\nu}_2$:

$$\Gamma_{h_k \rightarrow \nu_1 \bar{\nu}_2} = \frac{\sqrt{(m_{h_k}^2 - m_1^2 - m_2^2)^2 - 4m_1^2 m_2^2}}{8\pi m_{h_k}^3} \left\{ (|V_L|^2 + |V_R|^2) \frac{m_{h_k}^2 - m_1^2 - m_2^2}{2} - (V_L V_R^* + V_L^* V_R) m_1 m_2 \right\} \quad (\text{B.37})$$

We now proceed to find explicit expressions for each decay mode of h_k .

B.3.1 $h_k \rightarrow N \bar{N}$

For the decay of h_k to two heavy neutrinos N , we have

$$V_L^{N\bar{N}} = -\frac{is_j c_j m_N}{vs_\beta} V_{\varphi 1k}, \quad V_R^{N\bar{N}} = 0 \quad (\text{B.38})$$

yielding the decay width:

$$\Gamma_{h_k \rightarrow N \bar{N}} = \frac{s_j^4 m_N^2}{8\pi m_{h_k}^2 v^2 s_\beta^2} (m_{h_k}^2 - 4m_N^2)^{\frac{3}{2}} |V_{\varphi 1k}|^2 \quad (\text{B.39})$$

B.3.2 $h_k \rightarrow \nu_j \bar{N}$

For h_k decaying to a heavy neutrinos N and a SM neutrinos ν_j , we have

$$V_L^{N\bar{\nu}_j} = -\frac{is_j^2 m_N}{vs_\beta} V_{\varphi 1k}, \quad V_R^{N\bar{N}\bar{\nu}_j} = -\frac{is_j^2 m_N}{vs_\beta} V_{\varphi 1k} \quad (\text{B.40})$$

which gives the decay width:

$$\Gamma_{h_k \rightarrow N\bar{\nu}_j} = \frac{s_j^2 c_j^2 m_N^2}{16\pi m_{h_k}^3 v^2 s_\beta^2} (m_{h_k}^2 - m_N^2)^2 |V_{\varphi 1k}|^2 \quad (\text{B.41})$$

B.3.3 $h_k \rightarrow \ell_j^- \ell_j^+$

For h_k decaying to charged lepton pair $\ell_j^- \ell_j^+$, we have

$$V_L^{\ell_j^- \ell_j^+} = -\frac{iY_{jj}^l}{\sqrt{2}} V_{\varphi 2k}, \quad V_R^{\ell_j^- \ell_j^+} = -\frac{iY_{jj}^l}{\sqrt{2}} V_{\varphi 2k} \quad (\text{B.42})$$

yielding the decay width:

$$\Gamma_{h_k \rightarrow \ell_j^- \ell_j^+} = \frac{|Y_{jj}^l|^2}{16\pi m_{h_k}^2} (m_{h_k}^2 - 4m_{\ell_j})^{\frac{3}{2}} |V_{\varphi 2k}|^2 \quad (\text{B.43})$$

Appendix C

Signal Model Implementation

In the following lines one finds the $2HDM S+Z'+N$ model implementation with the `FeynRules` framework:

```
(* *****  
(* ***** Information ***** *)  
(* *****  
M$ModelName = "2HDM S_Zp3N";  
  
M$Information = {  
    Authors      -> {"Y. Burkard"},  
    Version       -> "2",  
    Date          -> "15.12.2022",  
    Institutions -> {"ETH Zurich; University of Zurich"},  
    Emails         -> {"yburkard@student.ethz.ch"},  
    URLs          -> ""  
};  
  
FeynmanGauge = True;  
  
(* *****  
(* ***** NLO Variables ***** *)  
(* *****  
  
(**FR$LoopSwitches = {{Gf, MW}};  
FR$RmDblExt = { ymb -> MB, ymc -> MC, ymdo -> MD, yme -> Me,  
    ymm -> MMU, yms -> MS, ymt -> MT, ymtau -> MTA, ymup -> MU};***)
```

```

(* ****)
(* ***** vevs ***** *)
(* ****)
(**M$vevs = { {Phi[2],vev} };**)

(* ****)
(* ***** Gauge groups ***** *)
(* ****)
M$GaugeGroups = {
U1Y == {
    Abelian      -> True,
    CouplingConstant -> g1,
    GaugeBoson     -> B,
    Charge         -> Y
},
SU2L == {
    Abelian      -> False,
    CouplingConstant -> gw,
    GaugeBoson     -> Wi,
    StructureConstant -> Eps,
    Representations -> {Ta,SU2D},
    Definitions     -> {Ta[a_,b_,c_]->PauliSigma[a,b,c]/2,
                           FSU2L[i_,j_,k_]:> I Eps[i,j,k]}
},
SU3C == {
    Abelian      -> False,
    CouplingConstant -> gs,
    GaugeBoson     -> G,
    StructureConstant -> f,
    Representations -> {T,Colour},
    SymmetricTensor -> dSUN
},
(******2HDMS_Zp3N*****)
U1X == {
    Abelian      -> True,
    CouplingConstant -> g1p,
    GaugeBoson     -> Bp,
}

```

```

    Charge          -> X
}

(*****END*****)
};

(* ****
Indices      **** *)
(* *****END*****)

IndexRange[Index[SU2W]] = Unfold[Range[3]];
IndexRange[Index[SU2D]] = Unfold[Range[2]];
IndexRange[Index[Gluon]] = NoUnfold[Range[8]];
IndexRange[Index[Colour]] = NoUnfold[Range[3]];
IndexRange[Index[Generation]] = Range[3];
(*****2HDMS_Zp3N*****)
(*IndexRange[Index[CPeven]] = Range[3];*)
IndexRange[Index[Two]] = Range[2];
IndexRange[Index[Three]] = Range[3];
(*****END*****)

IndexStyle[SU2W,      j];
IndexStyle[SU2D,      k];
IndexStyle[Gluon,     a];
IndexStyle[Colour,    m];
IndexStyle[Generation, f];
(*****2HDMS_Zp3N*****)
IndexStyle[Two, p];
IndexStyle[Three, q];
(*****END*****)

(* ****
Interaction orders ***
(* *** (as used by mg5) *** *)
(* *****END*****)

M$InteractionOrderHierarchy = {

```

```

{QCD, 1},
{QED, 2}
};

(* **** Particle classes **** *)
M$ClassesDescription = {

(* Gauge bosons: physical vector fields *)
V[1] == {
  ClassName      -> A,
  SelfConjugate  -> True,
  Mass           -> 0,
  Width          -> 0,
  ParticleName   -> "a",
  PDG            -> 22,
  PropagatorLabel -> "a",
  PropagatorType  -> W,
  PropagatorArrow -> None,
  FullName        -> "Photon"
},
V[2] == {
  ClassName      -> Z,
  SelfConjugate  -> True,
  Mass           -> {MZ, 91.1876},
  Width          -> {WZ, 2.4952},
  ParticleName   -> "Z",
  PDG            -> 23,
  PropagatorLabel -> "Z",
  PropagatorType  -> Sine,
  PropagatorArrow -> None,
  FullName        -> "Z"
},
V[3] == {
  ClassName      -> W,
  SelfConjugate  -> False,
}

```

```

Mass           -> {MW, Internal},
Width          -> {WW, 2.085},
ParticleName   -> "W+",
AntiParticleName -> "W-",
QuantumNumbers -> {Q -> 1},
PDG            -> 24,
PropagatorLabel -> "W",
PropagatorType  -> Sine,
PropagatorArrow  -> Forward,
FullName        -> "W"
},
V[4] == {
  ClassName      -> G,
  SelfConjugate  -> True,
  Indices         -> {Index[Gluon]},
  Mass            -> 0,
  Width           -> 0,
  ParticleName    -> "g",
  PDG             -> 21,
  PropagatorLabel -> "G",
  PropagatorType  -> C,
  PropagatorArrow  -> None,
  FullName        -> "G"
},
(*****2HDMS_Zp3N*****)
V[5] == {
  ClassName      -> Zp,
  SelfConjugate  -> True,
  Indices         -> {},
  Mass            -> {MZp, 500},
  Width           -> {WZp, 80.00},
  ParticleName    -> "Zp",
  PDG             -> 9900032,
  PropagatorLabel -> "Zp",
  PropagatorType  -> Sine,
  PropagatorArrow  -> None,
  FullName        -> "Zp"
},

```

```
(*****END*****)
```

```
(* Ghosts: related to physical gauge bosons *)
U[1] == {
  ClassName      -> ghA,
  SelfConjugate  -> False,
  Ghost          -> A,
  QuantumNumbers -> {GhostNumber -> 1},
  Mass           -> 0,
  Width          -> 0,
  PropagatorLabel -> "uA",
  PropagatorType  -> GhostDash,
  PropagatorArrow -> Forward
},
U[2] == {
  ClassName      -> ghZ,
  SelfConjugate  -> False,
  Ghost          -> Z,
  QuantumNumbers -> {GhostNumber -> 1},
  Mass           -> {MZ,91.1876},
  Width          -> {WZ, 2.4952},
  PropagatorLabel -> "uZ",
  PropagatorType  -> GhostDash,
  PropagatorArrow -> Forward
},
U[31] == {
  ClassName      -> ghWp,
  SelfConjugate  -> False,
  Ghost          -> W,
  QuantumNumbers -> {GhostNumber -> 1, Q -> 1},
  Mass           -> {MW,Internal},
  Width          -> {WW, 2.085},
  PropagatorLabel -> "uWp",
  PropagatorType  -> GhostDash,
  PropagatorArrow -> Forward
},
U[32] == {
  ClassName      -> ghWm,
```

```

SelfConjugate    -> False,
Ghost            -> Wbar,
QuantumNumbers   -> {GhostNumber -> 1, Q -> -1},
Mass             -> {MW, Internal},
Width            -> {WW, 2.085},
PropagatorLabel -> "uWm",
PropagatorType   -> GhostDash,
PropagatorArrow  -> Forward
},
U[4] == {
ClassName        -> ghG,
SelfConjugate    -> False,
Indices          -> {Index[Gluon]},
Ghost            -> G,
PDG              -> 82,
QuantumNumbers   -> {GhostNumber -> 1},
Mass             -> 0,
Width            -> 0,
PropagatorLabel -> "uG",
PropagatorType   -> GhostDash,
PropagatorArrow  -> Forward
},
(*****2HDMs_Zp3N*****)
U[5] == {
ClassName        -> ghZp,
SelfConjugate    -> False,
Indices          -> {},
Ghost            -> Zp,
QuantumNumbers   -> {GhostNumber -> 1},
Mass             -> {MZp, Internal},
Width            -> {WZp, 80.00},
PropagatorLabel -> "uZp",
PropagatorType   -> GhostDash,
PropagatorArrow  -> Forward
},
(*****END*****)

(* Gauge bosons: unphysical vector fields *)

```

```

V[11] == {
    ClassName      -> B,
    Unphysical     -> True,
    SelfConjugate -> True,
    Definitions   -> { B[mu_] -> -sw Z[mu]+cw A[mu] }
},
V[12] == {
    ClassName      -> Wi,
    Unphysical     -> True,
    SelfConjugate -> True,
    Indices        -> {Index[SU2W]},
    FlavorIndex   -> SU2W,
    Definitions   -> { Wi[mu_,1] -> (Wbar[mu]+W[mu])/Sqrt[2],
                           Wi[mu_,2] -> (Wbar[mu]-W[mu])/(I*Sqrt[2]),
                           Wi[mu_,3] -> cw Z[mu] + sw A[mu] }
},
(*****2HDMS_Zp3N*****)
V[6] == {
    ClassName      -> Bp,
    SelfConjugate -> True,
    Indices        -> {},
    Definitions   -> {Bp[mu_] -> Zp[mu]},
    Unphysical     -> True
},
(*****END*****)

(* Ghosts: related to unphysical gauge bosons *)
U[11] == {
    ClassName      -> ghB,
    Unphysical     -> True,
    SelfConjugate -> False,
    Ghost          -> B,
    Definitions   -> { ghB -> -sw ghZ + cw ghA}
},
U[12] == {
    ClassName      -> ghWi,
    Unphysical     -> True,
    SelfConjugate -> False,
}

```

```

Ghost          -> Wi,
Indices        -> {Index[SU2W]}, 
FlavorIndex    -> SU2W,
Definitions    -> { ghWi[1] -> (ghWp+ghWm)/Sqrt[2],
                      ghWi[2] -> (ghWm-ghWp)/(I*Sqrt[2]),
                      ghWi[3] -> cw ghZ+sw ghA}
},
(*****2HDMS_Zp3N*****)

U[6] == {
  ClassName      -> ghBp,
  SelfConjugate  -> False,
  Definitions    -> {ghBp -> ghZp},
  Indices        -> {},
  Unphysical     -> True,
  Ghost          -> Bp
},
(*****END*****)

(** Neutrino fields of 2HDMS_Zp3N**)
(*physical*)

F[1] == {
  ClassName      -> nL,
  ClassMembers   -> {nLe,nLm,nLt},
  Indices        -> {Index[Generation]},
  FlavorIndex    -> Generation,
  SelfConjugate  -> False,
  QuantumNumbers -> {LeptonNumber -> 1, Q -> 0},
  (*Mass          -> {MnL,{MnLe, 0},{MnLm, 0},{MnLt, 0}},*)
  Mass           -> 0,
  Width          -> 0,
  PropagatorLabel -> {"nL", "nule", "nulm", "nult"}, 
  (*PropagatorLabel -> {"v", "ve", "vm", "vt"},*)
  PropagatorType  -> S,
  PropagatorArrow -> Forward,
  PDG            -> {12,14,16},
  Unphysical     -> False,
  ParticleName    -> {"nLe","nLm","nLt"}, 
  AntiParticleName -> {"nLe~","nLm~","nLt~"}, 
  (*ParticleName   -> {"ve","vm","vt"},*)
}

```

```

(*AntiParticleName -> {"ve~","vm~","vt~"},*)
  FullName      -> {"Electron-neutrino", "Mu-neutrino", "Tau-neutrino"}
},
F[6] == {
  ClassName      -> nH,
  ClassMembers   -> {nH1,nH2,nH3},
  Indices        -> {Index[Generation]},
  FlavorIndex    -> Generation,
  SelfConjugate  -> False,
  QuantumNumbers -> {LeptonNumber -> 1, Q -> 0},
  Mass           -> {MnH,{MnH1, 200.00},{MnH2, 200.00},{MnH3, 200.00}},
  Width          -> 10^(-13),
  PropagatorLabel -> {"nH","nH1","nH2","nH3"},
  PropagatorType  -> Straight,
  PropagatorArrow -> Forward,
  PDG            -> {9910012,9910014,9910016},
  Unphysical      -> False,
  ParticleName    -> {"nH1","nH2","nH3"},
  AntiParticleName -> {"nH1~","nH2~","nH3~"},
  FullName        -> {"Heavy neutrino 1", "Heavy neutrino 2", "Heavy neutrino 3"}
},
(*unphysical*)
F[17] == {
  ClassName      -> nuSM,
  ClassMembers   -> {nuSMe, nuSMm, nuSMt},
  Indices        -> {Index[Generation]},
  FlavorIndex    -> Generation,
  SelfConjugate  -> False,
  FullName        -> {"Electron-neutrino (unphysical)",
    "Mu-neutrino (unphysical)",
    "Tau-neutrino (unphysical)" },
  Unphysical      -> True,
  Definitions     -> {nuSM[sp_,ff_] :> Module[{ff1,ff2,sp1,sp2},
    ULtl[ff,ff1] ProjM[sp,sp1] nL[sp1,ff1] + ULtr[ff,ff2] ProjM[sp,sp2] nH[sp2,ff2]]}
},
F[18] == {
  ClassName      -> nV,
  ClassMembers   -> {nV1,nV2,nV3},

```

```

Indices          -> {Index[Generation]},  

FlavorIndex     -> Generation,  

SelfConjugate   -> False,  

QuantumNumbers  -> {Y -> 0, X -> -1},  

FullName        -> {"Vector-like neutrino 1 (unphysical)",  

"Vector-like neutrino 2 (unphysical)", "Vector-like neutrino 3 (unphysical)"},  

Unphysical      -> True,  

Definitions     -> {nV[sp_,ff_] :> Module[{ff1,ff2,ff3,sp1,sp2,sp3},  

ULbl[ff,ff1] ProjM[sp,sp1] nL[sp1,ff1]+ ULbr[ff,ff2] ProjM[sp,sp2] nH[sp2,ff2]  

+ UR[ff,ff3] ProjP[sp,sp3] nH[sp3,ff3]]}  

},  

(*Right-handed component of unphysical vector-like neutrino*)  

F[19] == {  

  ClassName       -> nVR,  

  ClassMembers    -> {nVR},  

  Indices         -> {Index[Generation]},  

  FlavorIndex    -> Generation,  

  SelfConjugate   -> False,  

  QuantumNumbers  -> {Y -> 0, X -> -1},  

  FullName        -> {"RH component of vector-like neutrino (unphysical)"},  

  Unphysical      -> True,  

  Definitions     -> {nVR[sp_,ff_] :> Module[{sp2}, ProjP[sp,sp2] nV[sp2,ff]]}  

},  

(** End neutrino fields of 2HDMS_Zp3N ***)  

(* Fermions: physical fields *)  

F[2] == {  

  ClassName       -> l,  

  ClassMembers    -> {e, mu, ta},  

  Indices         -> {Index[Generation]},  

  FlavorIndex    -> Generation,  

  SelfConjugate   -> False,  

  Mass            -> {Ml, {Me,5.11*^-4}, {MMU,0.10566}, {MTA,1.777}},  

  Width           -> 0,  

  QuantumNumbers  -> {Q -> -1, LeptonNumber -> 1},  

  PropagatorLabel -> {"l", "e", "mu", "ta"},  

  PropagatorType  -> Straight,  

  PropagatorArrow -> Forward,  

  PDG             -> {11, 13, 15},

```

```

    ParticleName      -> {"e-", "mu-", "ta-"},  

    AntiParticleName -> {"e+", "mu+", "ta+"},  

    FullName         -> {"Electron", "Muon", "Tau"}  

},  

F[3] == {  

    ClassName       -> uq,  

    ClassMembers    -> {u, c, t},  

    Indices          -> {Index[Generation], Index[Colour]},  

    FlavorIndex     -> Generation,  

    SelfConjugate   -> False,  

    Mass             -> {Mu, {MU, 2.55*^-3}, {MC, 1.27}, {MT, 172}},  

    Width            -> {0, 0, {WT, 1.50833649}},  

    QuantumNumbers  -> {Q -> 2/3},  

    PropagatorLabel -> {"uq", "u", "c", "t"},  

    PropagatorType  -> Straight,  

    PropagatorArrow -> Forward,  

    PDG              -> {2, 4, 6},  

    ParticleName     -> {"u", "c", "t"},  

    AntiParticleName -> {"u~", "c~", "t~"},  

    FullName         -> {"u-quark", "c-quark", "t-quark"}  

},  

F[4] == {  

    ClassName       -> dq,  

    ClassMembers    -> {d, s, b},  

    Indices          -> {Index[Generation], Index[Colour]},  

    FlavorIndex     -> Generation,  

    SelfConjugate   -> False,  

    Mass             -> {Md, {MD, 5.04*^-3}, {MS, 0.101}, {MB, 4.7}},  

    Width            -> 0,  

    QuantumNumbers  -> {Q -> -1/3},  

    PropagatorLabel -> {"dq", "d", "s", "b"},  

    PropagatorType  -> Straight,  

    PropagatorArrow -> Forward,  

    PDG              -> {1, 3, 5},  

    ParticleName     -> {"d", "s", "b"},  

    AntiParticleName -> {"d~", "s~", "b~"},  

    FullName         -> {"d-quark", "s-quark", "b-quark"}  

},

```

```

(* Fermions: unphysical fields *)

F[11] == {
  ClassName      -> LL,
  Unphysical     -> True,
  Indices        -> {Index[SU2D], Index[Generation]},
  FlavorIndex    -> SU2D,
  SelfConjugate   -> False,
  QuantumNumbers -> {Y -> -1/2, X -> 0},
  Definitions    -> { LL[sp1_,1,ff_] :> Module[{sp2}, ProjM[sp1,sp2] nuSM[sp2,ff]], 
    LL[sp1_,2,ff_] :> Module[{sp2}, ProjM[sp1,sp2] 1[sp2,ff]] }
},
F[12] == {
  ClassName      -> 1R,
  Unphysical     -> True,
  Indices        -> {Index[Generation]},
  FlavorIndex    -> Generation,
  SelfConjugate   -> False,
  QuantumNumbers -> {Y -> -1, X -> 0},
  Definitions    -> { 1R[sp1_,ff_] :> Module[{sp2}, ProjP[sp1,sp2] 1[sp2,ff]] }
},
F[13] == {
  ClassName      -> QL,
  Unphysical     -> True,
  Indices        -> {Index[SU2D], Index[Generation], Index[Colour]},
  FlavorIndex    -> SU2D,
  SelfConjugate   -> False,
  QuantumNumbers -> {Y -> 1/6, X -> 1/3},
  Definitions    -> {
    QL[sp1_,1,ff_,cc_] :> Module[{sp2}, ProjM[sp1,sp2] uq[sp2,ff,cc]],
    QL[sp1_,2,ff_,cc_] :> Module[{sp2,ff2}, CKM[ff,ff2] ProjM[sp1,sp2] dq[sp2,ff2,cc]]}
},
F[14] == {
  ClassName      -> uR,
  Unphysical     -> True,
  Indices        -> {Index[Generation], Index[Colour]},
  FlavorIndex    -> Generation,
  SelfConjugate   -> False,
  QuantumNumbers -> {Y -> 2/3, X -> 1/3},
}

```

```

    Definitions      -> {uR[sp1_,ff_,cc_] :> Module[{sp2}, ProjP[sp1,sp2] uq[sp2,ff,cc]]}
},
F[15] == {
  ClassName      -> dR,
  Unphysical     -> True,
  Indices         -> {Index[Generation], Index[Colour]},
  FlavorIndex    -> Generation,
  SelfConjugate   -> False,
  QuantumNumbers  -> {Y -> -1/3, X -> 1/3},
  Definitions     -> {dR[sp1_,ff_,cc_] :> Module[{sp2}, ProjP[sp1,sp2] dq[sp2,ff,cc]]}
},
(** Higgs fields of 2HDMs_Zp3N **)
(**physical scalars**)
(*3 real CP-even fields*)
S[1] == {
  ClassName      -> CPevenH,
  ClassMembers   -> {hH, h, hS},
  Indices         -> {Index[Three]},
  FlavorIndex    -> Three,
  SelfConjugate   -> True,
  Mass           -> {MCPevenH, {MhH, 20000}, {Mh,125}, {MhS, 20000}},
  Width          -> {{WhH,0.006382339}, {Wh,0.00407}, {WhS,3.4952}},
  PropagatorLabel -> {"CPevenH", "hH", "h", "hS"},
  PropagatorType  -> D,
  PropagatorArrow -> None,
  PDG            -> {35, 25, 36},
  ParticleName    -> {"hH", "h" , "hS"},
  FullName        -> {"non-SM heavy Higgs boson H",
  "SM Higgs boson h", "non-SM heavy Higgs boson S"}
},
(*SM complex and real CP-odd fields*)
S[2] == {
  ClassName      -> G0,
  SelfConjugate   -> True,
  Goldstone      -> Z,
  Mass           -> {MZ, 91.1876},
  Width          -> {WZ, 2.4952},
  PropagatorLabel -> "Go",

```

```

PropagatorType -> D,
PropagatorArrow -> None,
PDG           -> 250,
ParticleName   -> "G0",
FullName       -> "G0"
},
S[3] == {
  ClassName      -> GP,
  SelfConjugate  -> False,
  Goldstone      -> W,
  Mass           -> {MW, Internal},
  QuantumNumbers -> {Q -> 1},
  Width          -> {WW, 2.085},
  PropagatorLabel -> "GP",
  PropagatorType  -> D,
  PropagatorArrow  -> None,
  PDG            -> 251,
  ParticleName    -> "G+",
  AntiParticleName -> "G-",
  FullName        -> "GP"
},
(*prime (non-SM) complex and real CP-odd fields*)
S[5] == {
  ClassName      -> hA,
  SelfConjugate  -> True,
  Mass           -> {MhA, 20000},
  Width          -> {WhA, 0.006382339},
  PropagatorLabel -> "hA",
  PropagatorType  -> D,
  PropagatorArrow  -> None,
  PDG            -> 40,
  ParticleName    -> "hA",
  FullName        -> "hA"
},
S[6] == {
  ClassName      -> HP,
  SelfConjugate  -> False,
  Mass           -> {MHP, 20000},

```

```

QuantumNumbers  -> {Q -> 1},
Width          -> {WHP, 0.006382339},
PropagatorLabel -> "chHp",
PropagatorType   -> D,
PropagatorArrow   -> None,
PDG             -> 37,
ParticleName     -> "H+",
AntiParticleName -> "H-",
FullName         -> "chHp"
},
(*S real CP-odd field*)
S[8] == {
  ClassName      -> GSo,
  SelfConjugate  -> True,
  Goldstone      -> Zp,
  Mass            -> {MZp, 270},
  Width           -> {WZp, 80.00},
  PropagatorLabel -> "GSo",
  PropagatorType   -> D,
  PropagatorArrow   -> None,
  PDG             -> 350,
  ParticleName    -> "GSo",
  FullName        -> "GSo"
},
(**unphysical scalars**)
(*phi1*)
S[10] == {
  ClassName      -> rho1,
  SelfConjugate  -> False,
  Unphysical     -> True,
  Definitions    -> {rho1 -> Vrho[1,1] GP + Vrho[1,2] HP}
},
S[11] == {
  ClassName      -> chiH1,
  SelfConjugate  -> True,
  Unphysical     -> True,
  Definitions    -> {chiH1 -> Vchi[1,1] G0 + Vchi[1,2] GSo + Vchi[1,3] hA}
},

```

```

S[12] == {
    ClassName      -> varphi1,
    SelfConjugate  -> True,
    Unphysical     -> True,
    Definitions    -> {varphi1 -> Vphi[1,1] hH + Vphi[1,2] h + Vphi[1,3] hS}
},
S[13] == {
    ClassName      -> Phi1,
    Unphysical     -> True,
    Indices        -> {Index[SU2D]}, 
    FlavorIndex   -> SU2D,
    SelfConjugate  -> False,
    QuantumNumbers -> {Y -> 1/2, X -> -1},
    Definitions    -> {Phi1[1] -> -I rho1,
                          Phi1[2] -> (vev*sbeta + varphi1 + I chiH1)/Sqrt[2]}
},
(*phi2*)
S[14] == {
    ClassName      -> rho2,
    SelfConjugate  -> False,
    Unphysical     -> True,
    Definitions    -> {rho2 -> Vrho[2,1] GP + Vrho[2,2] HP}
},
S[15] == {
    ClassName      -> chiH2,
    SelfConjugate  -> True,
    Unphysical     -> True,
    Definitions    -> {chiH2 -> Vchi[2,1] G0 + Vchi[2,2] GS0 + Vchi[2,3] hA}
},
S[16] == {
    ClassName      -> varphi2,
    SelfConjugate  -> True,
    Unphysical     -> True,
    Definitions    -> {varphi2 -> Vphi[2,1] hH + Vphi[2,2] h + Vphi[2,3] hS}
},
S[17] == {
    ClassName      -> Phi2,
    Unphysical     -> True,
}

```

```

Indices      -> {Index[SU2D]},  

FlavorIndex  -> SU2D,  

SelfConjugate -> False,  

QuantumNumbers -> {Y -> 1/2, X -> 0},  

Definitions   -> {Phi2[1] -> -I rho2,  

Phi2[2] -> (vev*cbeta + varphi2 + I chiH2)/Sqrt[2]}  

},  

(*phiS*)  

S[18] == {  

ClassName     -> chiHS,  

SelfConjugate -> True,  

Unphysical    -> True,  

Definitions   -> {chiHS -> Vchi[3,1] G0 + Vchi[3,2] GS0 + Vchi[3,3] hA}  

},  

S[19] == {  

ClassName     -> varphiS,  

SelfConjugate -> True,  

Unphysical    -> True,  

Definitions   -> {varphiS -> Vphi[3,1] hH + Vphi[3,2] h + Vphi[3,3] hS}  

},  

S[20] == {  

ClassName     -> PhiS,  

Unphysical    -> True,  

SelfConjugate -> False,  

QuantumNumbers -> {Y -> 0, X -> 1},  

Definitions   -> {PhiS -> (vevS + varphiS + I chiHS)/Sqrt[2]}  

}  

(** End Higgs fields of 2HDMs_Zp3N ***)  

};  

(* *****  

(* *****      Gauge      ***** *)  

(* *****      Parameters  ***** *)  

(* *****      (FeynArts) ***** *)  

(* *****  

GaugeXi[ V[1] ] = GaugeXi[A];

```

```

GaugeXi[ V[2] ] = GaugeXi[Z];
GaugeXi[ V[3] ] = GaugeXi[W];
GaugeXi[ V[4] ] = GaugeXi[G];
GaugeXi[ S[1] ] = 1;
GaugeXi[ S[2] ] = GaugeXi[Z];
GaugeXi[ S[3] ] = GaugeXi[W];
GaugeXi[ U[1] ] = GaugeXi[A];
GaugeXi[ U[2] ] = GaugeXi[Z];
GaugeXi[ U[31] ] = GaugeXi[W];
GaugeXi[ U[32] ] = GaugeXi[W];
GaugeXi[ U[4] ] = GaugeXi[G];
(*****2HDMS_Zp3N*****)
GaugeXi[ V[5] ] = GaugeXi[Zp];
GaugeXi[ S[4] ] = 1;
GaugeXi[ S[5] ] = GaugeXi[Zp];
GaugeXi[ U[5] ] = GaugeXi[Zp];
(*****END*****)

(* **** *)
(* ***** Parameters ***** *)
(* **** *)

(* The loop coefficient HEFT *)
sert[x_] := 1+ 7/30 x + 2/21 x^2 + 26/525 x^3;

M$Parameters = {

(* External parameters *)
aEWM1 == {
ParameterType    -> External,
BlockName        -> SMINPUTS,
OrderBlock       -> 1,
Value            -> 127.9,
InteractionOrder -> {QED,-2},
Description       -> "Inverse of the EW coupling constant at the Z pole"
},
Gf == {
}
}

```

```

ParameterType      -> External,
BlockName         -> SMINPUTS,
OrderBlock        -> 2,
Value             -> 1.16637*^-5,
InteractionOrder -> {QED,2},
TeX               -> Subscript[G,f],
Description       -> "Fermi constant"
},
aS    == {
ParameterType      -> External,
BlockName         -> SMINPUTS,
OrderBlock        -> 3,
Value             -> 0.1184,
InteractionOrder -> {QCD,2},
TeX               -> Subscript[\[Alpha],s],
Description       -> "Strong coupling constant at the Z pole"
},
ymdo == {
ParameterType -> External,
BlockName     -> YUKAWA,
OrderBlock    -> 1,
Value         -> 5.04*^-3,
Description   -> "Down Yukawa mass"
},
ymup == {
ParameterType -> External,
BlockName     -> YUKAWA,
OrderBlock    -> 2,
Value         -> 2.55*^-3,
Description   -> "Up Yukawa mass"
},
yms == {
ParameterType -> External,
BlockName     -> YUKAWA,
OrderBlock    -> 3,
Value         -> 0.101,
Description   -> "Strange Yukawa mass"
},

```

```

ymc == {
    ParameterType -> External,
    BlockName      -> YUKAWA,
    OrderBlock     -> 4,
    Value          -> 1.27,
    Description    -> "Charm Yukawa mass"
},
ymb == {
    ParameterType -> External,
    BlockName      -> YUKAWA,
    OrderBlock     -> 5,
    Value          -> 4.7,
    Description    -> "Bottom Yukawa mass"
},
ymt == {
    ParameterType -> External,
    BlockName      -> YUKAWA,
    OrderBlock     -> 6,
    Value          -> 172,
    Description    -> "Top Yukawa mass"
},
yme == {
    ParameterType -> External,
    BlockName      -> YUKAWA,
    OrderBlock     -> 11,
    Value          -> 5.11*^-4,
    Description    -> "Electron Yukawa mass"
},
ymm == {
    ParameterType -> External,
    BlockName      -> YUKAWA,
    OrderBlock     -> 13,
    Value          -> 0.10566,
    Description    -> "Muon Yukawa mass"
},
ymtau == {
    ParameterType -> External,
    BlockName      -> YUKAWA,

```

```

OrderBlock    -> 15,
Value         -> 1.777,
Description   -> "Tau Yukawa mass"
},
cab1 == {
  ParameterType -> External,
  BlockName     -> CKMBLOCK,
  OrderBlock    -> 1,
  Value         -> 0.227736,
  TeX          -> Subscript[\[Theta], c],
  Description   -> "Cabibbo angle"
},
(* Internal Parameters *)
aEW == {
  ParameterType -> Internal,
  Value         -> 1/aEWM1,
  InteractionOrder -> {QED,2},
  TeX          -> Subscript[\[Alpha], EW],
  Description   -> "Electroweak coupling contant"
},
MW == {
  ParameterType -> Internal,
  Value         -> Sqrt[MZ^2/2+Sqrt[MZ^4/4-Pi/Sqrt[2]*aEW/Gf*MZ^2]],
  TeX          -> Subscript[M,W],
  Description   -> "W mass"
},
sw2 == {
  ParameterType -> Internal,
  Value         -> 1-(MW/MZ)^2,
  Description   -> "Squared Sin of the Weinberg angle"
},
ee == {
  ParameterType -> Internal,
  Value         -> Sqrt[4 Pi aEW],
  InteractionOrder -> {QED,1},
  TeX          -> e,
  Description   -> "Electric coupling constant"
},

```

```

cw == {
    ParameterType -> Internal,
    Value         -> Sqrt[1-sw2],
    TeX          -> Subscript[c,w],
    Description   -> "Cosine of the Weinberg angle"
},
sw == {
    ParameterType -> Internal,
    Value         -> Sqrt[sw2],
    TeX          -> Subscript[s,w],
    Description   -> "Sine of the Weinberg angle"
},
gw == {
    ParameterType   -> Internal,
    Definitions     -> {gw->ee/sw},
    InteractionOrder -> {QED,1},
    TeX            -> Subscript[g,w],
    Description     -> "Weak coupling constant at the Z pole"
},
g1 == {
    ParameterType   -> Internal,
    Definitions     -> {g1->ee/cw},
    InteractionOrder -> {QED,1},
    TeX            -> Subscript[g,1],
    Description     -> "U(1)Y coupling constant at the Z pole"
},
gs == {
    ParameterType   -> Internal,
    Value           -> Sqrt[4 Pi aS],
    InteractionOrder -> {QCD,1},
    TeX            -> Subscript[g,s],
    ParameterName   -> G,
    Description     -> "Strong coupling constant at the Z pole"
},
yl == {
    ParameterType   -> Internal,
    Indices         -> {Index[Generation], Index[Generation]},
    Definitions     -> {yl[i_?NumericQ, j_?NumericQ] :> 0 /; (i != j)},
}

```

```

Value           -> {yl[1,1] -> Sqrt[2] yme / (vev*cbeta),
yl[2,2] -> Sqrt[2] ymm / (vev*cbeta),
yl[3,3] -> Sqrt[2] ymtau / (vev*cbeta)},
InteractionOrder -> {QED, 1},
ParameterName   -> {yl[1,1] -> ye, yl[2,2] -> ym, yl[3,3] -> ytau},
TeX            -> Superscript[y, 1],
Description     -> "Lepton Yukawa couplings"
},
yu == {
ParameterType  -> Internal,
Indices        -> {Index[Generation], Index[Generation]},
Definitions   -> {yu[i_?NumericQ, j_?NumericQ] :> 0 /; (i != j)},
Value          -> {yu[1,1] -> Sqrt[2] ymup/(vev*cbeta),
yu[2,2] -> Sqrt[2] ymc/(vev*cbeta),
yu[3,3] -> Sqrt[2] ymt/(vev*cbeta)},
InteractionOrder -> {QED, 1},
ParameterName   -> {yu[1,1] -> yup, yu[2,2] -> yc, yu[3,3] -> yt},
TeX            -> Superscript[y, u],
Description     -> "Up-type Yukawa couplings"
},
yd == {
ParameterType  -> Internal,
Indices        -> {Index[Generation], Index[Generation]},
Definitions   -> {yd[i_?NumericQ, j_?NumericQ] :> 0 /; (i != j)},
Value          -> {yd[1,1] -> Sqrt[2] ymdo/(vev*cbeta),
yd[2,2] -> Sqrt[2] yms/(vev*cbeta),
yd[3,3] -> Sqrt[2] ymb/(vev*cbeta)},
InteractionOrder -> {QED, 1},
ParameterName   -> {yd[1,1] -> ydo, yd[2,2] -> ys, yd[3,3] -> yb},
TeX            -> Superscript[y, d],
Description     -> "Down-type Yukawa couplings"
},
(* N. B. : only Cabibbo mixing! *)
CKM == {
ParameterType -> Internal,
Indices        -> {Index[Generation], Index[Generation]},
Unitary        -> True,
Value          -> {CKM[1,1] -> Cos[cabi], CKM[1,2] -> Sin[cabi], CKM[1,3] -> 0,
}

```

```

CKM[2,1] -> -Sin[cabi], CKM[2,2] -> Cos[cabi], CKM[2,3] -> 0,
CKM[3,1] -> 0, CKM[3,2] -> 0, CKM[3,3] -> 1},
TeX -> Superscript[V,CKM],
Description -> "CKM-Matrix"
},
(*****2HDMS_Zp3N*****)
(*U1X gauge symmetry*)
g1p == {
ParameterType -> External,
BlockName -> BSMIMPUTS,
InteractionOrder -> {QED,1},
TeX -> Subscript[g,1p],
Value -> 0.2,
Description -> "U(1)_X coupling constant at the Zp pole"
},
(*neutrino sector*)
alphaE == {
ParameterType -> External,
BlockName -> BSMIMPUTS,
TeX -> Subscript[\[Alpha],e],
Value -> 0.1,
Description -> "Electron-1 mixing angle"
},
alphaMu == {
ParameterType -> External,
BlockName -> BSMIMPUTS,
TeX -> Subscript[\[Alpha],\[Mu]],
Value -> 0.1,
Description -> "Muon-2 mixing angle"
},
alphaTau == {
ParameterType -> External,
BlockName -> BSMIMPUTS,
TeX -> Subscript[\[Alpha],\[Tau]],
Value -> 0.1,
Description -> "Tau-3 mixing angle"
},
YukN == {

```

```

ParameterType -> Internal,
Indices       -> {Index[Generation],Index[Generation]},
Definitions -> {YukN[i_?NumericQ, j_?NumericQ] :> 0 /; (i != j)},
Value      -> {YukN[1,1] -> Sqrt[2]* Sin[alphaE]*MnH1/(vev*sbeta),
                  YukN[2,2] -> Sqrt[2]* Sin[alphaMu]*MnH1/(vev*sbeta),
                  YukN[3,3] -> Sqrt[2]* Sin[alphaTau]*MnH1/(vev*sbeta)},
InteractionOrder -> {QED, 1},
Description -> "Yukawa neutrino matrix"
},
MNN == {
ParameterType -> Internal,
Indices       -> {Index[Generation],Index[Generation]},
Definitions -> {MNN[i_?NumericQ, j_?NumericQ] :> 0 /; (i != j)},
Value      -> {MNN[1,1] -> Cos[alphaE]*MnH1,
                  MNN[2,2] -> Cos[alphaMu]*MnH2,
                  MNN[3,3] -> Cos[alphaTau]*MnH3},
InteractionOrder -> {QED, 1},
Description -> "Dirac heavy neutrino matrix"
},
ULtl == {
ParameterType -> Internal,
Indices       -> {Index[Generation], Index[Generation]},
Definitions      -> {
ULtl[1,1] -> Cos[alphaE],
ULtl[1,2] -> 0,
ULtl[1,3] -> 0,
ULtl[2,1] -> 0,
ULtl[2,2] -> Cos[alphaMu],
ULtl[2,3] -> 0,
ULtl[3,1] -> 0,
ULtl[3,2] -> 0,
ULtl[3,3] -> Cos[alphaTau]},
Description -> "Projection of LH physical light neutrinos
onto LH unphysical neutrinos"
},
ULtr == {
ParameterType -> Internal,
Indices       -> {Index[Generation], Index[Generation]},

```

```

Definitions      -> {
ULtr[1,1] -> Sin[alphaE],
ULtr[1,2] -> 0,
ULtr[1,3] -> 0,
ULtr[2,1] -> 0,
ULtr[2,2] -> Sin[alphaMu],
ULtr[2,3] -> 0,
ULtr[3,1] -> 0,
ULtr[3,2] -> 0,
ULtr[3,3] -> Sin[alphaTau]},
Description -> "Projection of physical heavy neutrinos
onto LH unphysical neutrinos"
},

ULbl == {
ParameterType -> Internal,
Indices      -> {Index[Generation], Index[Generation]},
Definitions      -> {
ULbl[1,1] -> -Sin[alphaE],
ULbl[1,2] -> 0,
ULbl[1,3] -> 0,
ULbl[2,1] -> 0,
ULbl[2,2] -> -Sin[alphaMu],
ULbl[2,3] -> 0,
ULbl[3,1] -> 0,
ULbl[3,2] -> 0,
ULbl[3,3] -> -Sin[alphaTau]},
Description -> "Projection of LH physical light neutrinos
onto unphysical vector-like neutrinos"
},

ULbr == {
ParameterType -> Internal,
Indices      -> {Index[Generation], Index[Generation]},
Definitions      -> {
ULbr[1,1] -> Cos[alphaE],
ULbr[1,2] -> 0,
ULbr[1,3] -> 0,
ULbr[2,1] -> 0,
ULbr[2,2] -> Cos[alphaMu],
}
}

```

```

ULbr[2,3] -> 0,
ULbr[3,1] -> 0,
ULbr[3,2] -> 0,
ULbr[3,3] -> Cos[alphaTau}],
Description -> "Projection of physical heavy light neutrinos
onto unphysical vector-like neutrinos"
},
UR == {
ParameterType -> Internal,
Indices -> {Index[Generation], Index[Generation]},
Definitions -> {
UR[1,1] -> 1, UR[1,2] -> 0, UR[1,3] -> 0,
UR[2,1] -> 0, UR[2,2] -> 1, UR[2,3] -> 0,
UR[3,1] -> 0, UR[3,2] -> 0, UR[3,3] -> 1},
Description -> "Projection of RH physical heavy neutrinos
onto RH unphysical vector-like neutrinos"
},
(*Higgs sector*)
vev == {
ParameterType -> Internal,
InteractionOrder -> {QED,-1},
Value -> 2*MW*sW/eW,
Description -> "SM vacuum expectation value"
},
vevS == {
ParameterType -> Internal,
InteractionOrder -> {QED,-1},
Value -> MZp/(2*g1p),
Description -> "Complex scalar vacuum expectation value"
},
betaH == {
ParameterType -> External,
BlockName -> BSMIMPUTS,
Value -> 0.1,
TeX -> \Beta,
Description -> "beta"
},
sbeta == {

```

```

ParameterType    -> Internal,
Value          -> Sin[betaH],
TeX            -> Subscript[s,\[Beta]],
Description     -> "sin beta"
},
cbeta == {
ParameterType    -> Internal,
Value          -> Cos[betaH],
TeX            -> Subscript[c,\[Beta]],
Description     -> "cos beta"
},
tbeta == {
ParameterType    -> Internal,
Value          -> sbeta/cbeta,
TeX            -> Subscript[t,\[Beta]],
Description     -> "tan beta (v1/v2)"
},
lam1 == {
ParameterType    -> Internal,
Definitions     -> {lam1 ->
(1/(2 vev^2 sbeta^2))((cbeta^2 vevS^2 / (vev^2 sbeta^2 cbeta^2 + vevS^2))MhA^2
- Vphi[1,1]^2 MhH^2 - Vphi[1,2]^2 Mh^2 - Vphi[1,3]^2 MhS^2)},
InteractionOrder -> {QED, 2},
Description      -> "Higgs 1 (non-SM) quartic coupling"
},
lam2 == {
ParameterType    -> Internal,
Definitions     -> {lam2 ->
(1/(2 vev^2 cbeta^2))((sbeta^2 vevS^2 / (vev^2 sbeta^2 cbeta^2 + vevS^2))MhA^2
- Vphi[2,1]^2 MhH^2 - Vphi[2,2]^2 Mh^2 - Vphi[2,3]^2 MhS^2)},
InteractionOrder -> {QED, 2},
Description      -> "Higgs 2 (SM) quartic coupling"
},
lamS == {
ParameterType    -> Internal,
Definitions     -> {lamS ->
(1/(2 vevS^2))((vev^2 sbeta^2 cbeta^2 / (vev^2 sbeta^2 cbeta^2 + vevS^2))MhA^2
- Vphi[3,1]^2 MhH^2 - Vphi[3,2]^2 Mh^2 - Vphi[3,3]^2 MhS^2)},

```

```

InteractionOrder -> {QED, 2},
Description      -> "Complex scalar quartic coupling"
},
lamD == {
ParameterType   -> Internal,
Definitions     -> {lamD ->
(1/vev^2)((vevS^2/(vev^2 sbeta^2 cbeta^2 + vevS^2))*MhA^2 - (1/(sbeta*cbeta))
(Vphi[1,1]*Vphi[2,1]*MhH^2 + Vphi[1,2]*Vphi[2,2]*Mh^2 + Vphi[1,3]*Vphi[2,3]*MhS^2)
-2*MHP^2)},
InteractionOrder -> {QED, 2},
Description      -> "1122 quartic coupling"
},
lamM == {
ParameterType   -> Internal,
Definitions     -> {lamM ->
(2/vev^2)(MHP^2 - (vevS^2 / (vev^2 sbeta^2 cbeta^2 + vevS^2)) MhA^2)},
InteractionOrder -> {QED, 2},
Description      -> "1221 quartic coupling"
},
lamS1 == {
ParameterType   -> Internal,
Definitions     -> {lamS1 ->
-((1/(vev*vevS*sbeta))(Vphi[1,1]*Vphi[3,1]*MhH^2 + Vphi[1,2]*Vphi[3,2]*Mh^2
+ Vphi[1,3]*Vphi[3,3]*MhS^2) + (cbeta^2/(vev^2 sbeta^2 cbeta^2 + vevS^2))MhA^2)},
InteractionOrder -> {QED, 2},
Description      -> "SS11 quartic coupling"
},
lamS2 == {
ParameterType   -> Internal,
Definitions     -> {lamS2 ->
-((1/(vev*vevS*cbeta))(Vphi[2,1]*Vphi[3,1]*MhH^2 + Vphi[2,2]*Vphi[3,2]*Mh^2
+ Vphi[2,3]*Vphi[3,3]*MhS^2) + (sbeta^2/(vev^2 sbeta^2 cbeta^2 + vevS^2))MhA^2)},
InteractionOrder -> {QED, 2},
Description      -> "SS22 quartic coupling"
},
xiH == {
ParameterType   -> Internal,
Definitions     -> {xiH -> (Sqrt[2] sbeta cbeta vevS /

```

```

(vev^2 sbeta^2 cbeta^2 + vevS^2)) MhA^2},
InteractionOrder -> {QED, 1},
Description      -> "S12 cubic coupling"
},
mu1sq == {
    ParameterType -> Internal,
    Definitions   -> {mu1sq -> lam1 sbeta^2 vev^2 + (1/2)
(vev^2 cbeta^2 (lamD + lamM) + vevS^2 lamS1 + Sqrt[2] xiH cbeta vevS / sbeta)},
    TeX          -> Subscript[\[Mu]^2,1],
    Description   -> "Squared coefficient of the quadratic piece
of the Higgs 1 (non-SM) potential"
},
mu2sq == {
    ParameterType -> Internal,
    Definitions   -> {mu2sq -> lam2 cbeta^2 vev^2 + (1/2)
(vev^2 sbeta^2 (lamD + lamM) + vevS^2 lamS2 + Sqrt[2] xiH sbeta vevS / cbeta)},
    TeX          -> Subscript[\[Mu]^2,2],
    Description   -> "Squared coefficient of the quadratic piece
of the Higgs 2 (SM) potential"
},
muSsq == {
    ParameterType -> Internal,
    Definitions   -> {muSsq -> lamS vevS^2 + ((vev^2)/2)
(sbeta^2 lamS1 + cbeta^2 lamS2 + Sqrt[2] xiH sbeta cbeta / vevS)},
    TeX          -> Subscript[\[Mu]^2,S],
    Description   -> "Squared coefficient of the quadratic piece
of the complex scalar potential"
},
Vrho == {
    ParameterType -> Internal,
    Indices       -> {Index[Two], Index[Two]},
    Orthogonal    -> True,
    Value         -> {Vrho[1,1] -> sbeta, Vrho[1,2] -> -cbeta,
                      Vrho[2,1] -> cbeta, Vrho[2,2] -> sbeta},
    ComplexParameter -> False,
    Description   -> "Basis transformation matrix for complex scalars"
},
Vchi == {

```

```

ParameterType -> Internal,
Indices       -> {Index[Three], Index[Three]},
Orthogonal    -> True,
Value         -> {
Vchi[1,1]   -> sbeta,
Vchi[1,2]   -> -cbeta vev sbeta cbeta / Sqrt[vev^2 sbeta^2 cbeta^2 + vevS^2],
Vchi[1,3]   -> cbeta vevS / Sqrt[vev^2 sbeta^2 cbeta^2 + vevS^2],
Vchi[2,1]   -> cbeta,
Vchi[2,2]   -> sbeta vev sbeta cbeta / Sqrt[vev^2 sbeta^2 cbeta^2 + vevS^2],
Vchi[2,3]   -> -sbeta vevS / Sqrt[vev^2 sbeta^2 cbeta^2 + vevS^2],
Vchi[3,1]   -> 0,
Vchi[3,2]   -> vevS / Sqrt[vev^2 sbeta^2 cbeta^2 + vevS^2],
Vchi[3,3]   -> vev sbeta cbeta / Sqrt[vev^2 sbeta^2 cbeta^2 + vevS^2}],
ComplexParameter -> False,
Description -> "Basis transformation matrix for real CP-odd scalars"
},
om12 == {
ParameterType      -> External,
BlockName -> BSMIMPUTS,
TeX           -> Subscript[\[Omega],12],
Value        -> 0.1,
Description     -> "CP-even mixing angle 1"
},
om1S == {
ParameterType      -> External,
BlockName -> BSMIMPUTS,
TeX           -> Subscript[\[Omega],1S],
Value        -> 0.0,
Description     -> "CP-even mixing angle 2"
},
om2S == {
ParameterType      -> External,
BlockName -> BSMIMPUTS,
TeX           -> Subscript[\[Omega],2S],
Value        -> 0.0,
Description     -> "CP-even mixing angle 3"
},
Vphi == {

```

```

ParameterType -> Internal,
Indices       -> {Index[Three], Index[Three]},
Orthogonal    -> True,
Value         -> {
Vphi[1,1]   -> Cos[om12]*Cos[om1S],
Vphi[1,2]   -> -(Cos[om12]*Sin[om1S]*Sin[om2S]+Sin[om12]*Cos[om2S]),
Vphi[1,3]   -> -Cos[om12]*Sin[om1S]*Cos[om2S]+Sin[om12]*Sin[om2S],
Vphi[2,1]   -> Sin[om12]*Cos[om1S],
Vphi[2,2]   -> Cos[om12]*Cos[om2S]-Sin[om12]*Sin[om1S]*Sin[om2S],
Vphi[2,3]   -> -(Cos[om12]*Sin[om2S]+Sin[om12]*Sin[om1S]*Cos[om2S]),
Vphi[3,1]   -> Sin[om1S],
Vphi[3,2]   -> Cos[om1S]*Sin[om2S],
Vphi[3,3]   -> Cos[om1S]*Cos[om2S]},
ComplexParameter -> False,
Description -> "Basis transformation matrix for real CP-even scalars"
},
(*****
Vphi == {
ParameterType -> Internal,
Indices       -> {Index[Three], Index[Three]},
Orthogonal    -> True,
Value         -> {Vphi[1,1] -> 1, Vphi[1,2] -> 0, Vphi[1,3] -> 0,
                  Vphi[2,1] -> 0, Vphi[2,2] -> 1, Vphi[2,3] -> 0,
                  Vphi[3,1] -> 0, Vphi[3,2] -> 0, Vphi[3,3] -> 1},
ComplexParameter -> False,
Description -> "Basis transformation matrix for real CP-even scalars"
},
*****)
coughH == {TeX -> Subscript[c, H],
ParameterType -> Internal,
InteractionOrder -> {HIG, 1},
Value -> -gs^2/(4Pi(3Pi vev*cbeta))*Vphi[2,2]*sert[(MhH/2/MT)^2]
},
cough == {TeX -> Subscript[c, H],
ParameterType -> Internal,
InteractionOrder -> {HIG, 1},
Value -> -gs^2/(4Pi(3Pi vev*cbeta))*Vphi[2,1]*sert[(Mh/2/MT)^2]
}

```

```

(******END*****)
};

(* *****
LGauge := Block[{mu,nu,ii,aa},
  ExpandIndices[-1/4 FS[B,mu,nu] FS[B,mu,nu] - 1/4 FS[Wi,mu,nu,ii] FS[Wi,mu,nu,ii]
  - 1/4 FS[G,mu,nu,aa] FS[G,mu,nu,aa], FlavorExpand->SU2W]];

LFermions := Block[{mu},
  ExpandIndices[I*(  

    QLbar.Ga[mu].DC[QL, mu] + LLbar.Ga[mu].DC[LL, mu] + uRbar.Ga[mu].DC[uR, mu]  

    + dRbar.Ga[mu].DC[dR, mu] + lRbar.Ga[mu].DC[lR, mu])  

(******2HDMS_Zp3N*****)  

    + nVbar.Ga[mu].DC[nV, mu]  

(******END*****)
  , FlavorExpand->{SU2W,SU2D}]/.{CKM[a_,b_] Conjugate[CKM[a_,c_]]->IndexDelta[b,c],
  CKM[b_,a_] Conjugate[CKM[c_,a_]]->IndexDelta[b,c]}];

LHiggs := Block[{ii,mu, feynmangaugerules},
  feynmangaugerules = If[Not[FeynmanGauge], {GO|GP|GPbar ->0}, {}];
  ExpandIndices[DC[Phi2bar[ii],mu] DC[Phi2[ii],mu] - (mu2sq Phi2bar[ii] Phi2[ii]
  - lam2 Phi2bar[ii] Phi2[ii] Phi2bar[jj] Phi2[jj])
(******2HDMS_Zp3N*****)
  + DC[Phi1bar[ii],mu] DC[Phi1[ii],mu] + DC[PhiSbar,mu] DC[PhiS,mu]
  - (mu1sq Phi1bar[ii] Phi1[ii] - lam1 Phi1bar[ii] Phi1[ii] Phi1bar[jj] Phi1[jj]
  + muSsq PhiSbar PhiS - lamS PhiSbar PhiS PhiSbar PhiS
  - lamD Phi1bar[ii] Phi1[ii] Phi2bar[jj] Phi2[jj]
  - lamM Phi1bar[ii] Phi2[ii] Phi2bar[jj] Phi1[jj]
  - lamS1 PhiSbar PhiS Phi1bar[jj] Phi1[jj] - lamS2 PhiSbar PhiS Phi2bar[jj] Phi2[jj]
  - xiH (Phi1bar[ii] Phi2[ii] PhiSbar + Phi2bar[ii] Phi1[ii] PhiS))
(******END*****)
  , FlavorExpand->{SU2D,SU2W}]/.feynmangaugerules
];

```

```

LYukawa := Block[{sp,ii,jj,cc,ff1,ff2,ff3,yuk,feynmangaugerules},
  feynmangaugerules = If[Not[FeynmanGauge], {G0|GP|GPbar ->0}, {}];

yuk = ExpandIndices[
  -yd[ff2, ff3] CKM[ff1, ff2] QLbar[sp, ii, ff1, cc].dR [sp, ff3, cc] Phi2[ii] -
  yl[ff1, ff3] LLbar[sp, ii, ff1].lR [sp, ff3] Phi2[ii] -
  yu[ff1, ff2] QLbar[sp, ii, ff1, cc].uR [sp, ff2, cc] Phi2bar[jj] Eps[ii, jj]
  (*****2HDMS_Zp3N*****)
  - ((1/2) MNN[ff1,ff2] nVbar[sp1,ff1].nV[sp1,ff2]
  + YukN[ff1,ff2] LLbar[sp2,ii,ff1].nVR[sp2,ff2] Phi1bar[jj] Eps[ii, jj])
  (*****END*****)
  , FlavorExpand -> SU2D];
yuk = yuk /. { CKM[a_, b_] Conjugate[CKM[a_, c_]] -> IndexDelta[b, c],
  CKM[b_, a_] Conjugate[CKM[c_, a_]] -> IndexDelta[b, c]};
yuk+HC[yuk]/.feynmangaugerules
];

LHEFT := Block[{mu,nu,b,feynmangaugerules},
LCPE = -1/4 couphH FS[G, mu, nu, b] FS[G, mu, nu, b] hH
- 1/4 couph FS[G, mu, nu, b] FS[G, mu, nu, b] h;
ExpandIndices[LCPE, FlavorExpand->{SU2D,SU2W,CPevenscalar}]
];
LBSM:= LGauge + LFermions + LHiggs + LYukawa + LHEFT;

```

Appendix D

Digitalized Values for Literature Distributions

We provide the numerical values for the histograms corresponding to different SM background channels found in [1] after digitalization. Values are given with 0.1 precision in terms of the y -axis in ascending x order.

D.1 Gluon Fusion Category

D.1.1 $p_{T2} < 20$ GeV

- $h \rightarrow WW^*$: [7.9, 15.0, 14.5, 6.2, 1.3, 0.8]
- Drell-Yan+Nonprompt+Minor Background: [55.3, 70.4, 40.4, 10.7, 4.3, 1.6]
- SM Total: [103.8, 150.55, 119.995, 63.65, 36.15, 22.95]
- Data: [105, 149, 124, 66, 38, 22]

D.1.2 $p_{T2} > 20$ GeV

- $h \rightarrow WW^*$: [10.1, 17.4, 22.2, 22.2, 17.4, 10.1, 2.8, 0.3]
- Drell-Yan+Nonprompt+Minor Background: [63.6, 71.3, 66.8, 51.8, 36.9, 25.3, 15.9, 4.5]
- SM Total: [402.5, 523.9, 547.2, 530.2, 479.7, 444.1, 330.0, 155.9]
- Data: [402, 524, 547, 530, 480, 444, 330, 156]

D.2 Z -Higgs Production Category

D.2.1 1-jet

- $Z \rightarrow Zh$: [1.7, 6.0, 10.0, 11.8, 8.7, 3.3, 0.9, 0.5, 0.0, 0.3]
- SM Total: [36.5, 121.9, 255.8, 346.6, 327.6, 187.3, 79.6, 42.6, 20.6, 26.2]
- Data: [25, 120, 227, 356, 345, 165, 84, 32, 15, 25]

D.2.2 2-jet

- $Z \rightarrow Zh$: [2.1, 3.5, 5.8, 6.1, 4.6, 3.7, 2.3, 1.7, 1.0, 0.8, 0.5, 0.3, 0.3, 0.1, 0.0, 0.7]
- SM Total: [18.1, 35.8, 79.1, 122.7, 130.9, 111.9, 89.1, 61.4, 44.8, 30.5, 23.5, 18.4, 12.7, 9.7, 7.8, 31.2]
- Data: [18, 40, 73, 118, 145, 128, 111, 69, 44, 39, 34, 22, 14, 15, 5, 46]

Appendix E

Standard Model Normalization Parameters

Here we display the values for the SM normalization parameters after fitting with the χ^2 and likelihood functions for both categories.

E.1 Scalar Mediated Neutrino Production

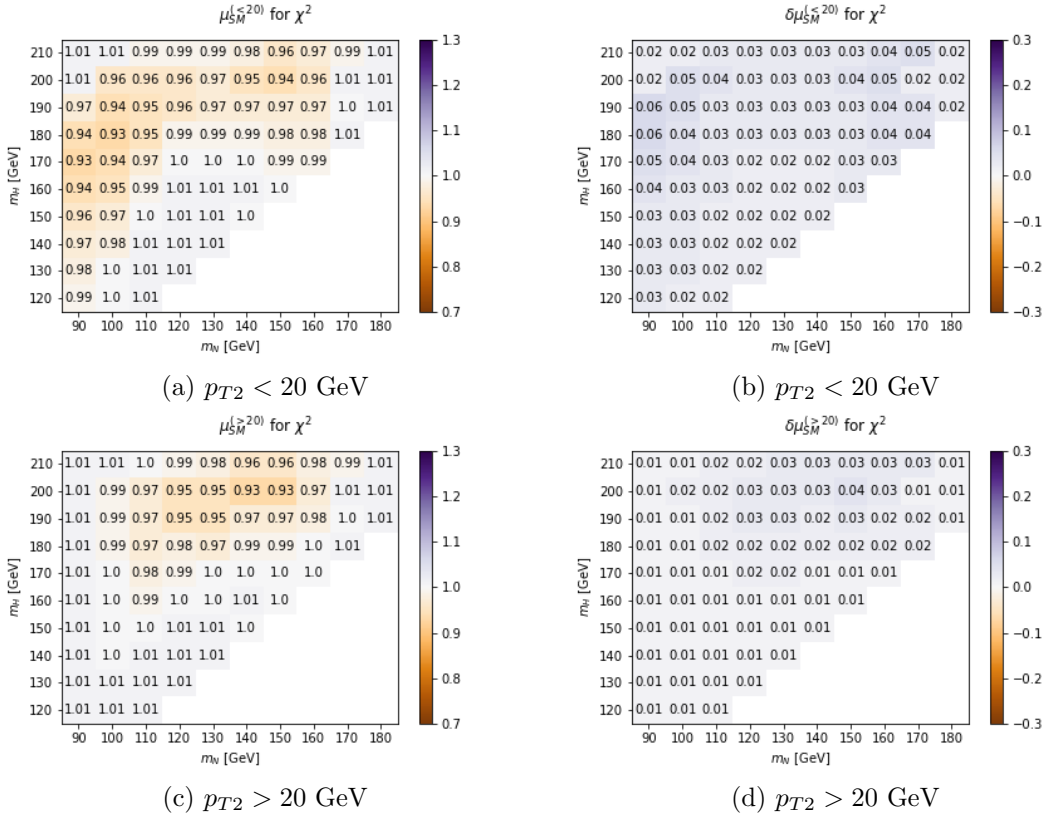


Figure E.1: $\mu_{\text{SM}}^{(k)}$ values and associated errors $\delta\mu_{\text{SM}}^{(k)}$ after fitting for $N\nu$ process with the χ^2 function

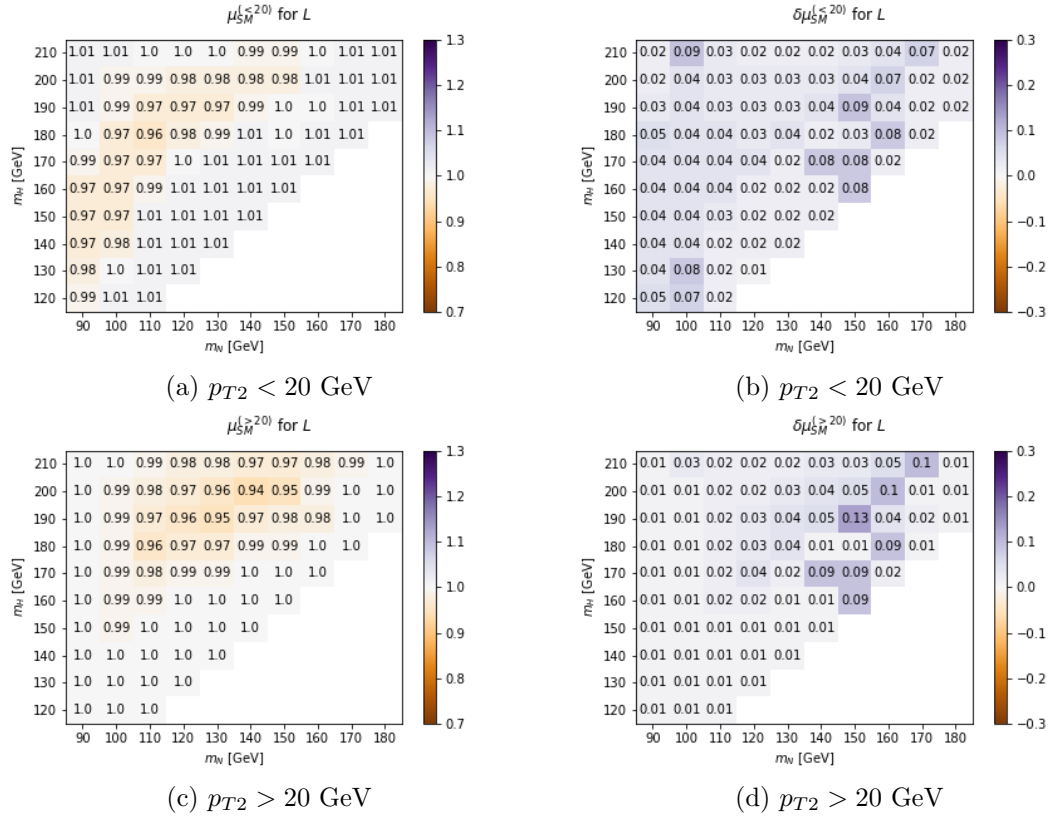


Figure E.2: $\mu_{\text{SM}}^{(k)}$ values and associated errors $\delta\mu_{\text{SM}}^{(k)}$ after fitting for $N\nu$ process with the likelihood function

E.2 Z' Mediated Neutrino Production

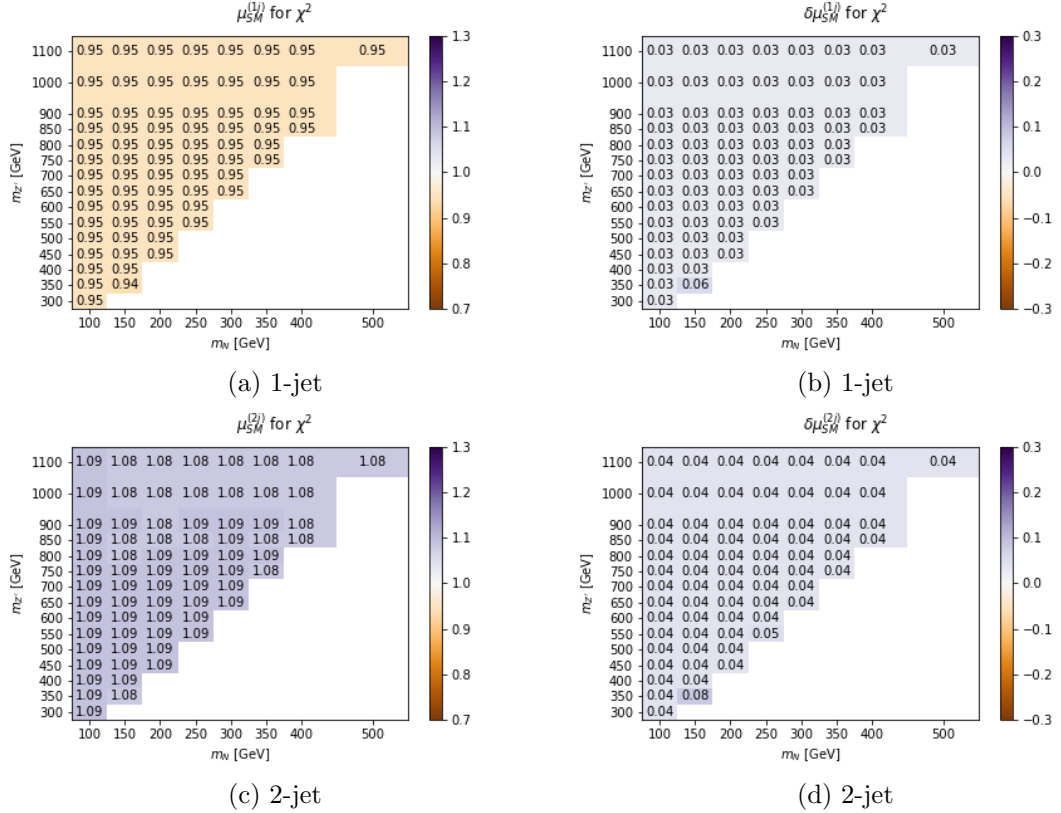


Figure E.3: $\mu_{SM}^{(k)}$ values and associated errors $\delta\mu_{SM}^{(k)}$ after fitting for NN process with the χ^2 function

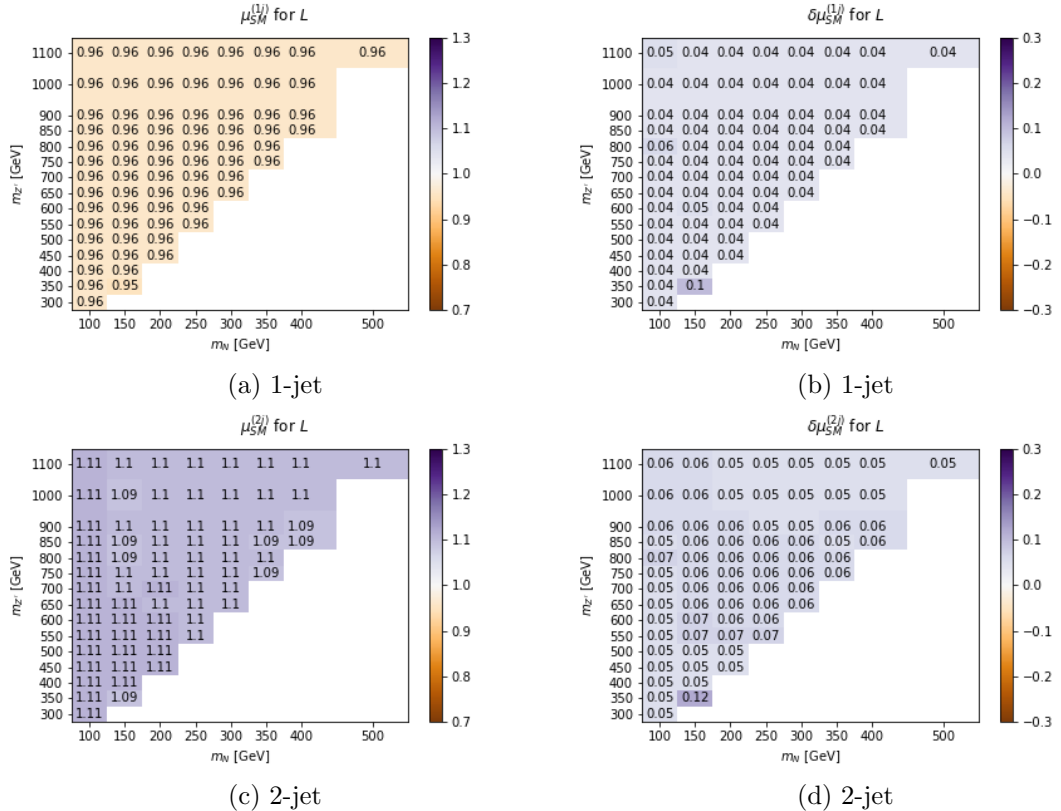


Figure E.4: $\mu_{SM}^{(k)}$ values and associated errors $\delta\mu_{SM}^{(k)}$ after fitting for NN process with the likelihood function

Appendix F

Selection Efficiencies

The efficiencies obtained after applying the selection criteria on BSM samples is displayed in the following sections.

F.1 Scalar Mediated Neutrino Production

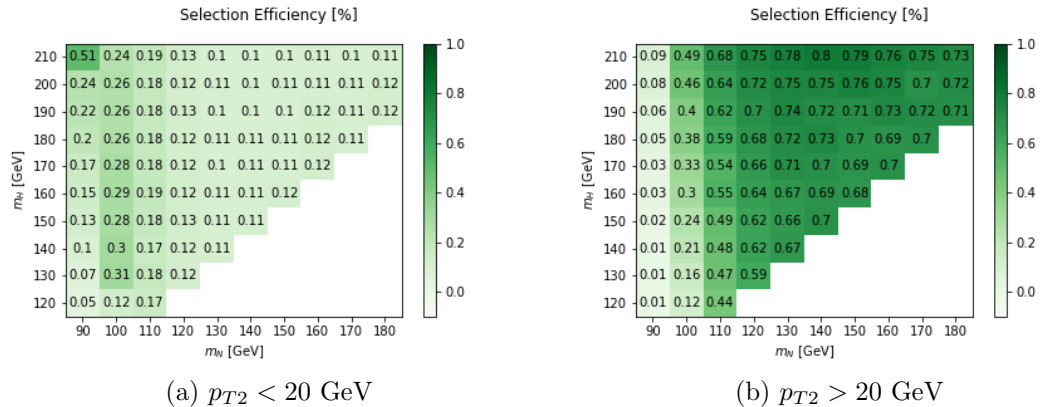


Figure F.1: Selection efficiencies for BSM samples

F.2 Z' Mediated Neutrino Production

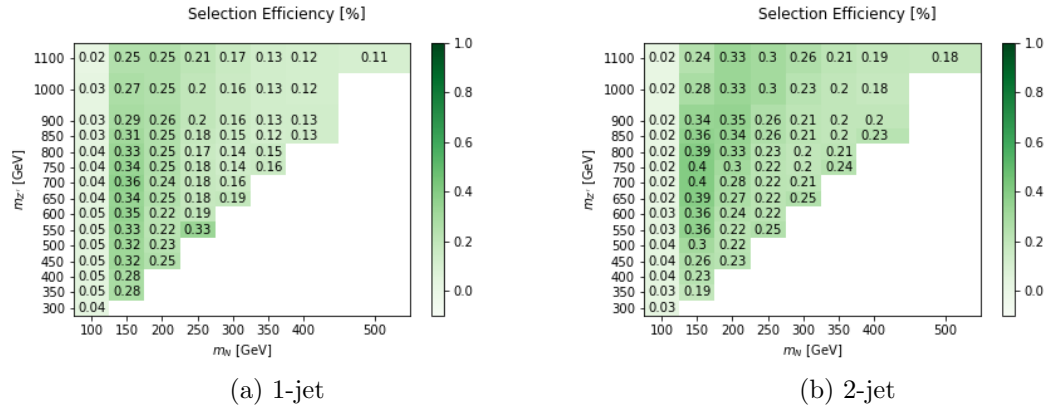


Figure F.2: Selection efficiencies for BSM samples

Appendix G

Normalized Signal Distributions

In the following sections we present the normalized m_T^H distributions for each subcategory and mass combination.

G.1 Scalar Mediated Neutrino Production

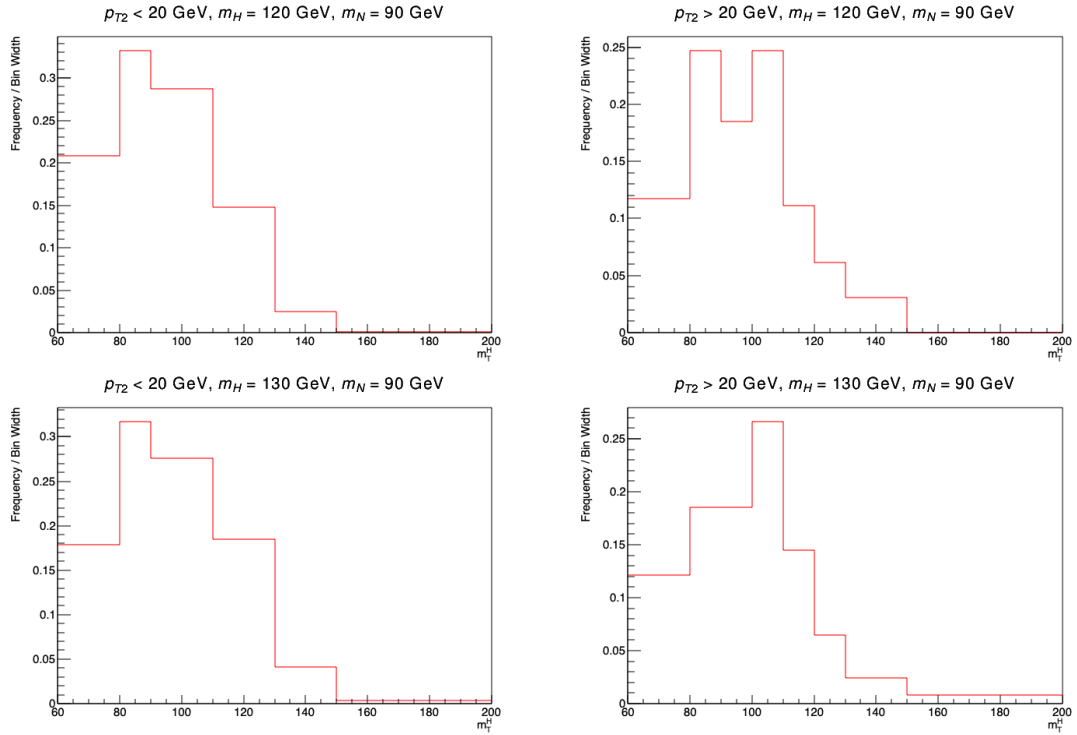


Figure G.1: Histograms for $N\nu$ process for masses $m_H = (120, 130)$ GeV and $m_N = 90$ GeV

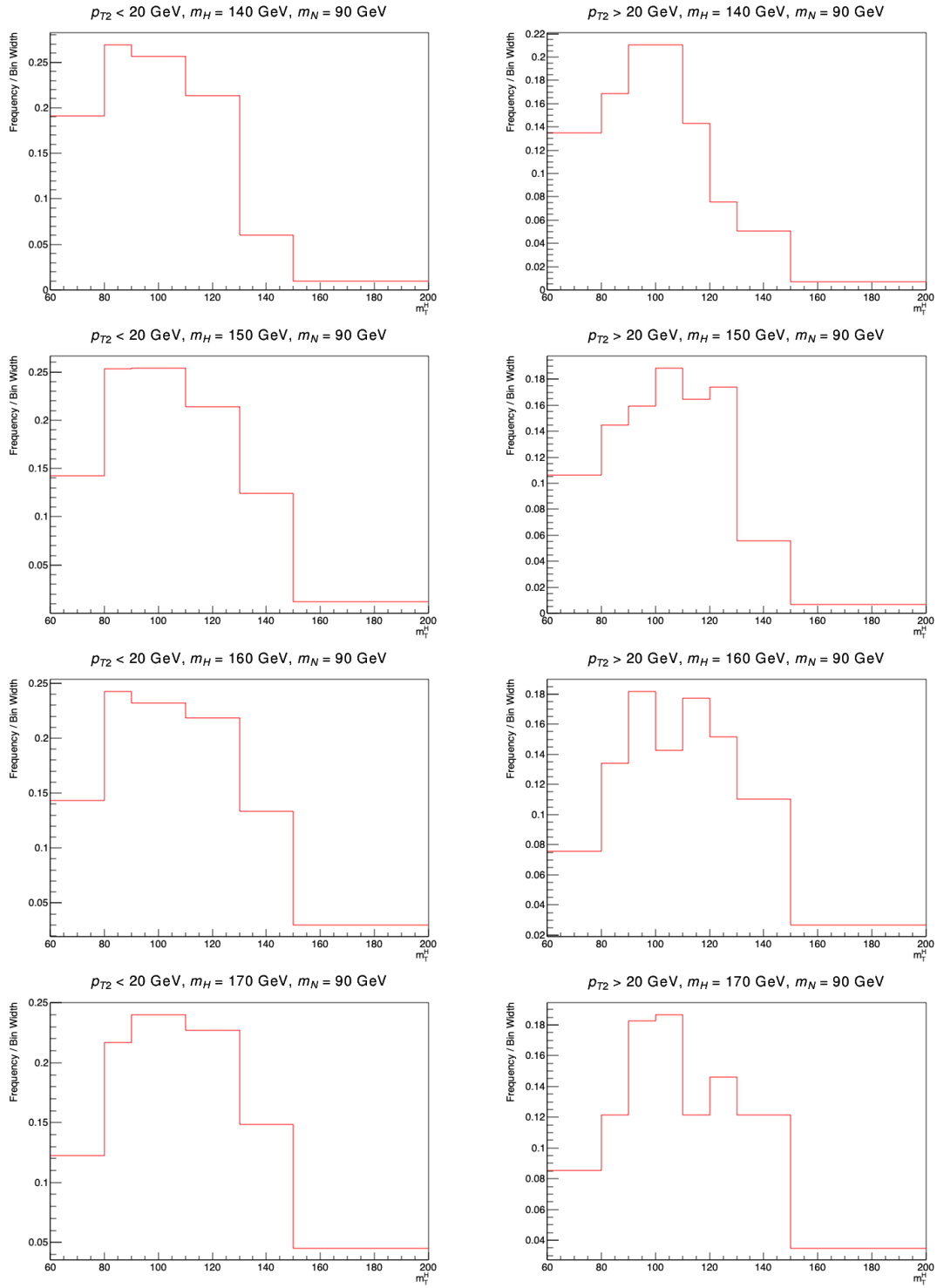


Figure G.2: Histograms for $N\nu$ process for masses $m_H = (140, 150, 160, 170)$ GeV and $m_N = 90$ GeV

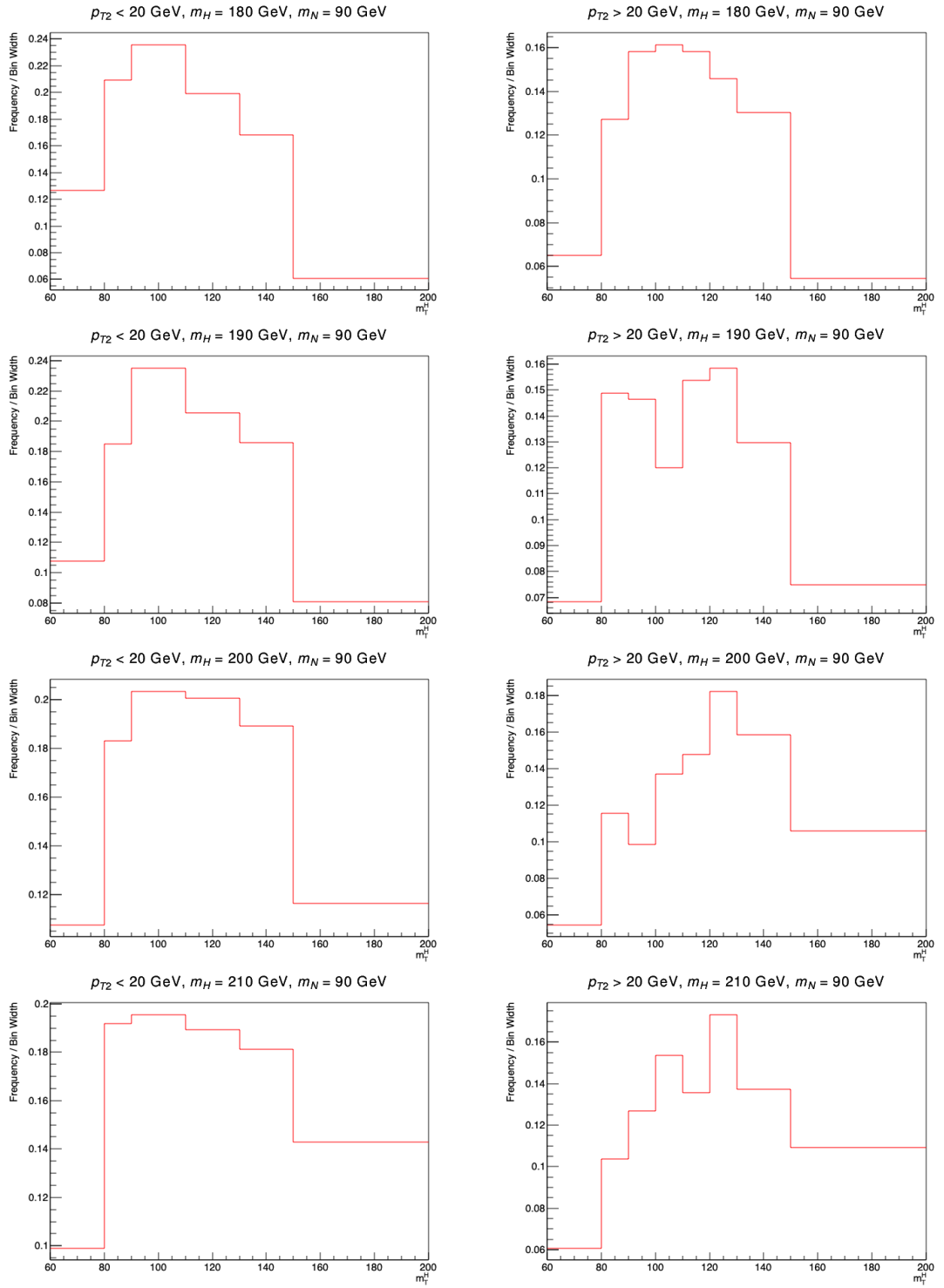


Figure G.3: Histograms for $N\nu$ process for masses $m_H = (180, 190, 200, 210)$ GeV and $m_N = 90$ GeV

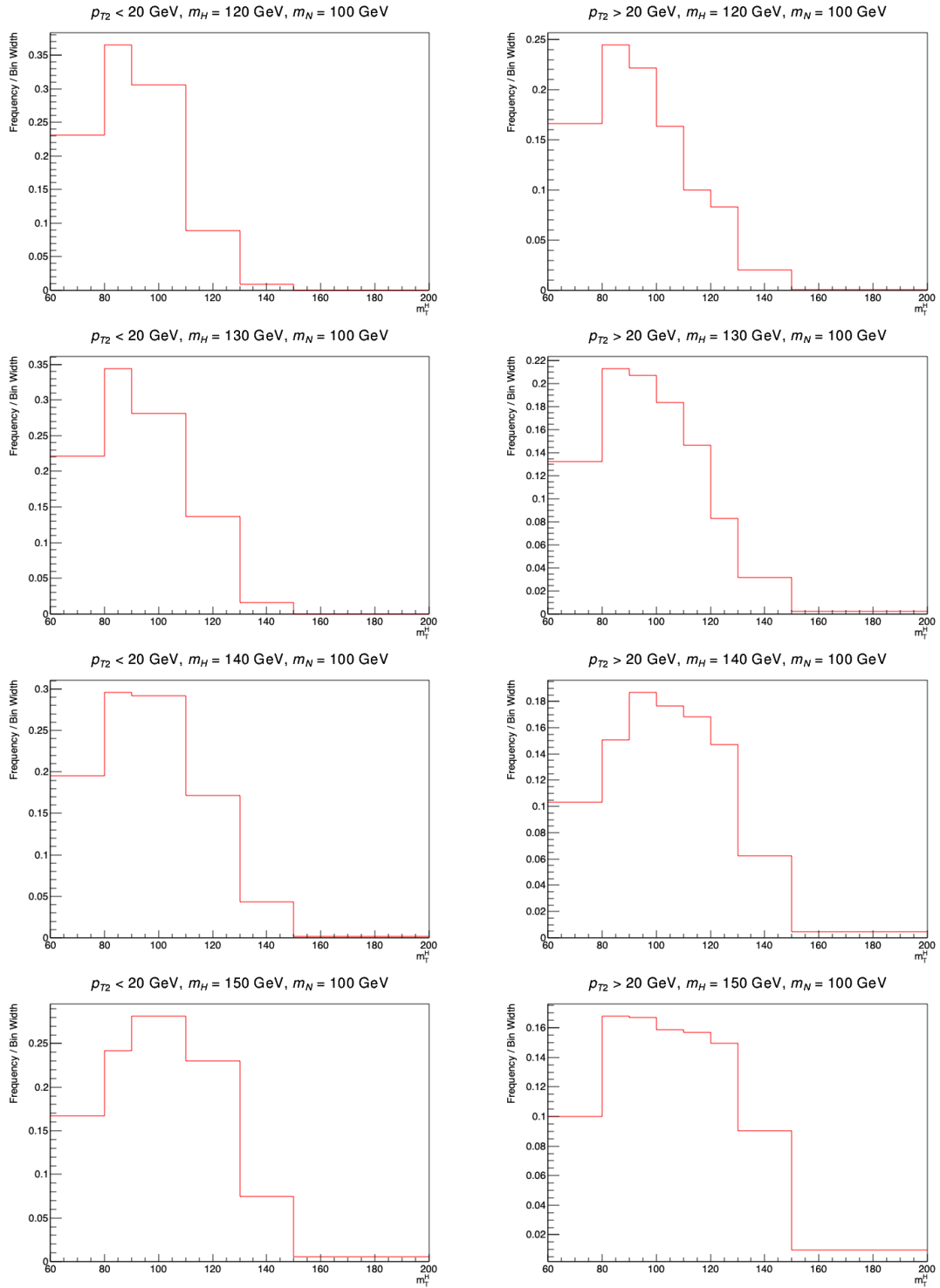


Figure G.4: Histograms for $N\nu$ process for masses $m_H = (120, 130, 140, 150)$ GeV and $m_N = 100$ GeV

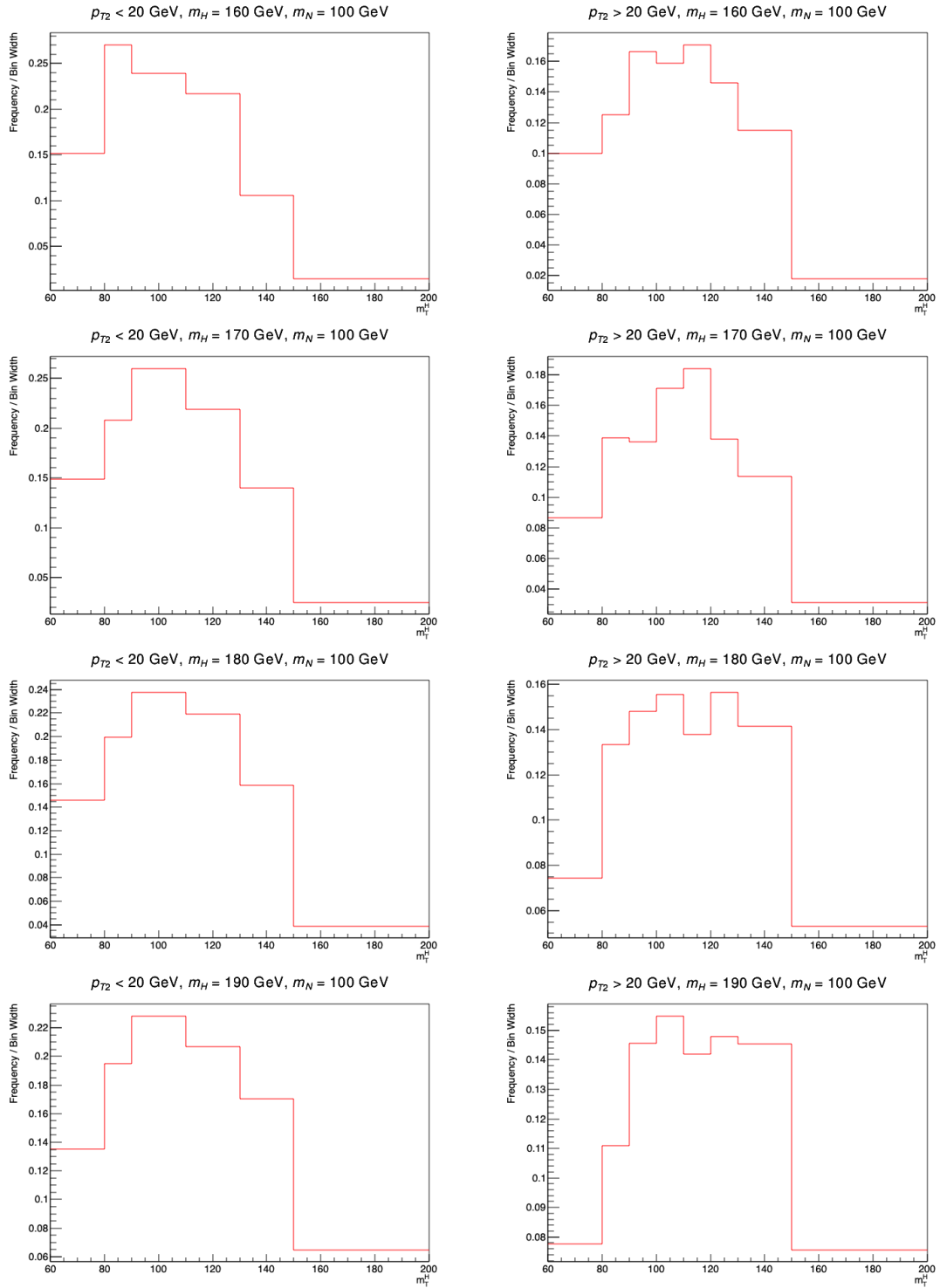


Figure G.5: Histograms for $N\nu$ process for masses $m_H = (160, 170, 180, 190)$ GeV and $m_N = 100$ GeV

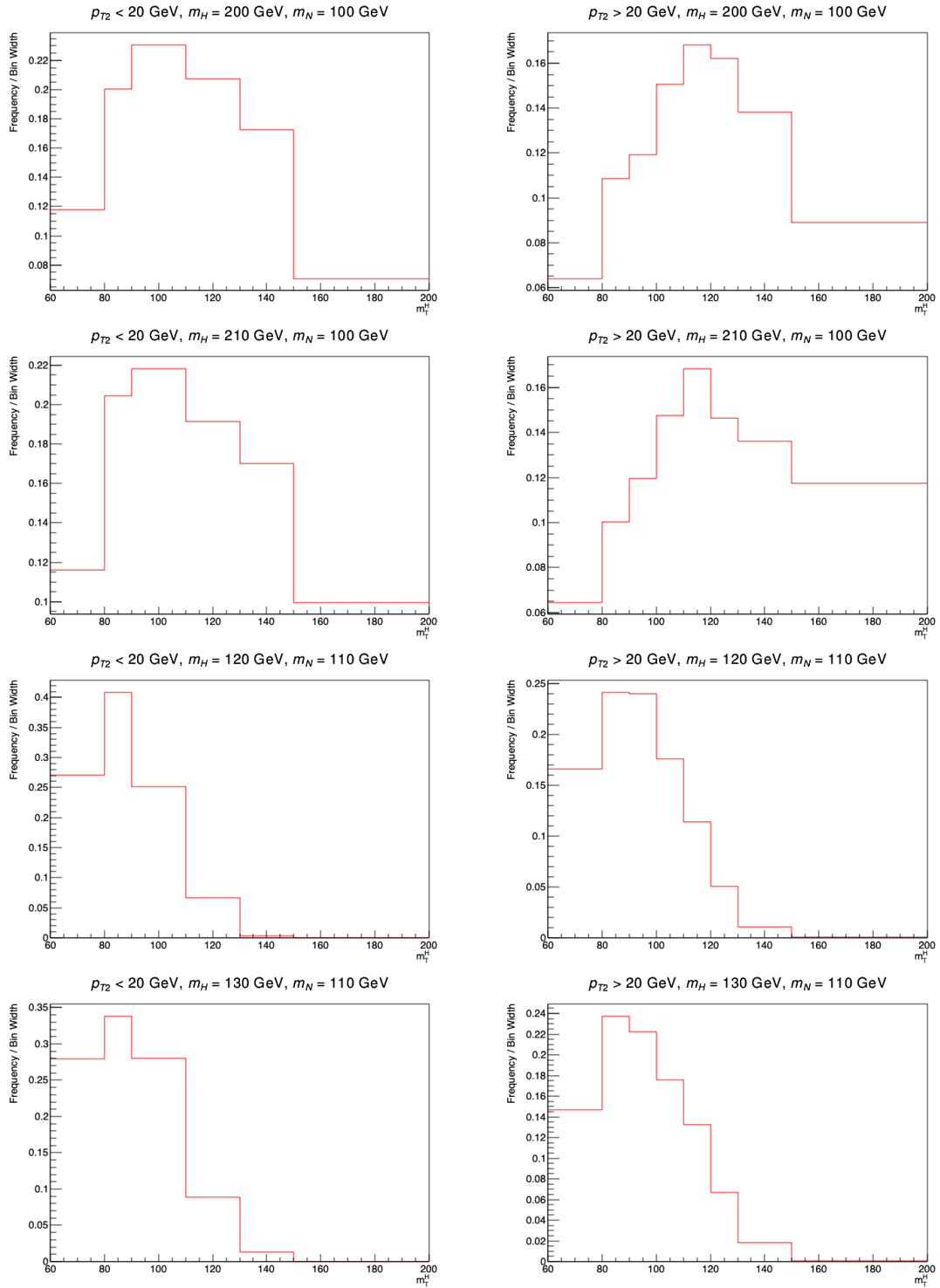


Figure G.6: Histograms for $N\nu$ process for masses $m_H = (200, 210)$ GeV and $m_N = 100$ GeV, and masses $m_H = (120, 130)$ and $m_N = 110$ GeV

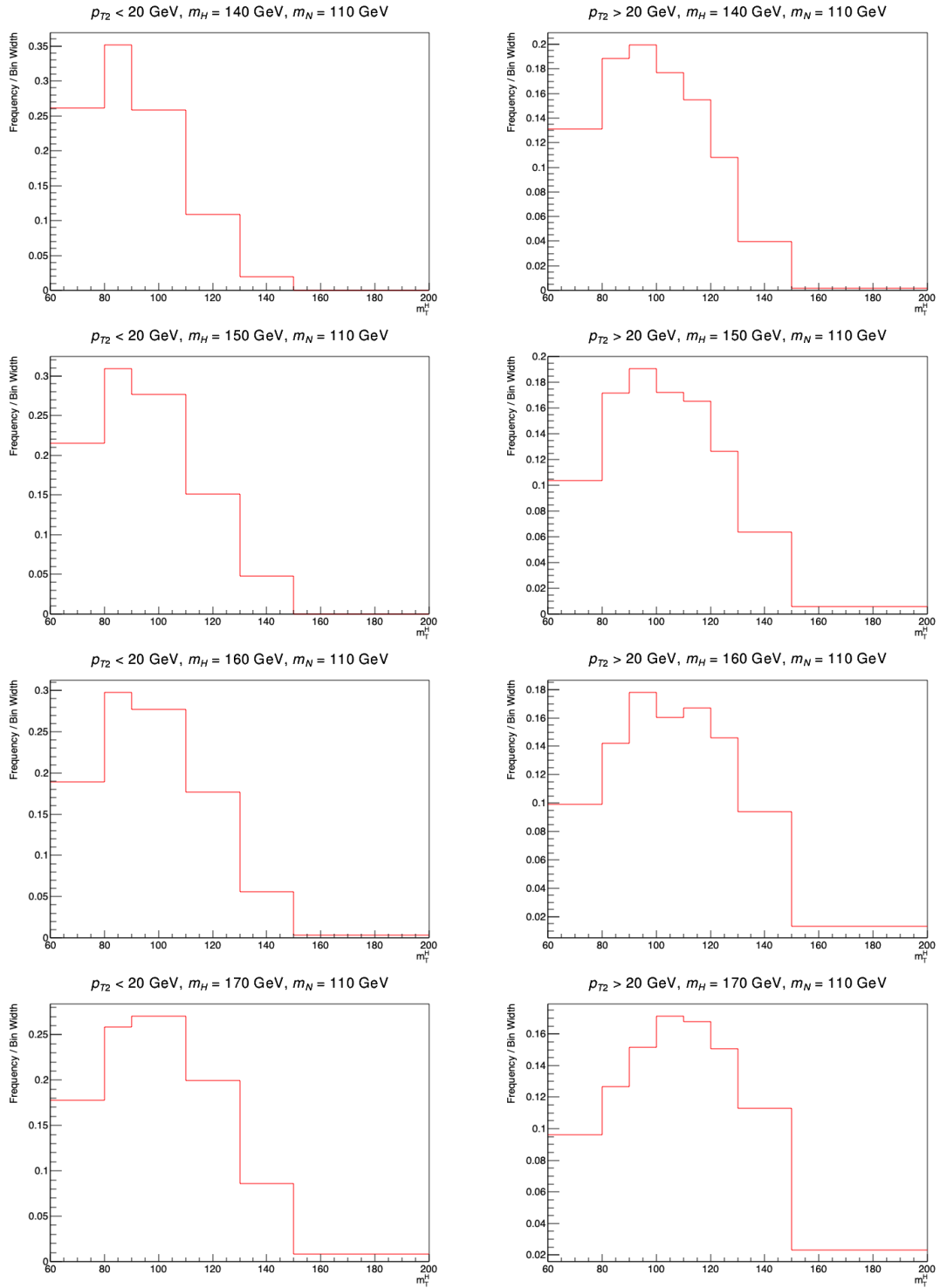


Figure G.7: Histograms for $N\nu$ process for masses $m_H = (140, 150, 160, 170) \text{ GeV}$ and $m_N = 110 \text{ GeV}$

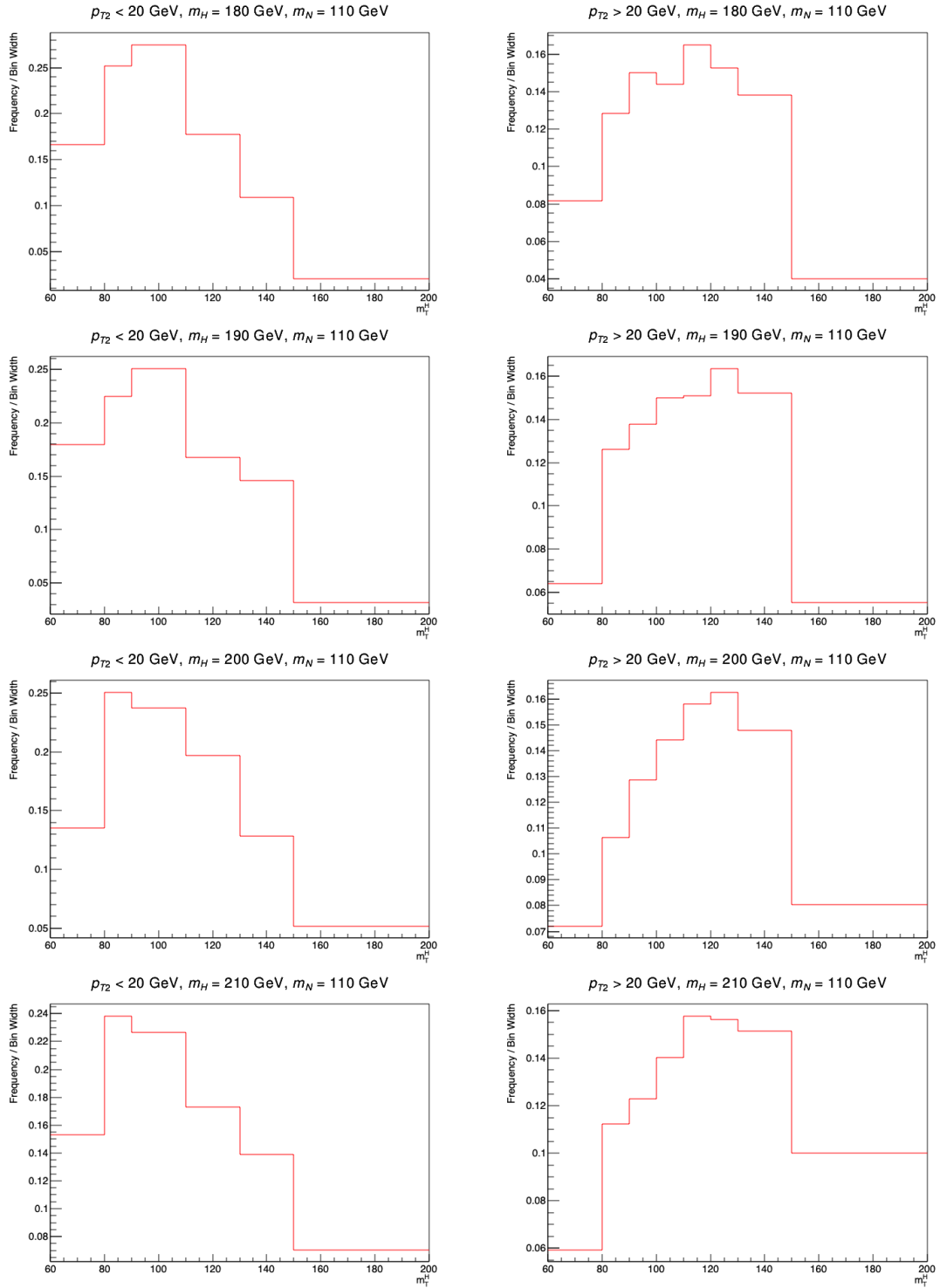


Figure G.8: Histograms for $N\nu$ process for masses $m_H = (180, 190, 200, 210)$ GeV and $m_N = 110$ GeV

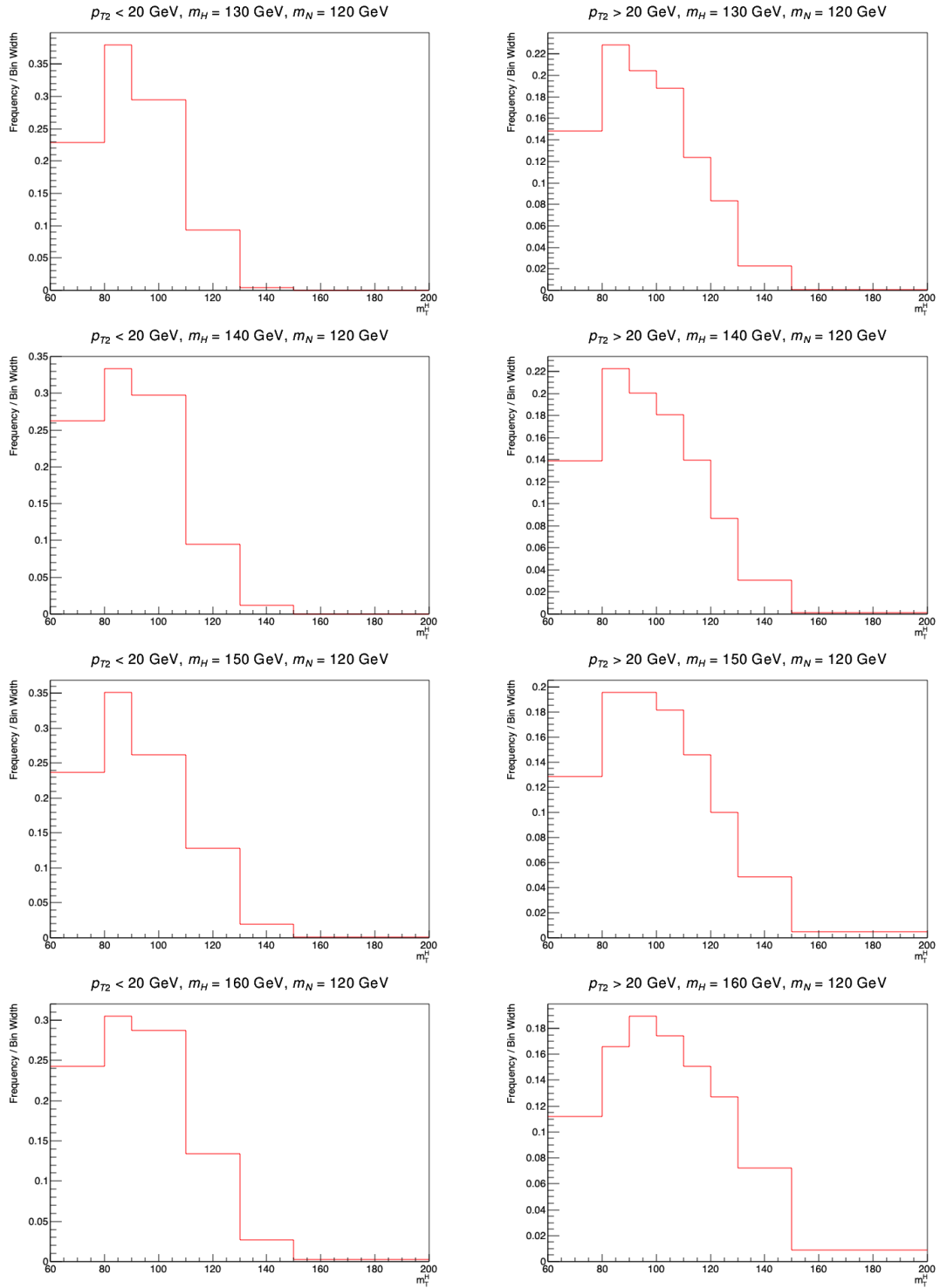


Figure G.9: Histograms for $N\nu$ process for masses $m_H = (130, 140, 150, 160)$ GeV and $m_N = 120$ GeV

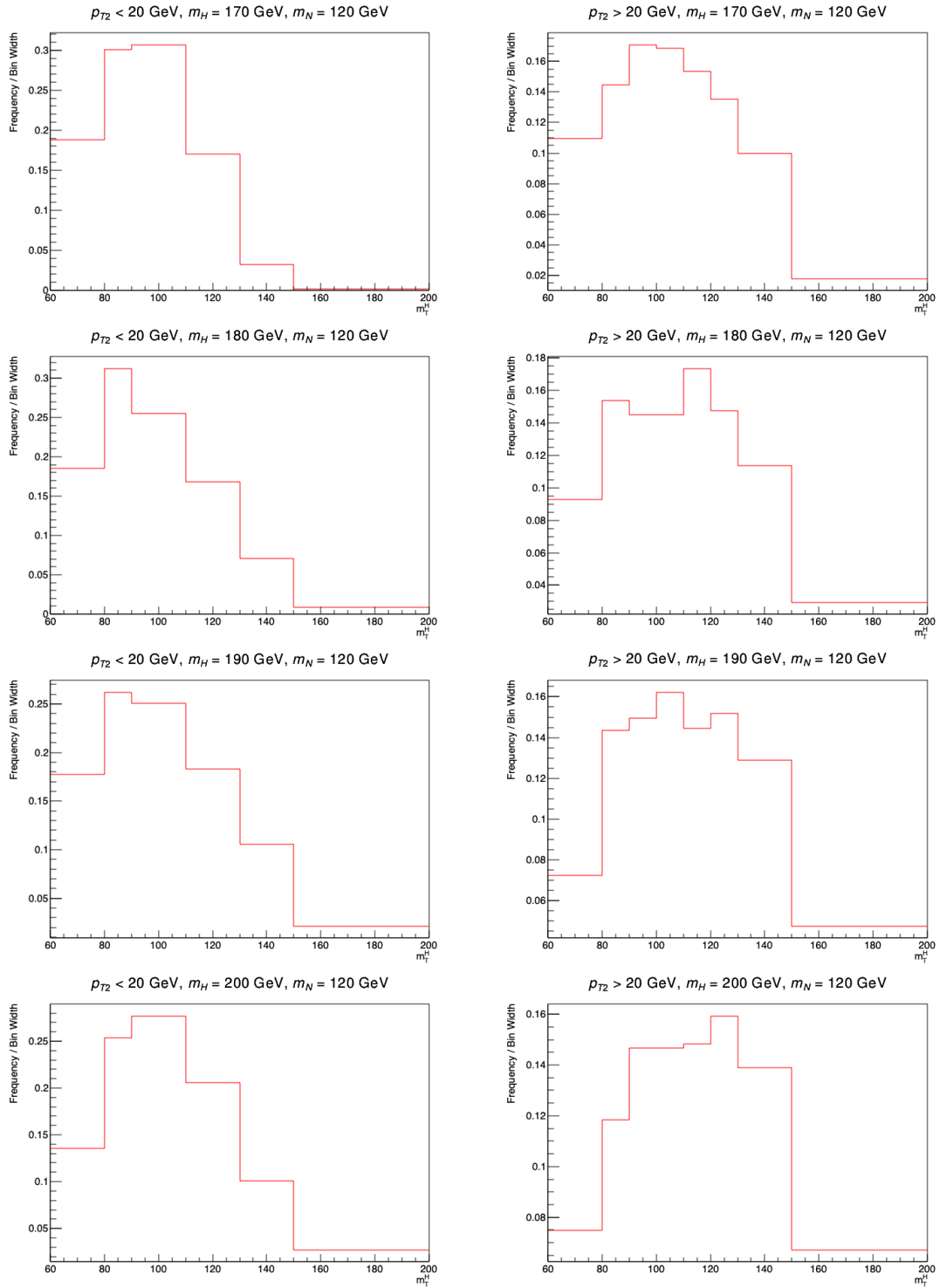


Figure G.10: Histograms for $N\nu$ process for masses $m_H = (170, 180, 190, 200)$ GeV and $m_N = 120$ GeV

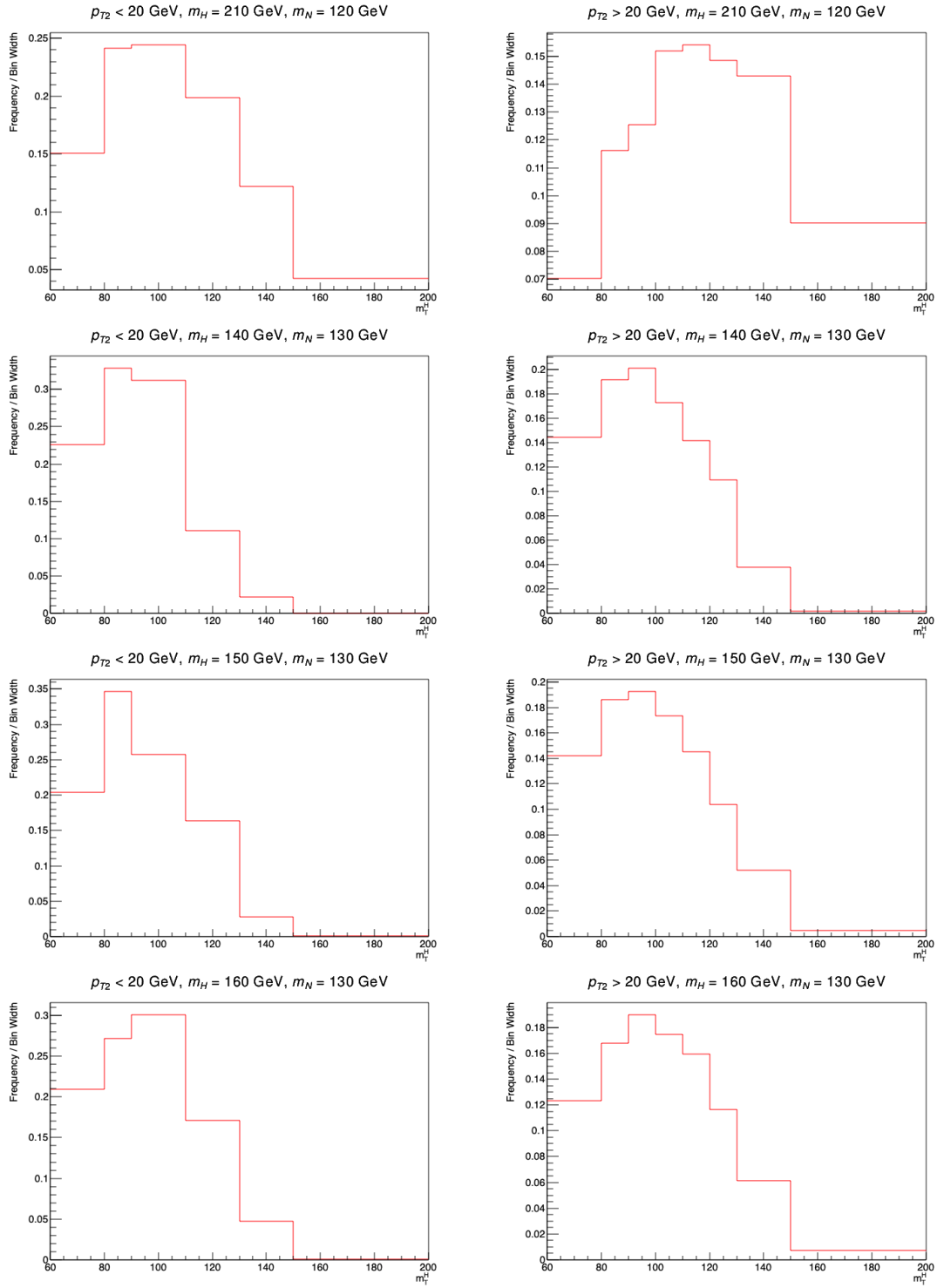


Figure G.11: Histograms for $N\nu$ process for masses $m_H = 210 \text{ GeV}$ and $m_N = 120 \text{ GeV}$, and masses $m_H = (140, 150, 160)$ and $m_N = 130 \text{ GeV}$

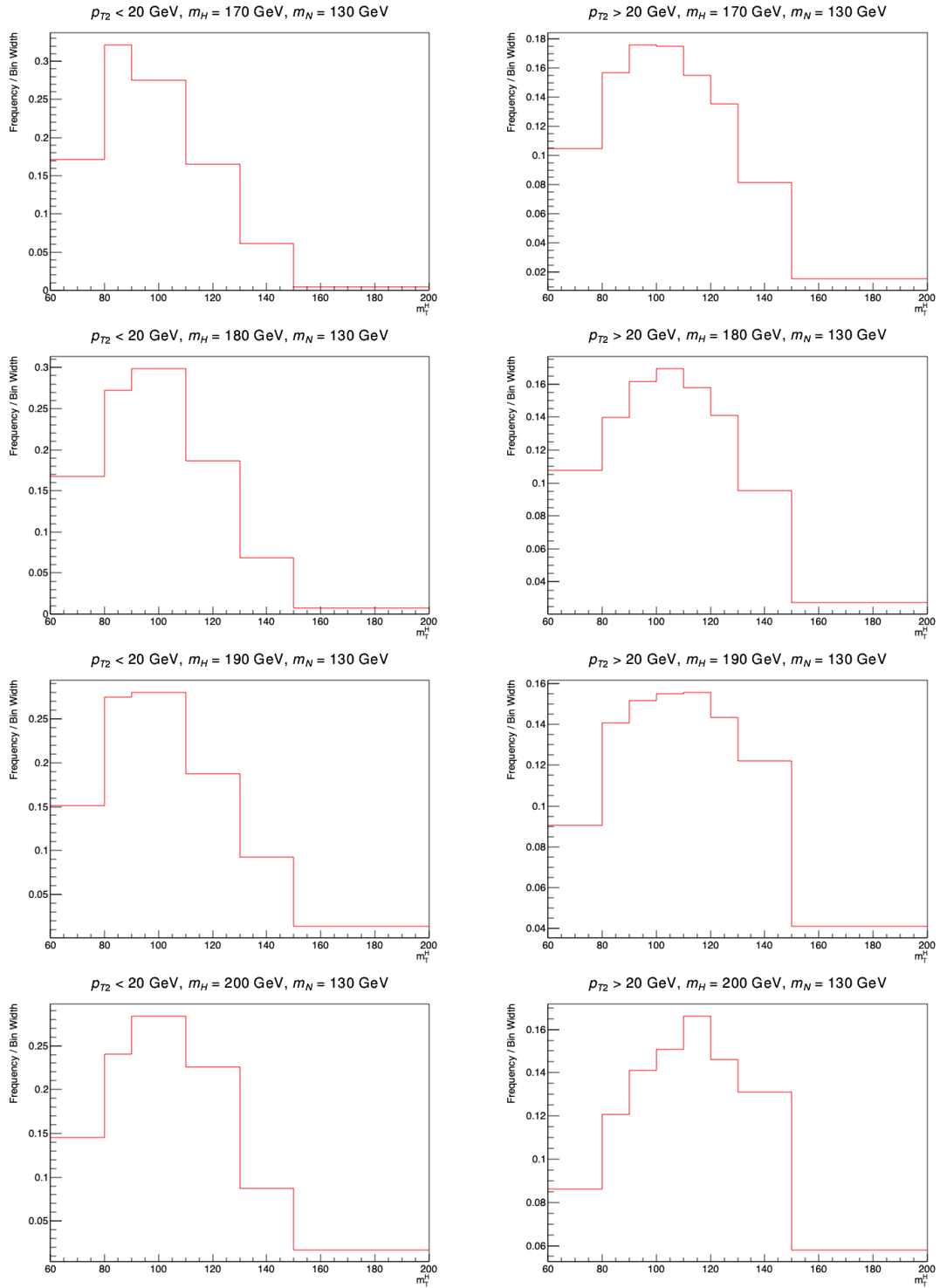


Figure G.12: Histograms for $N\nu$ process for masses $m_H = (170, 180, 190, 200)$ GeV and $m_N = 130$ GeV

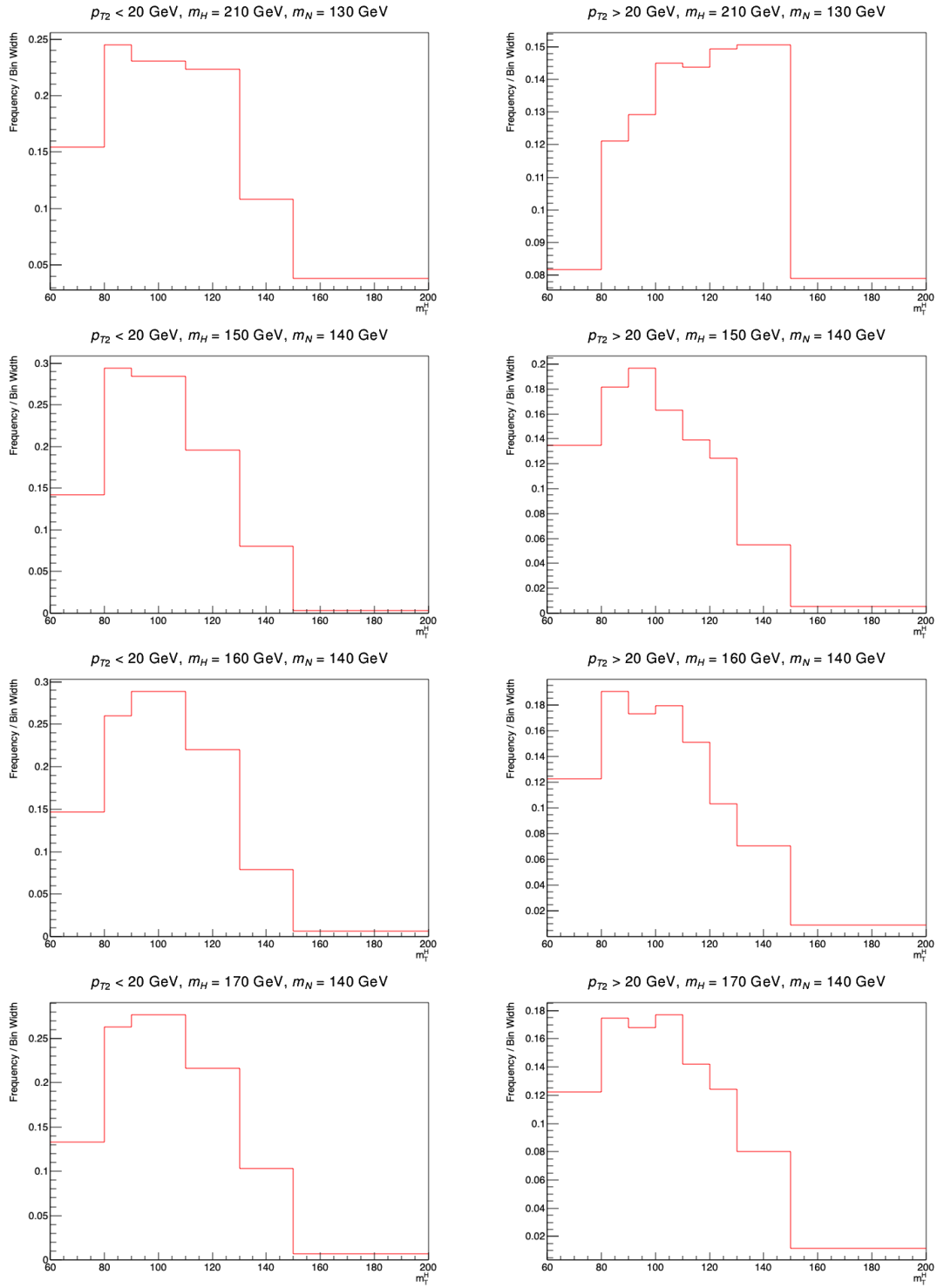


Figure G.13: Histograms for $N\nu$ process for masses $m_H = 210 \text{ GeV}$ and $m_N = 130 \text{ GeV}$, and masses $m_H = (150, 160, 170)$ and $m_N = 140 \text{ GeV}$

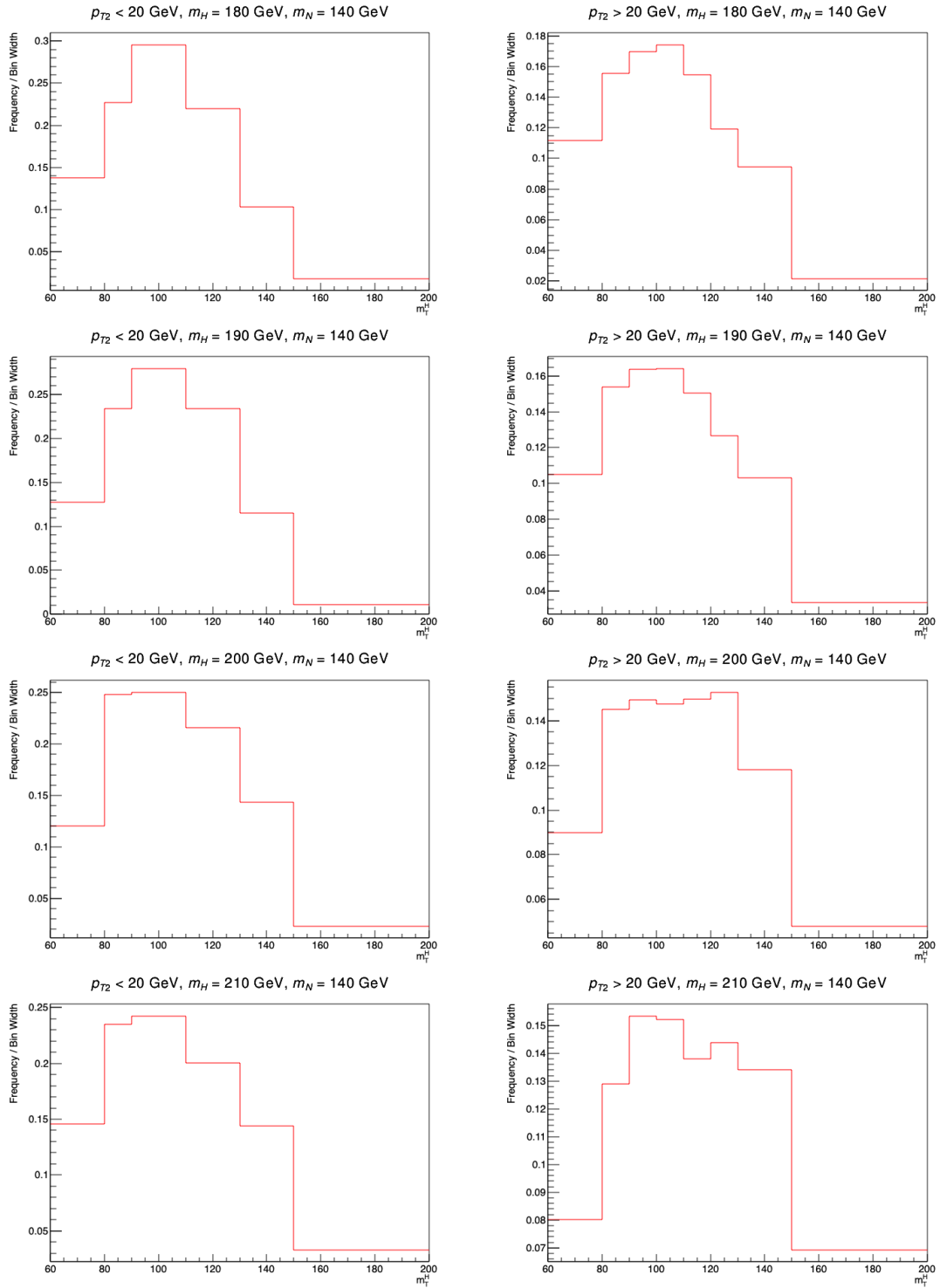


Figure G.14: Histograms for $N\nu$ process for masses $m_H = (180, 190, 200, 210)$ GeV and $m_N = 140$ GeV

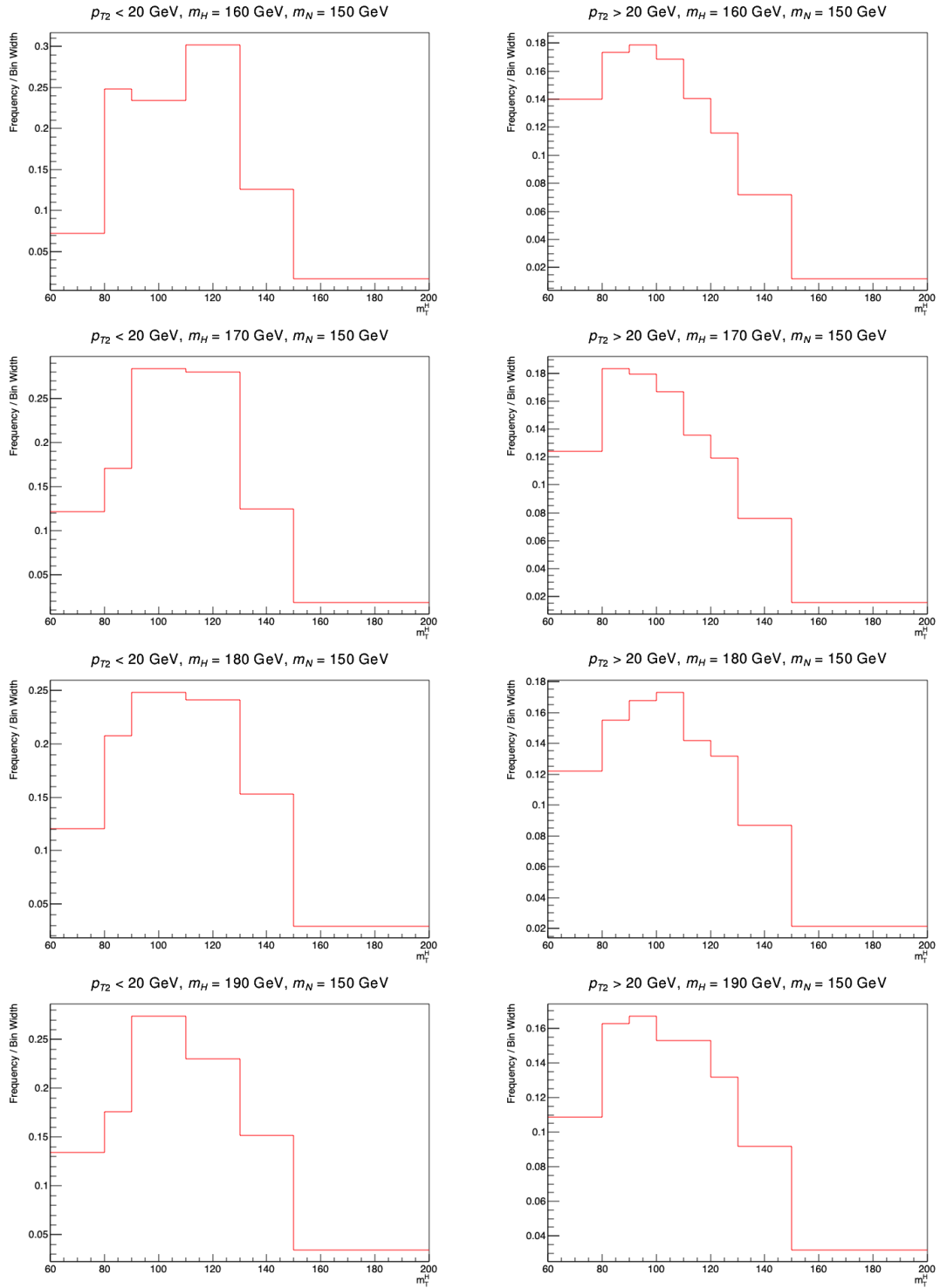


Figure G.15: Histograms for $N\nu$ process for masses $m_H = (160, 170, 180, 190)$ GeV and $m_N = 150$ GeV

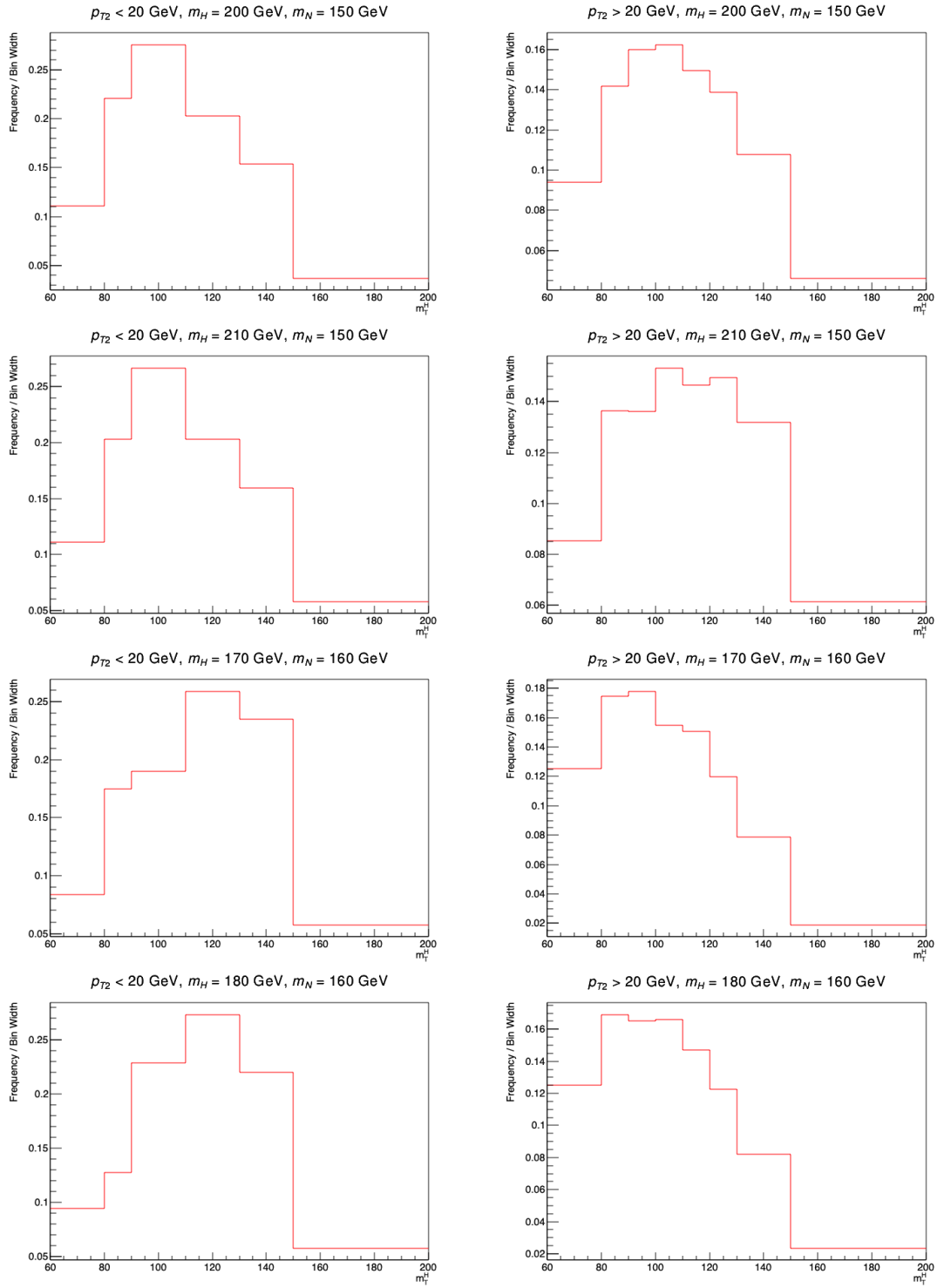


Figure G.16: Histograms for $N\nu$ process for masses $m_H = (200, 210)$ GeV and $m_N = 150$ GeV, and masses $m_H = (170, 180)$ GeV and $m_N = 160$ GeV

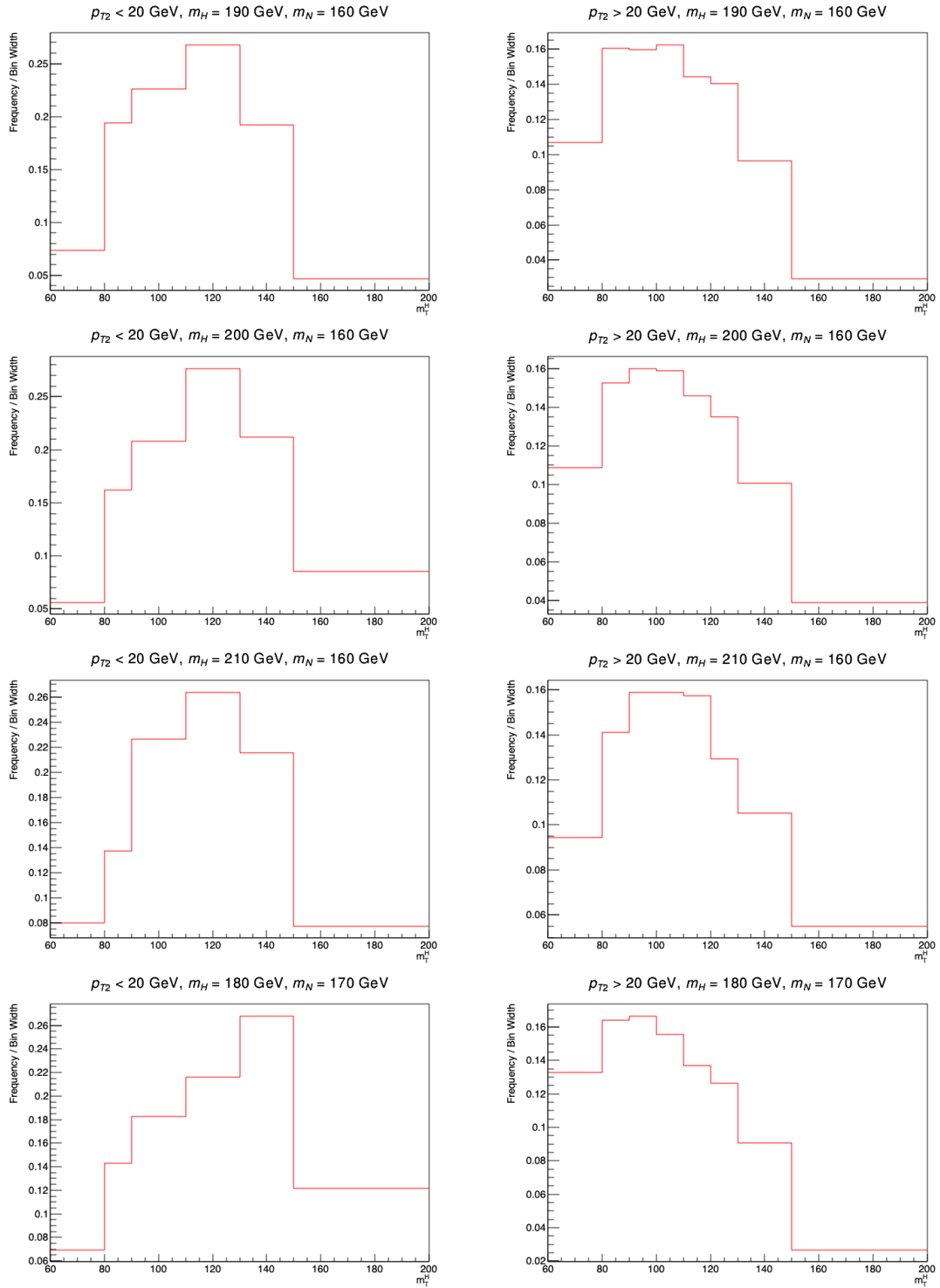


Figure G.17: Histograms for $N\nu$ process for masses masses $m_H = (190, 200, 210) \text{ GeV}$ and $m_N = 160$, and masses $m_H = 180 \text{ GeV}$ and $m_N = 170 \text{ GeV}$

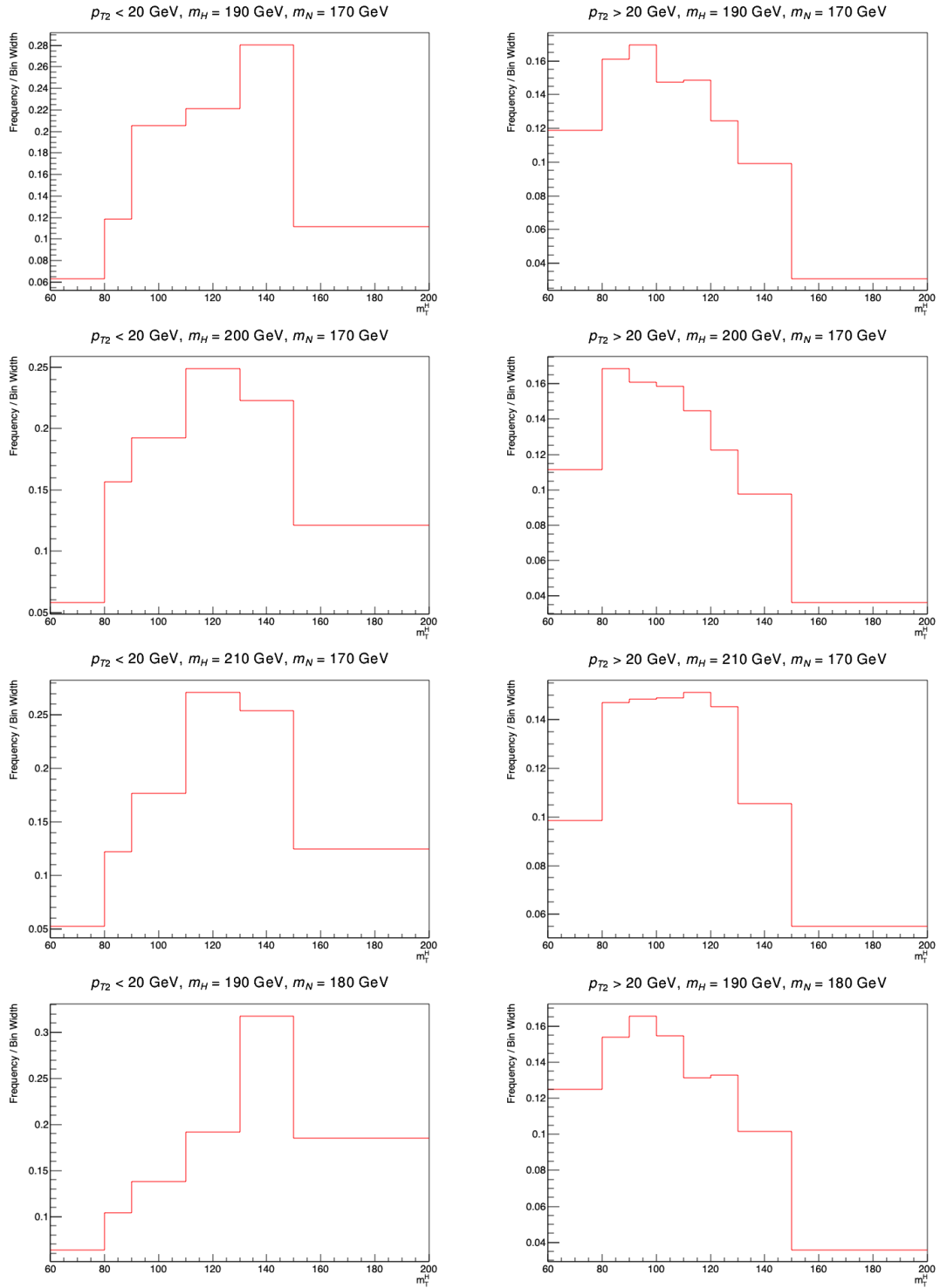


Figure G.18: Histograms for $N\nu$ process for masses $m_H = (190, 200, 210) \text{ GeV}$ and $m_N = 170$, and masses $m_H = 190 \text{ GeV}$ and $m_N = 180 \text{ GeV}$

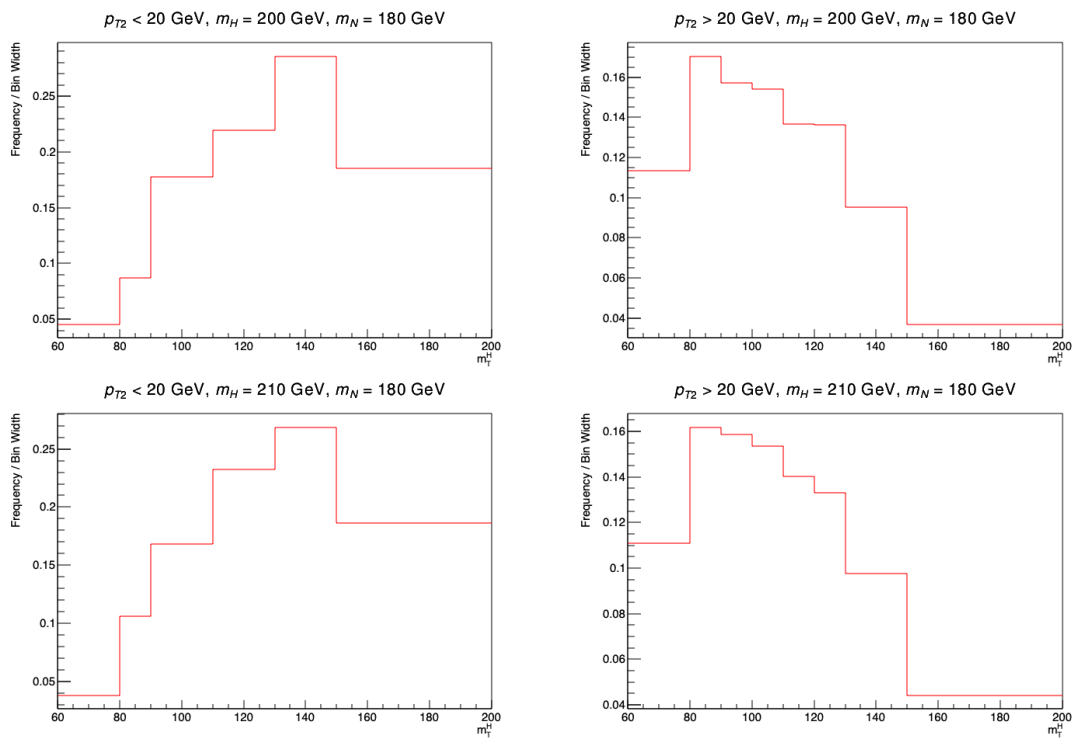


Figure G.19: Histograms for $N\nu$ process for masses $m_H = (200, 210)$ GeV and $m_N = 180$ GeV

G.2 Z' Mediated Neutrino Production

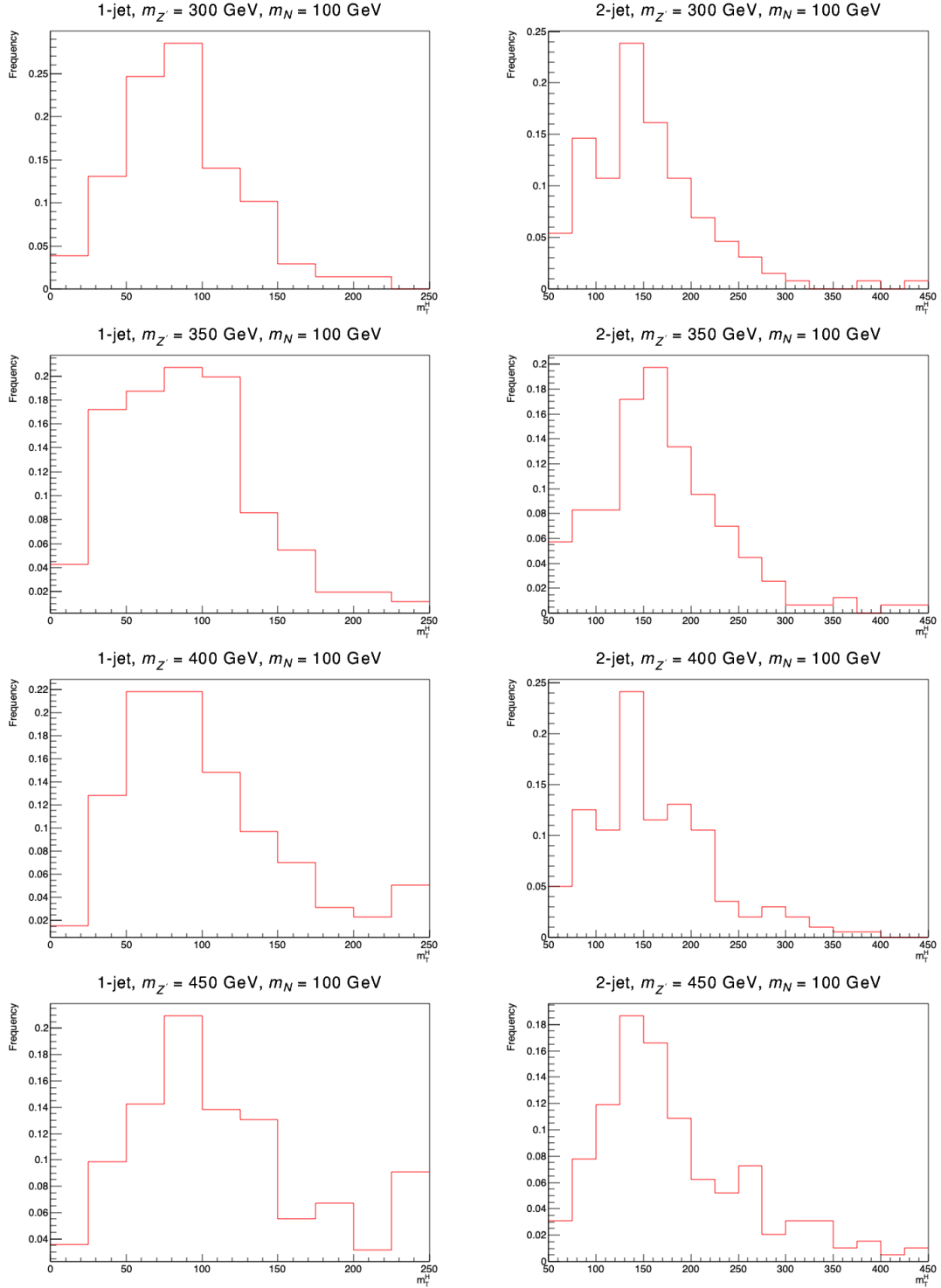


Figure G.20: Histograms for NN process for masses $m_{Z'} = (300, 350, 400, 450)$ GeV and $m_N = 100$ GeV

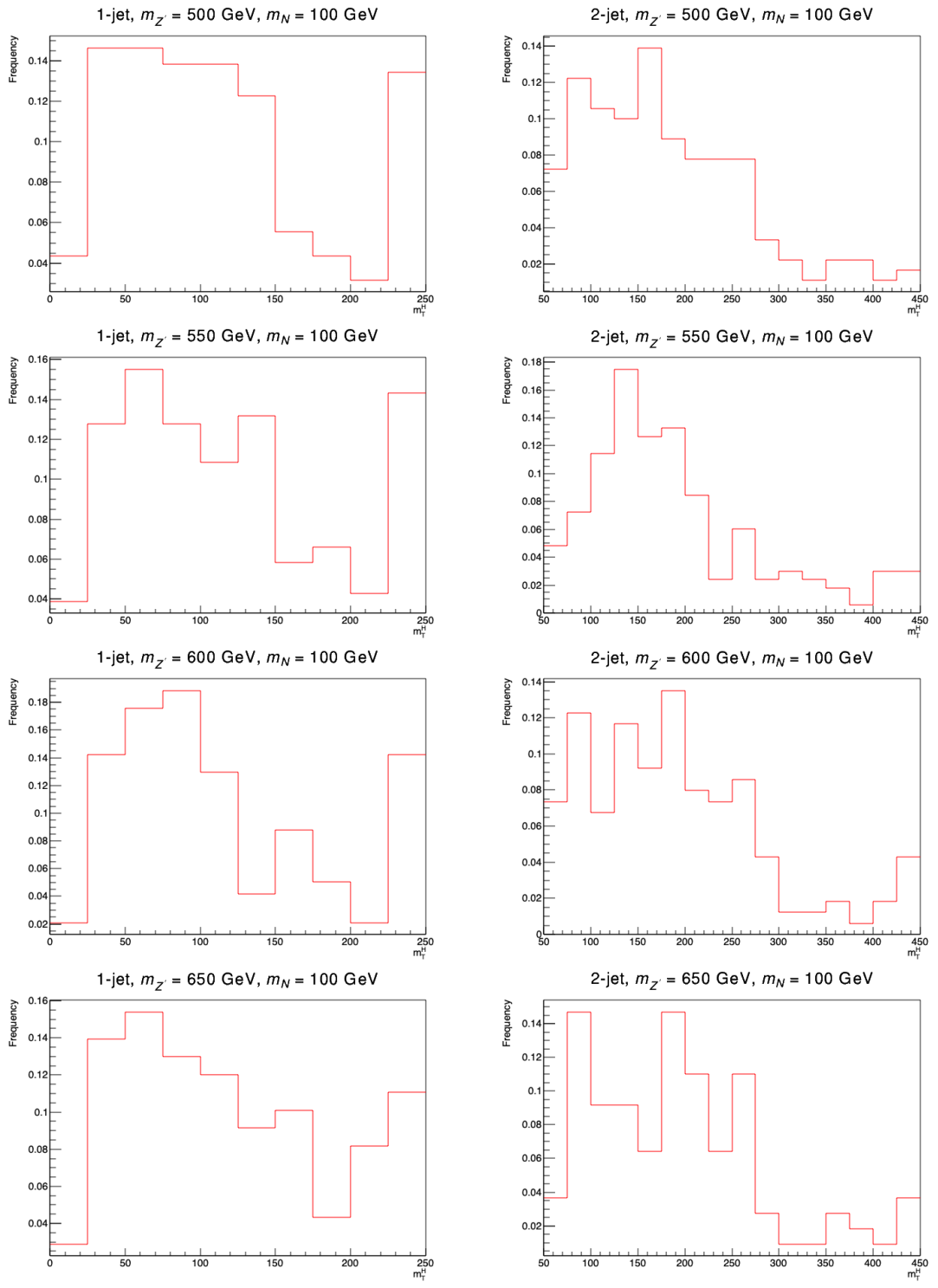


Figure G.21: Histograms for NN process for masses $m_{Z'} = (500, 550, 600, 650)$ GeV and $m_N = 100$ GeV

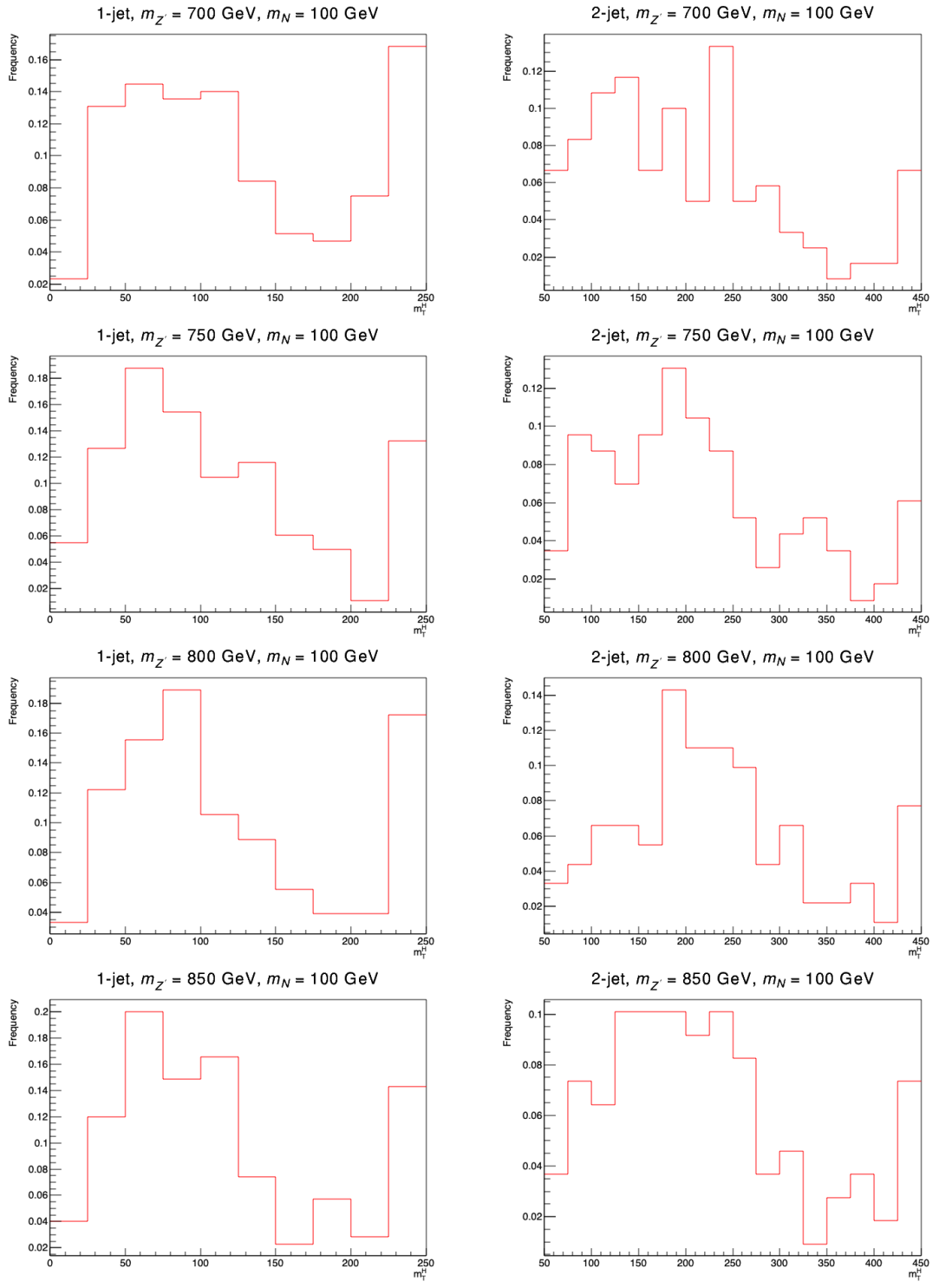


Figure G.22: Histograms for NN process for masses $m_{Z'} = (700, 750, 800, 850)$ GeV and $m_N = 100$ GeV

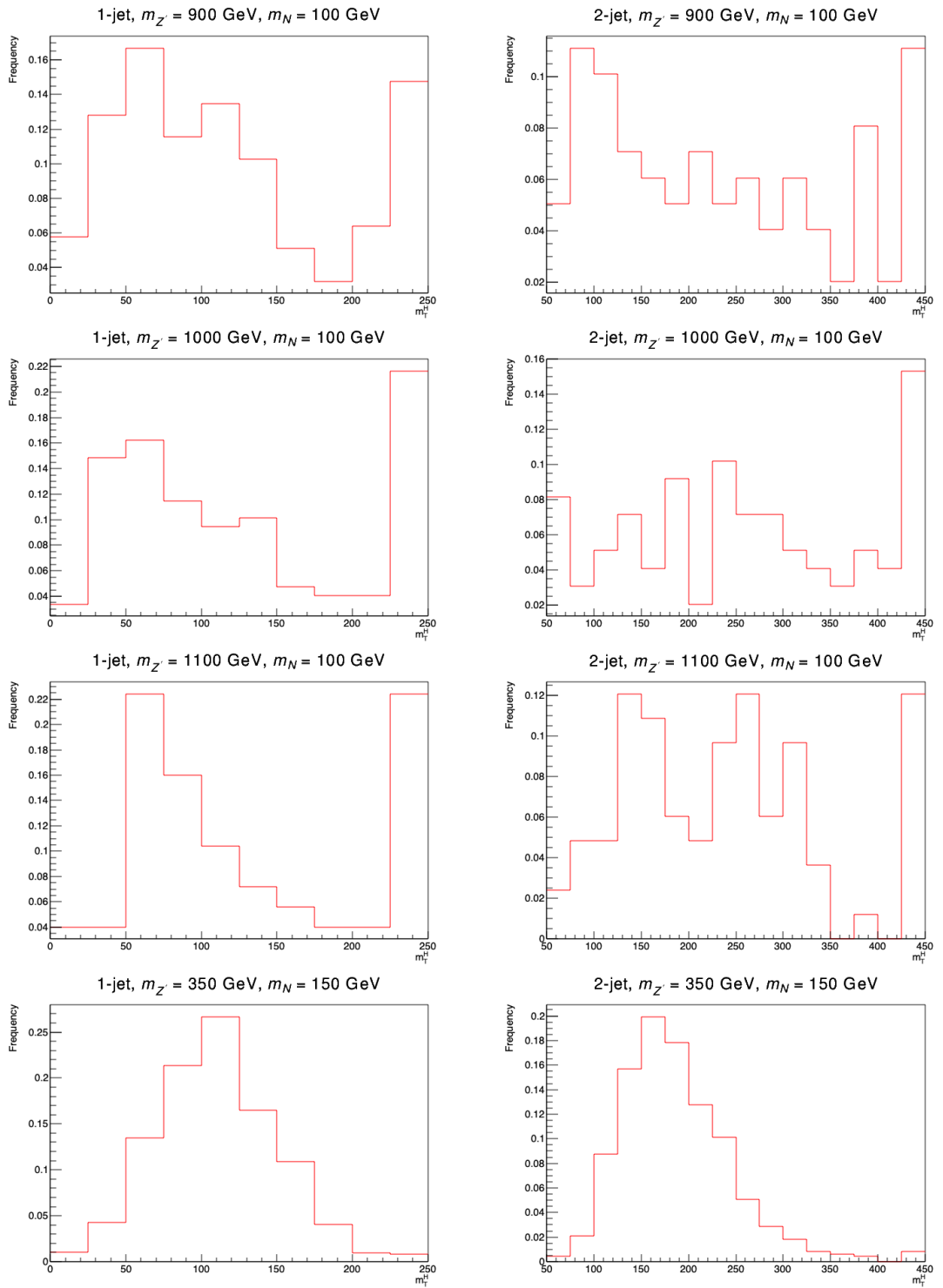


Figure G.23: Histograms for NN process for masses $m_{Z'} = (900, 1000, 1100)$ GeV and $m_N = 100$ GeV, and masses $m_{Z'} = 350$ GeV and $m_N = 150$ GeV

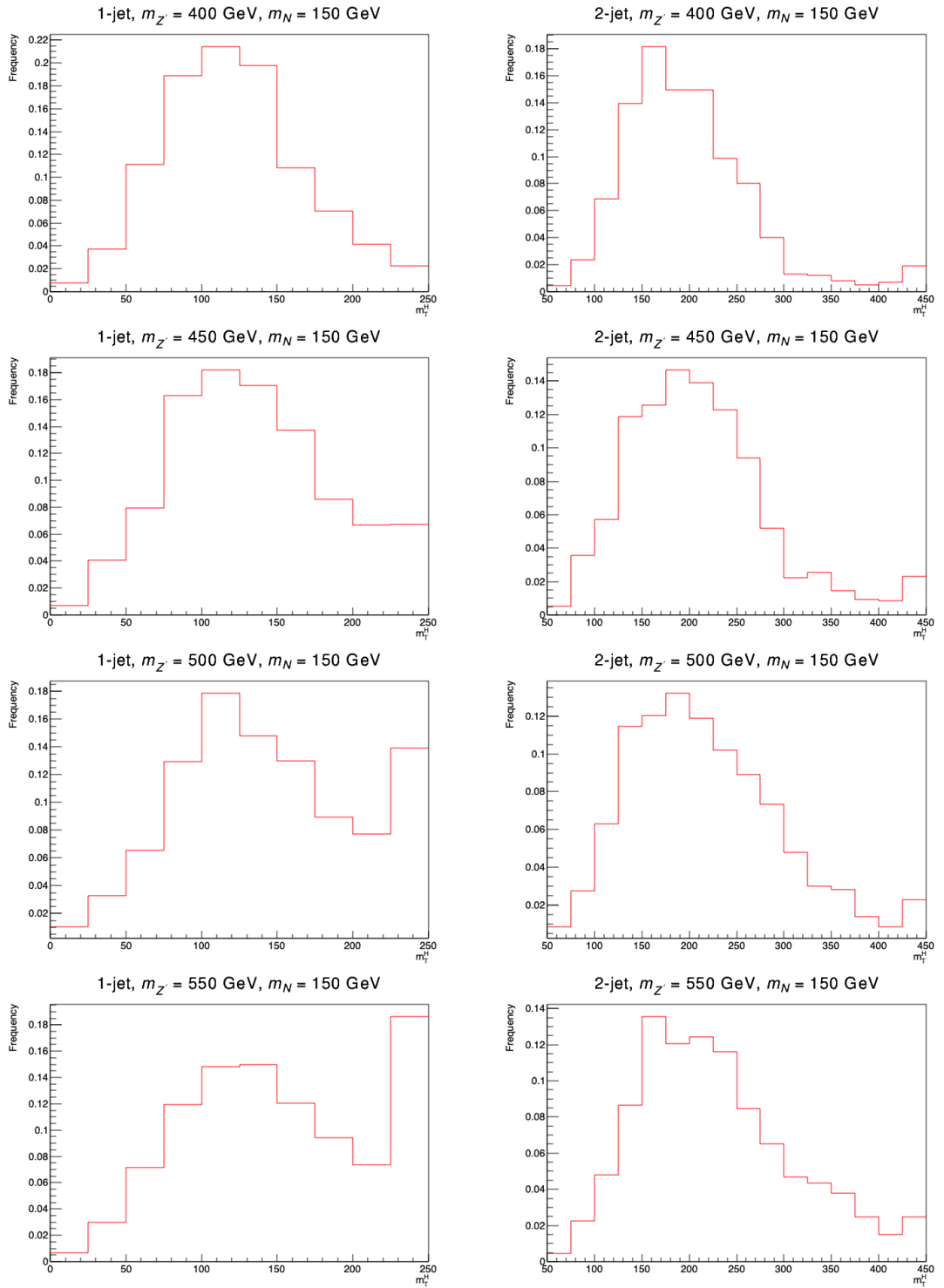


Figure G.24: Histograms for NN process for masses $m_{Z'} = (400, 450, 500, 550)$ GeV and $m_N = 150$ GeV

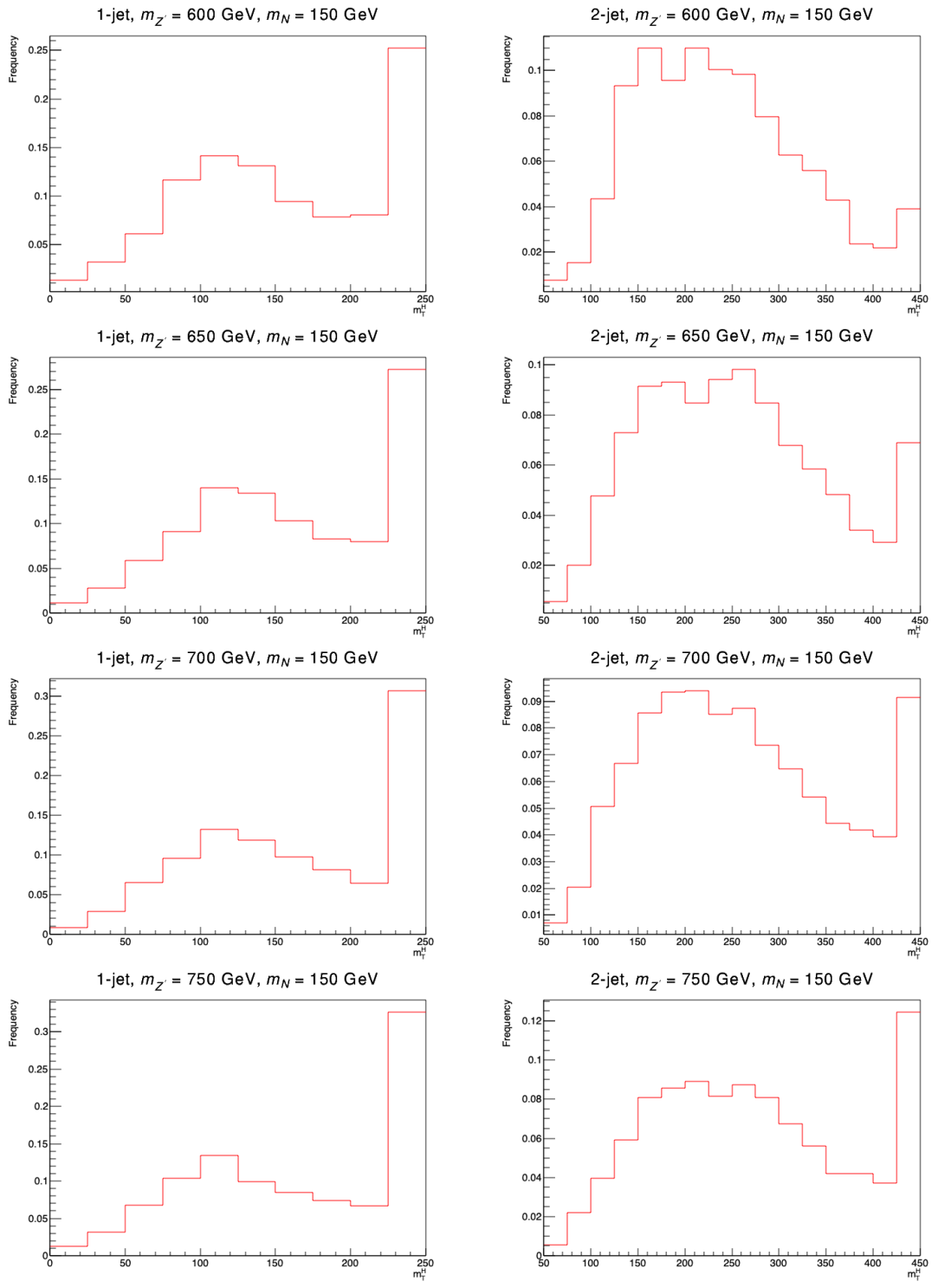


Figure G.25: Histograms for NN process for masses $m_{Z'} = (600, 650, 700, 750)$ GeV and $m_N = 150$ GeV

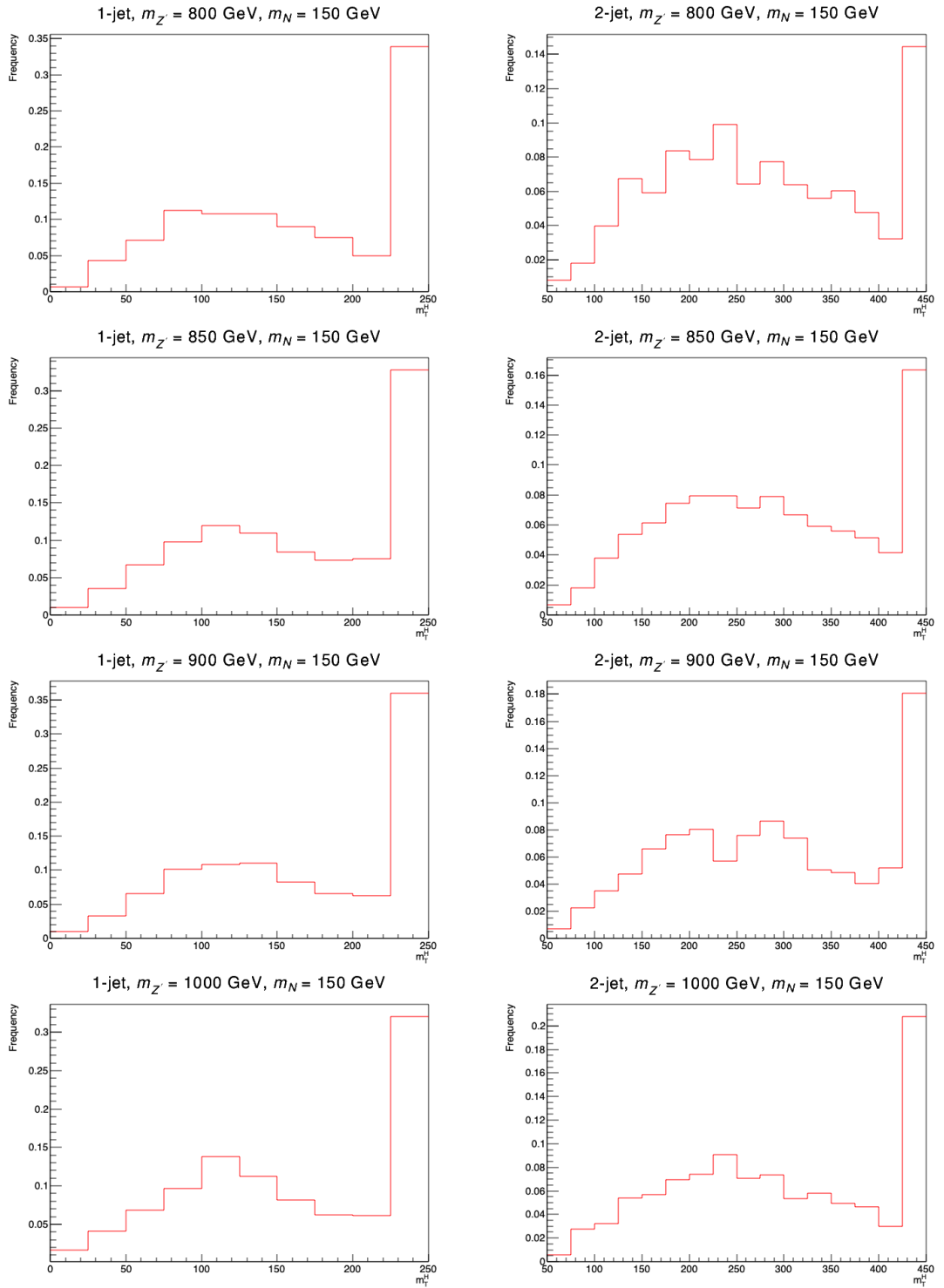


Figure G.26: Histograms for NN process for masses $m_{Z'} = (800, 850, 900, 1000)$ GeV and $m_N = 150$ GeV

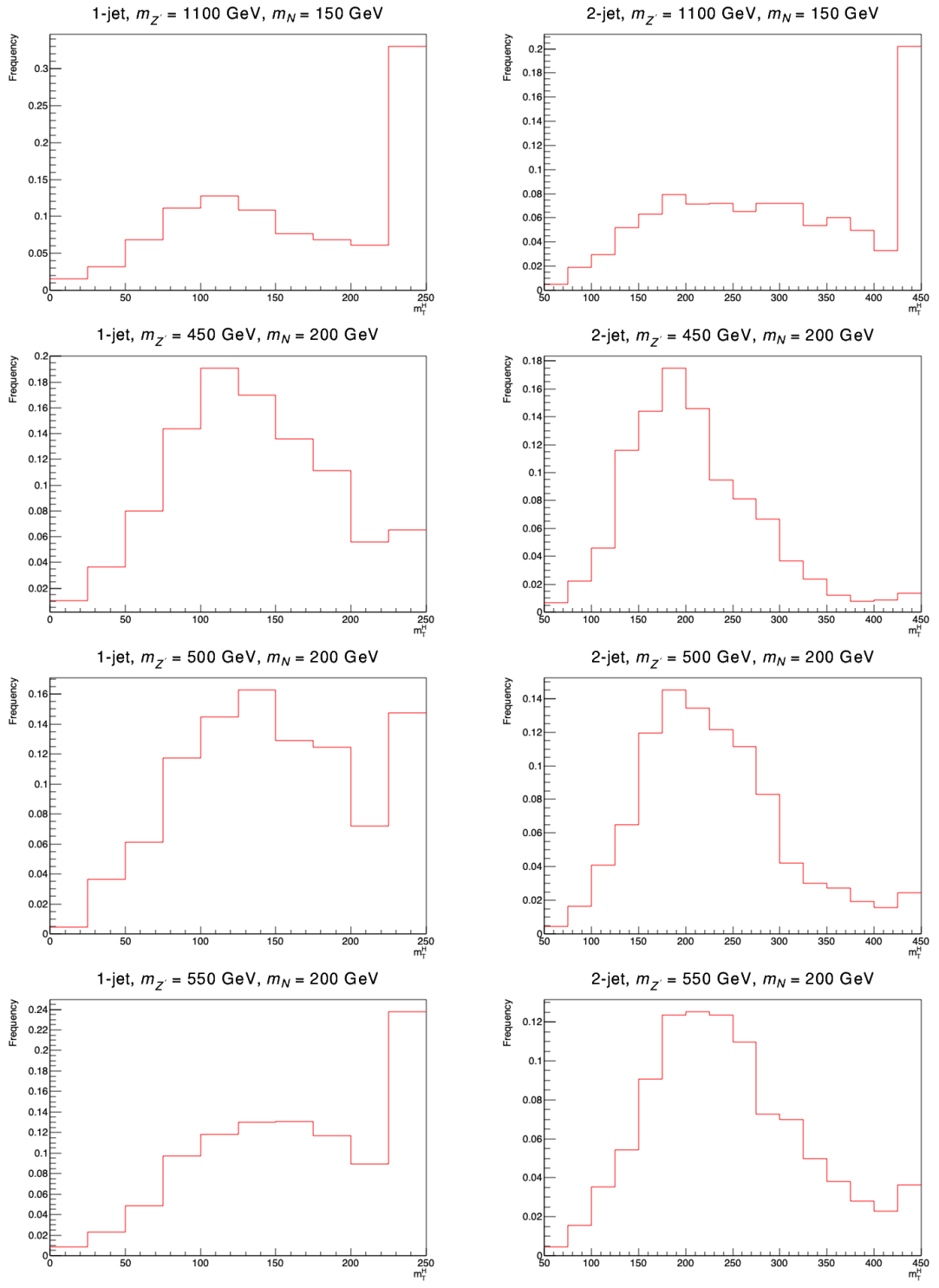


Figure G.27: Histograms for NN process for masses $m_{Z'} = 1100$ GeV and $m_N = 150$ GeV, and $m_{Z'} = (450, 500, 550)$ GeV and $m_N = 200$ GeV

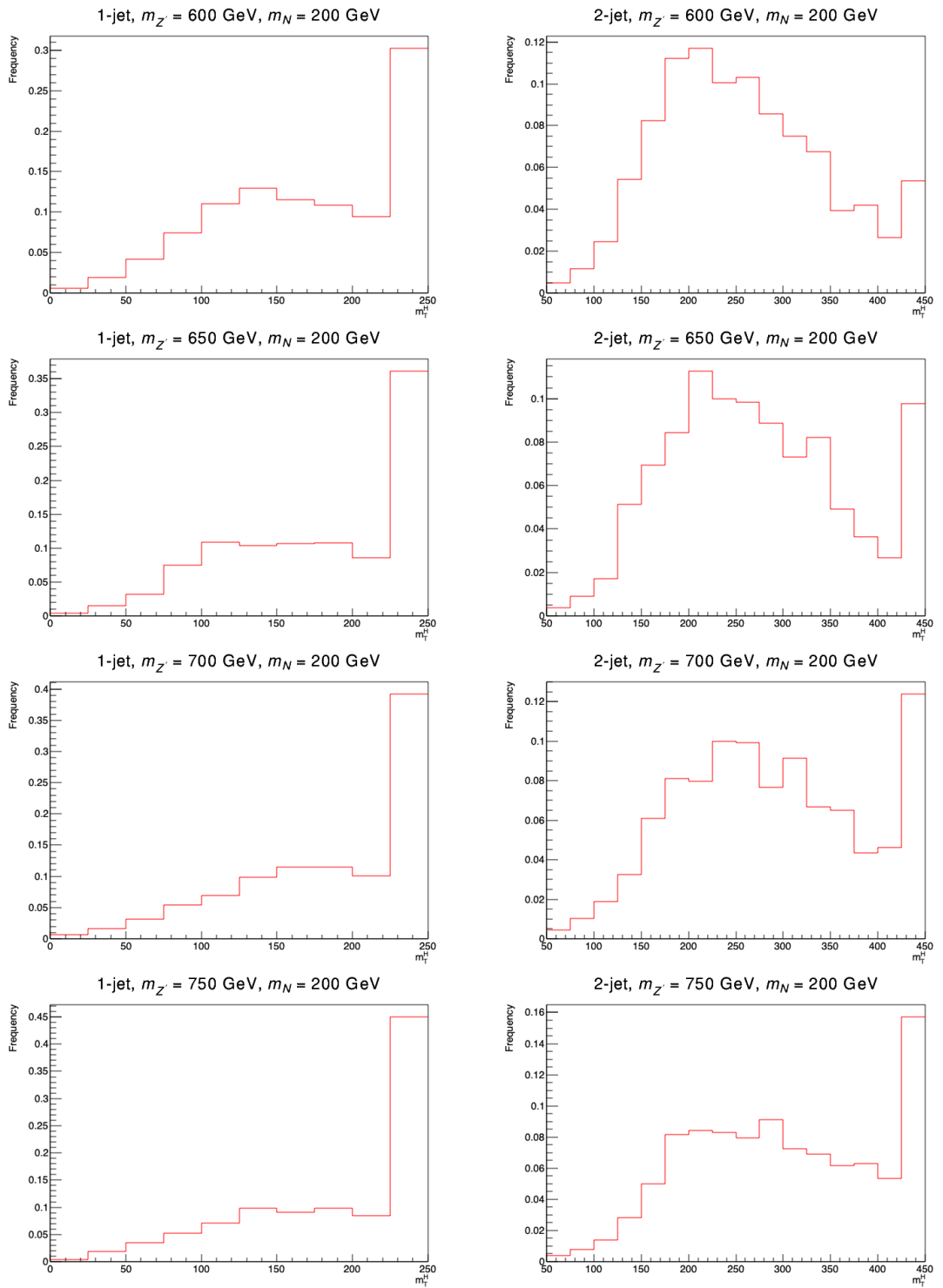


Figure G.28: Histograms for NN process for masses $m_{Z'} = (600, 650, 700, 750)$ GeV and $m_N = 200$ GeV

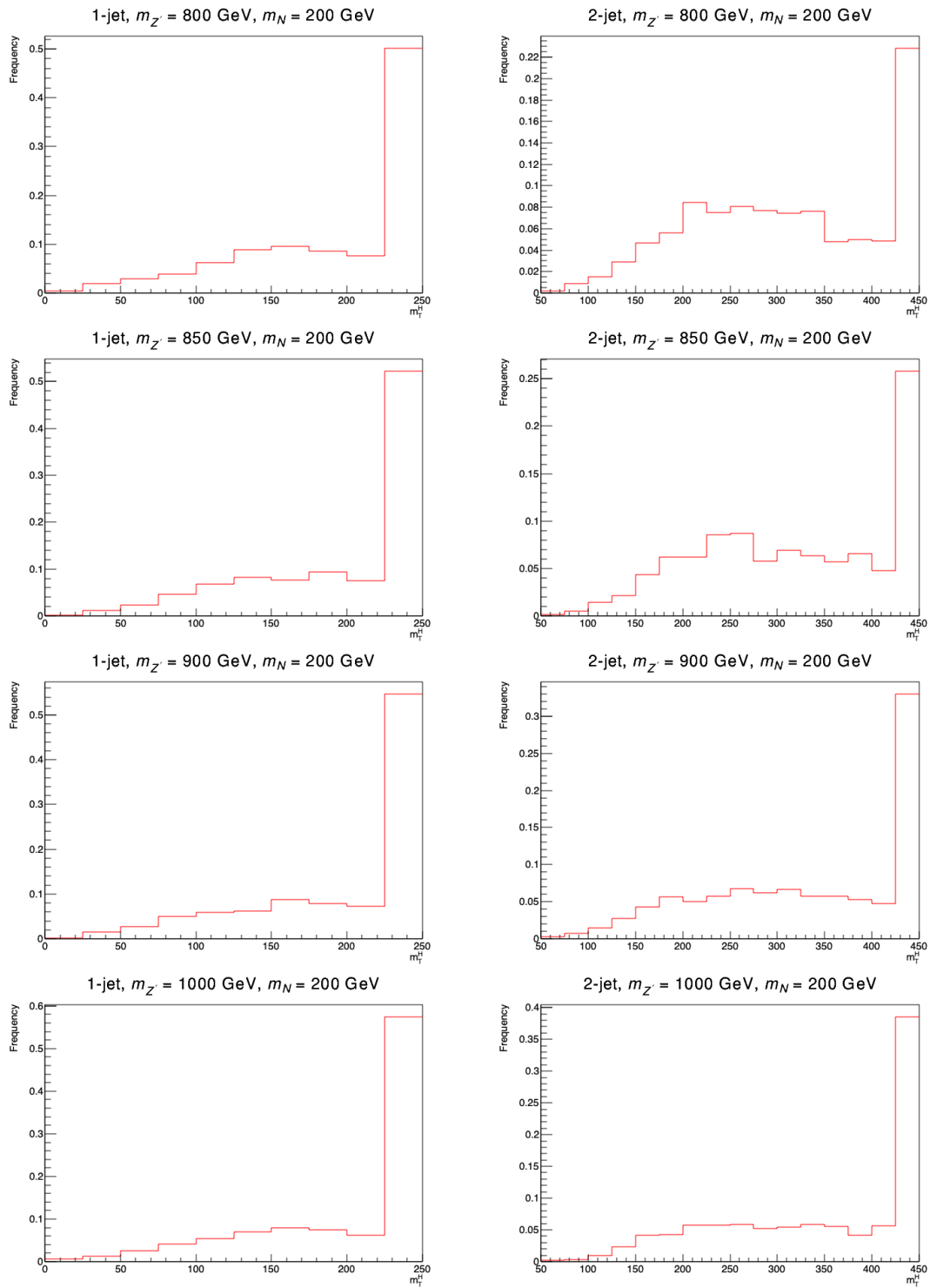


Figure G.29: Histograms for NN process for masses $m_{Z'} = (800, 850, 900, 1000)$ GeV and $m_N = 200$ GeV

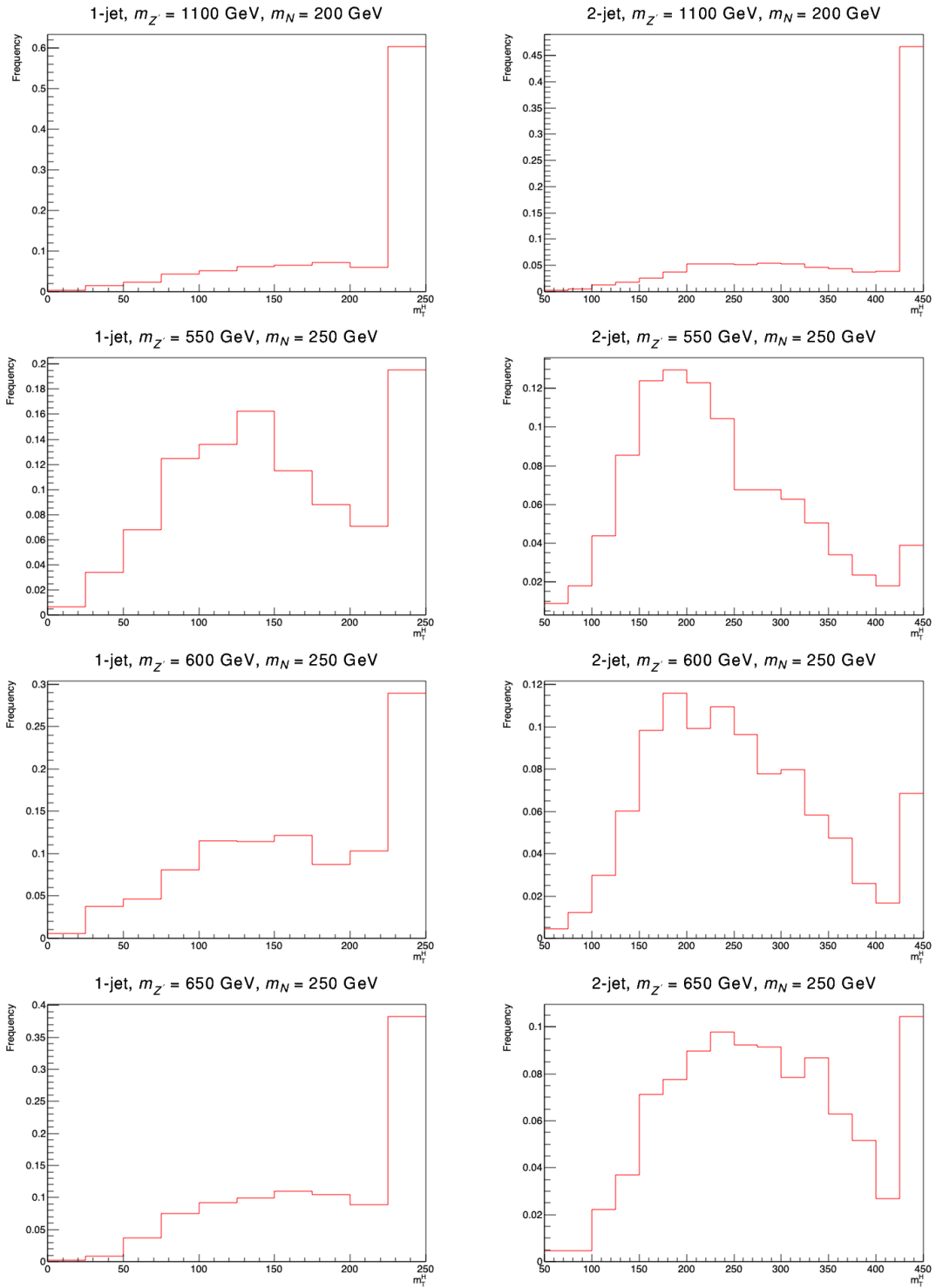


Figure G.30: Histograms for NN process for masses $m_{Z'} = 1100 \text{ GeV}$ and $m_N = 200 \text{ GeV}$, and masses $m_{Z'} = (550, 600, 650) \text{ GeV}$ and $m_N = 250 \text{ GeV}$

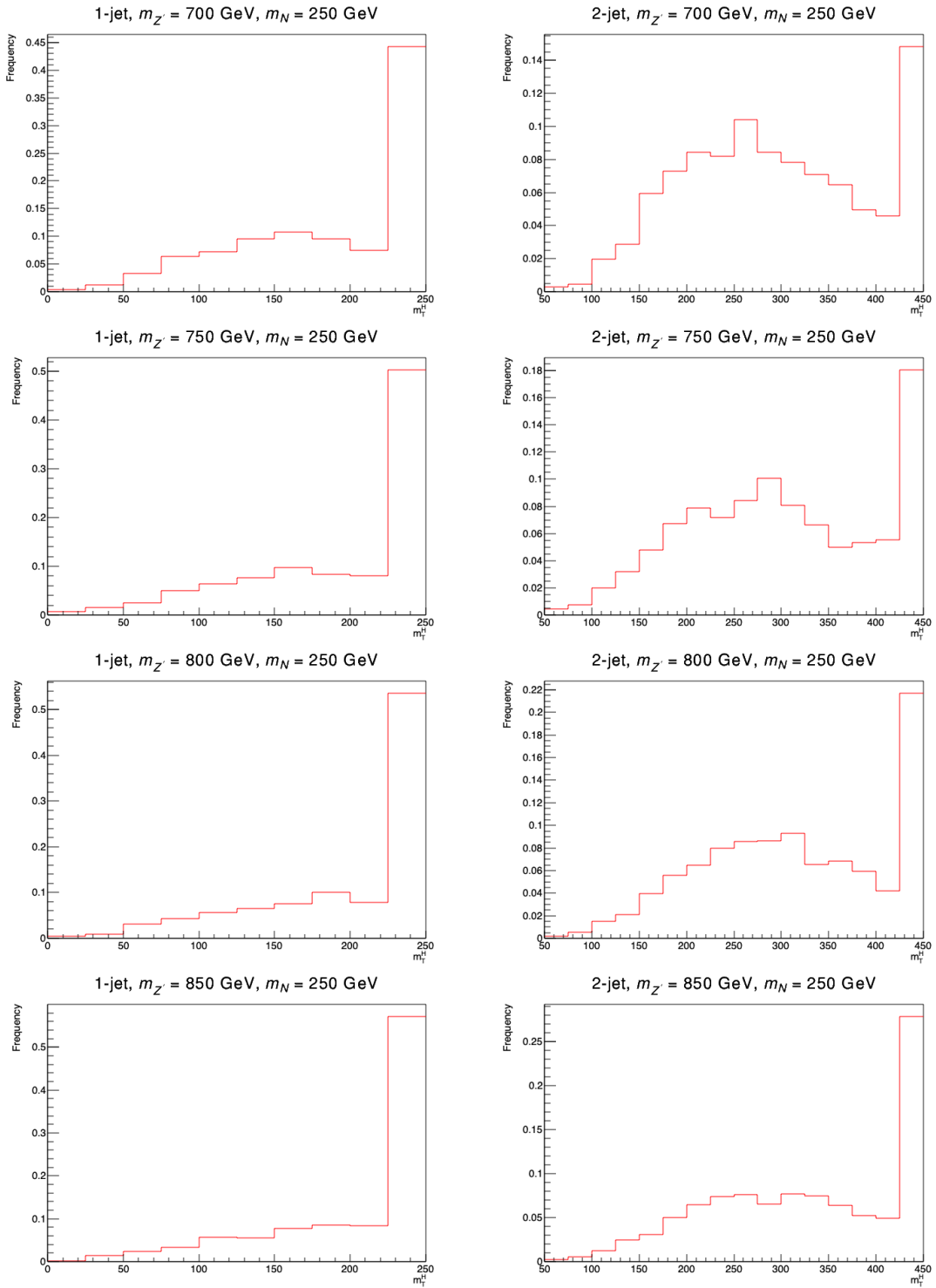


Figure G.31: Histograms for NN process for masses $m_{Z'} = (700, 750, 800, 850)$ GeV and $m_N = 250$ GeV

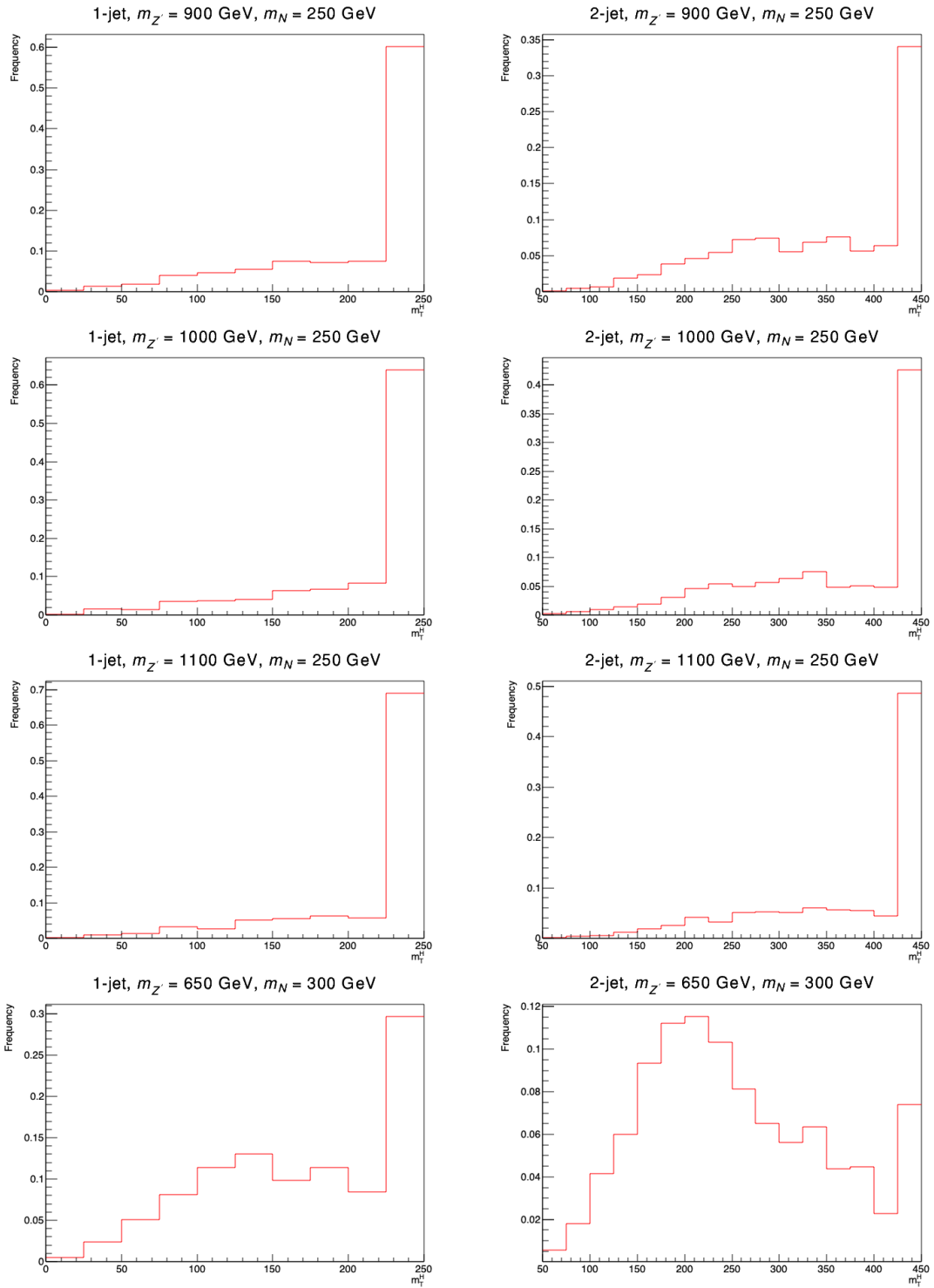


Figure G.32: Histograms for NN process for masses $m_{Z'} = (900, 1000, 1100) \text{ GeV}$ and $m_N = 250 \text{ GeV}$, and masses $m_{Z'} = 650 \text{ GeV}$ and $m_N = 300 \text{ GeV}$

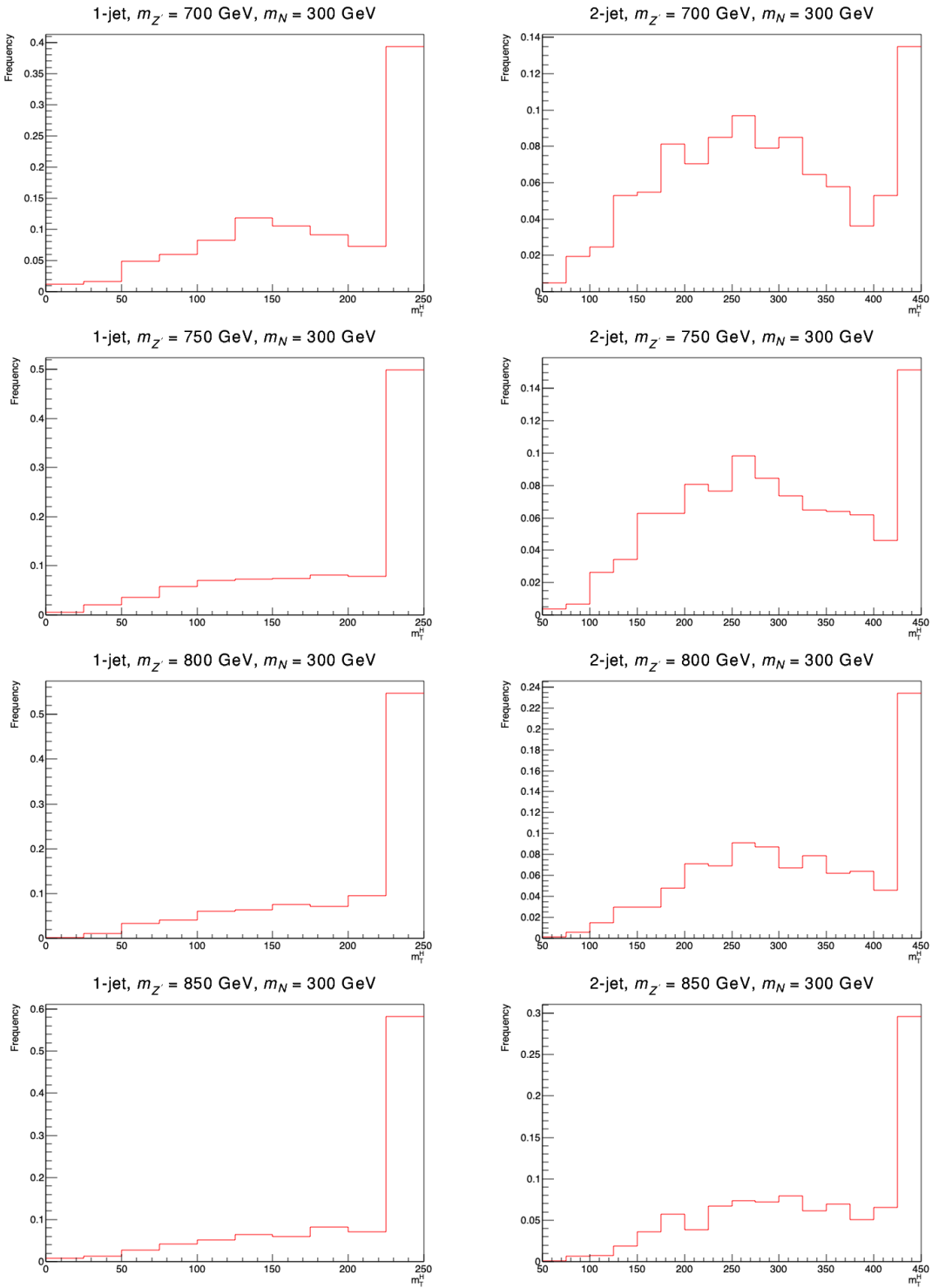


Figure G.33: Histograms for NN process for masses $m_{Z'} = (700, 750, 800, 850)$ GeV and $m_N = 300$ GeV

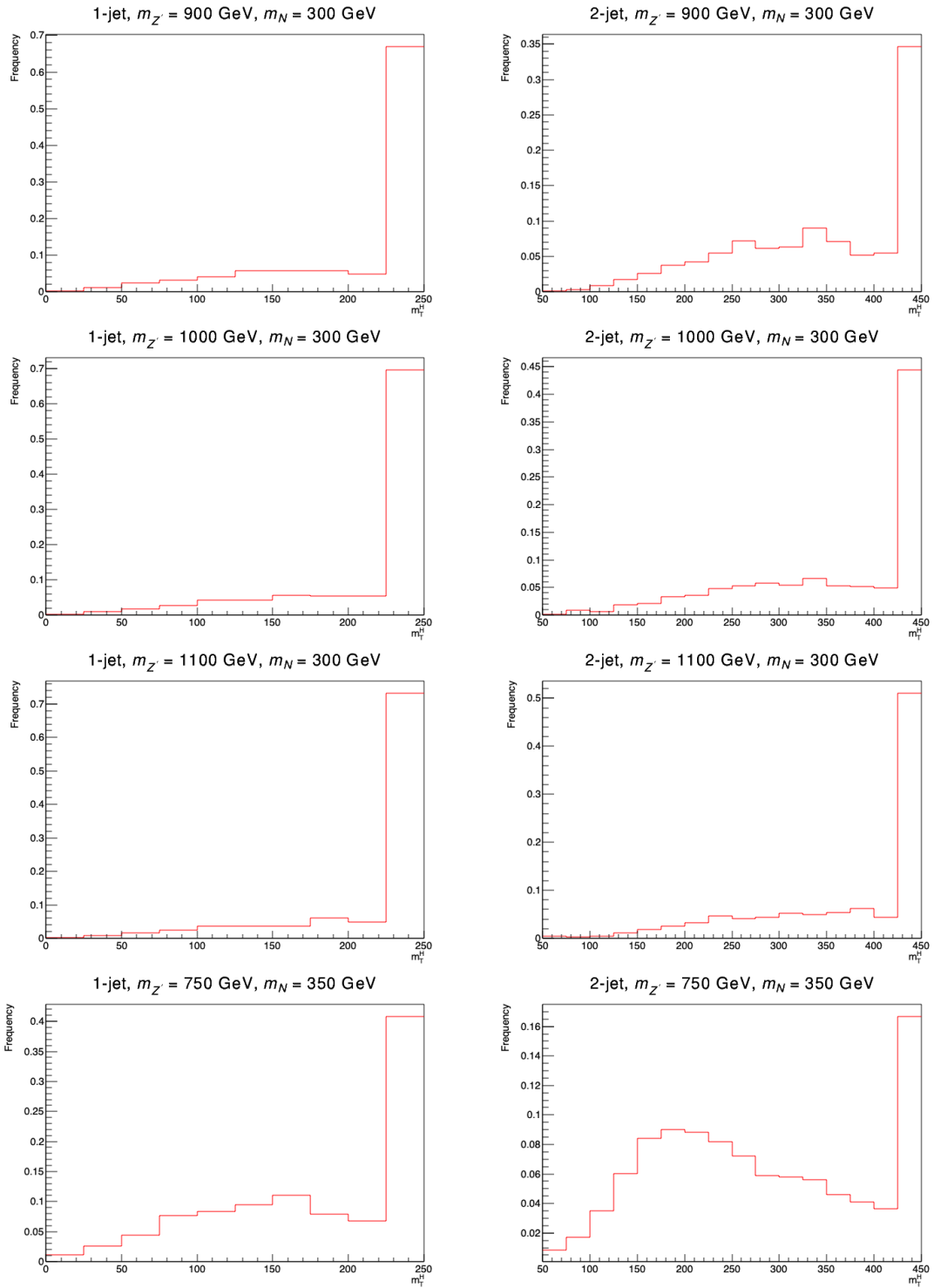


Figure G.34: Histograms for NN process for masses $m_{Z'} = (900, 1000, 1100)$ GeV and $m_N = 300$ GeV, and masses $m_{Z'} = 750$ GeV and $m_N = 350$ GeV

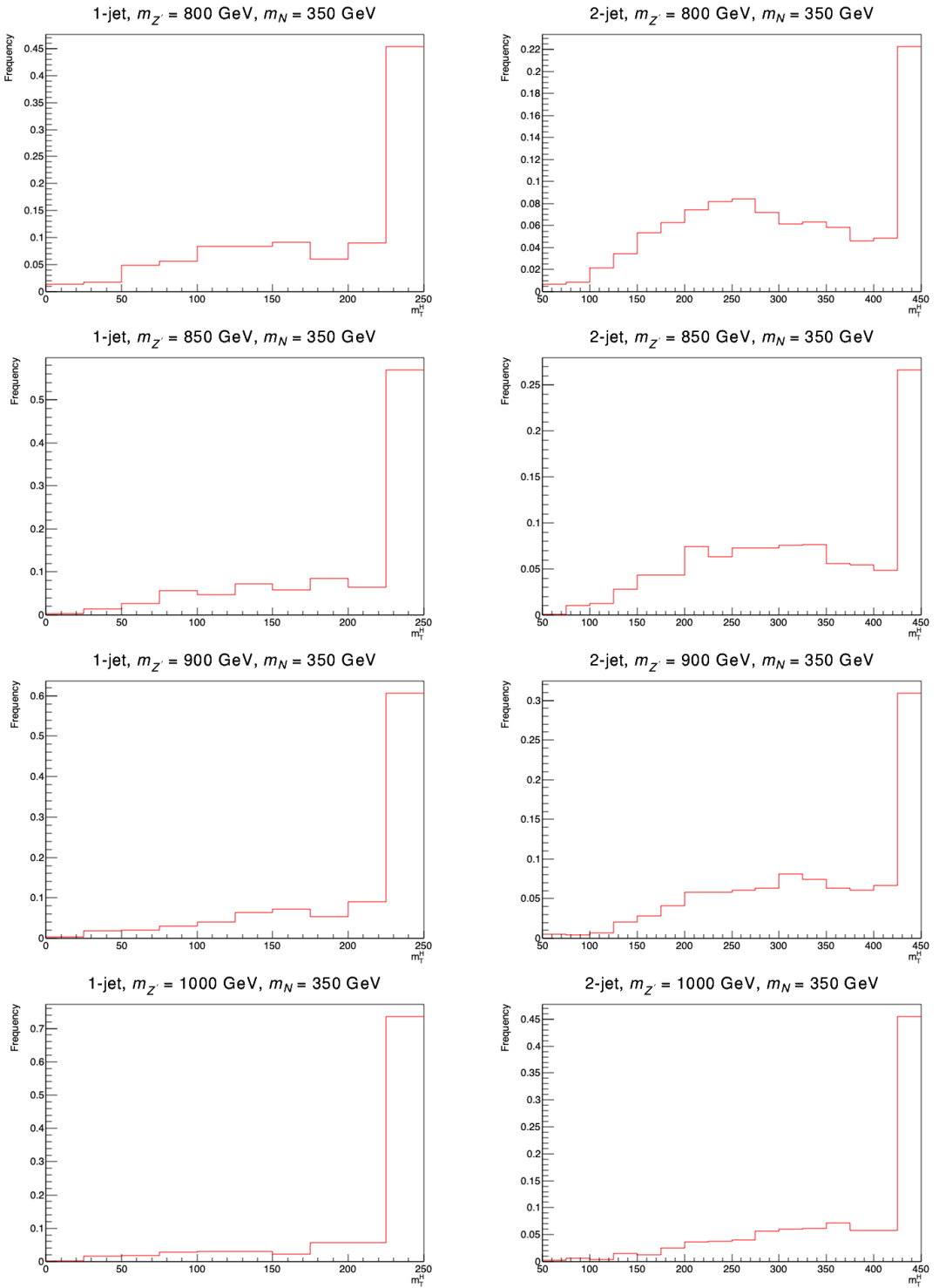


Figure G.35: Histograms for NN process for masses $m_{Z'} = (800, 850, 900, 1000)$ GeV and $m_N = 350$ GeV

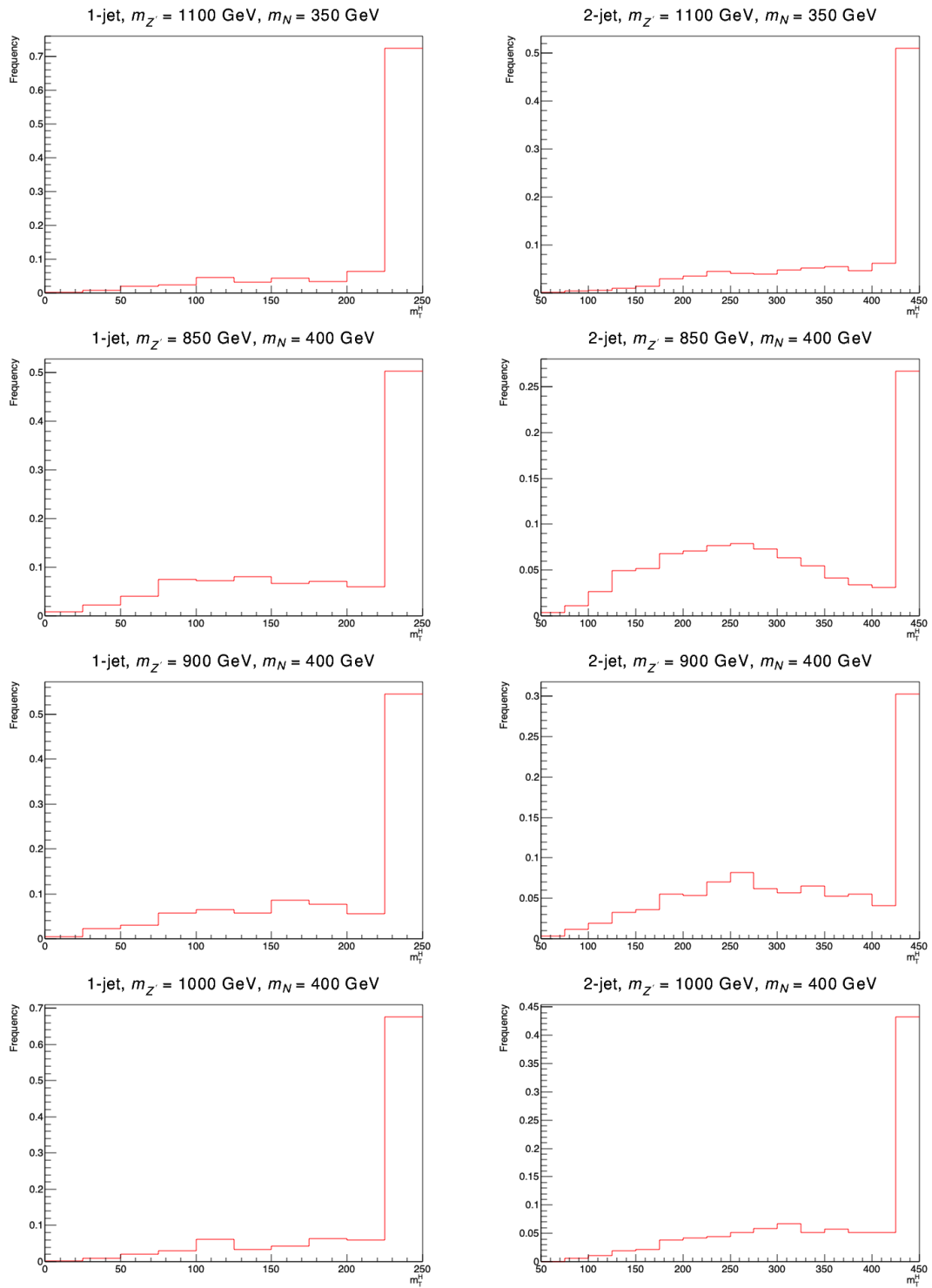


Figure G.36: Histograms for NN process for masses masses $m_{Z'} = 1100$ GeV and $m_N = 350$ GeV, and masses $m_{Z'} = (850, 900, 1000)$ GeV and $m_N = 400$ GeV

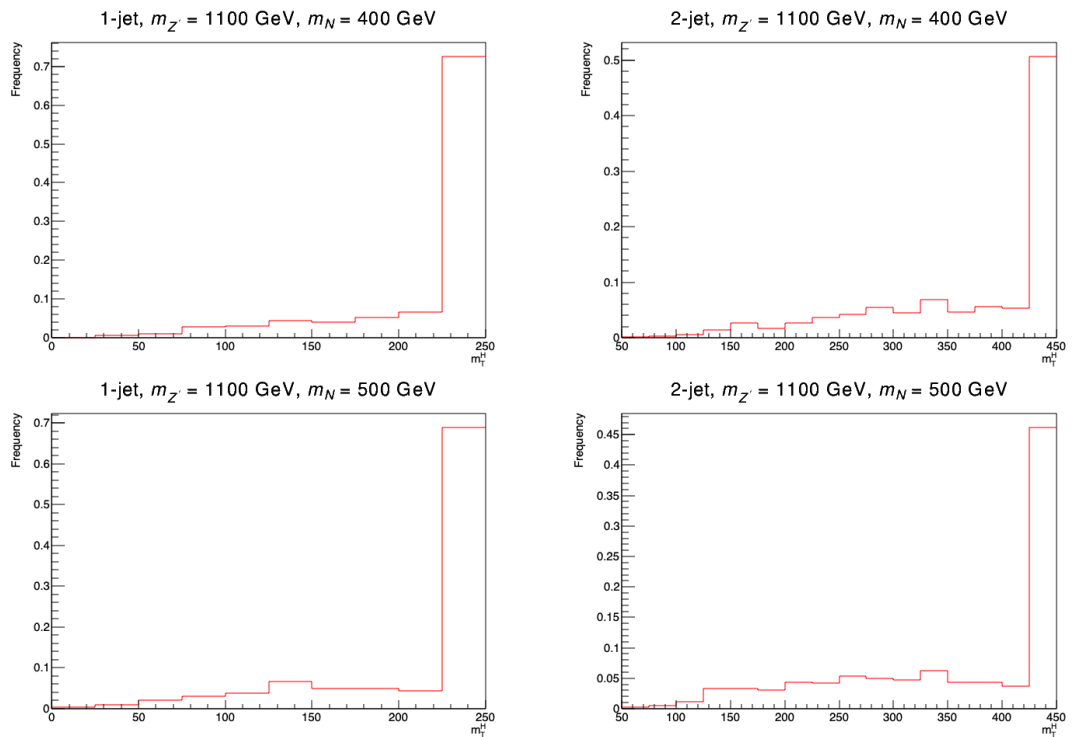


Figure G.37: Histograms for NN process for masses $m_{Z'} = 110 \text{ GeV}$ and $m_N = (400, 500) \text{ GeV}$